STABILITY INVESTIGATIONS OF TUNNELS IN A COAL MINE IN CHINA THROUGH 3D-DISCONTINUUM NUMERICAL MODELING AND FIELD DEFORMATION MONITORING DATA

by

Srisharan Shreedharan

A Thesis Submitted to the Faculty of the

DEPARTMENT OF MINING & GEOLOGICAL ENGINEERING

In Partial Fulfillment of the Requirements

For the Degree of

MASTER OF SCIENCE

WITH A MAJOR IN MINING, GEOLOGICAL & GEOPHYSICAL ENGINEERING

In the Graduate College

THE UNIVERSITY OF ARIZONA

2016

STATEMENT BY AUTHOR

This thesis has been submitted in partial fulfillment of requirements for a master's degree at the University of Arizona and is deposited in the University Library to be made available to borrowers under rules of the Library.

Brief quotations from this thesis are allowable without special permission, provided that an accurate acknowledgement of the source is made. Requests for permission for extended quotation from or reproduction of this manuscript in whole or in part may be granted by the head of the major department or the Dean of the Graduate College when in his or her judgment the proposed use of the material is in the interests of scholarship. In all other instances, however, permission must be obtained from the author.

SIGNED: Srisharan Shreedharan

APPROVAL BY THESIS DIRECTOR

This thesis has been approved on the date shown below:

_____ _____

Pinnaduwa Kulatilake Date

Professor of Geological Engineering

ACKNOWLEDGMENTS

I would like to thank all the people who have helped me reach this pivotal stage in my research career. First and foremost, I wish to express my deepest gratitude to my thesis advisor, Prof. Pinnaduwa Kulatilake. Not only did he let me identify and solve research problems independently, he has always been a constant presence as a voice of reason, encouragement and criticism. I also thank him for going beyond his role as my advisor by involving me in a variety of research problems spanning laboratory and computational questions, and for his coursework which have helped me grow as a scholar. I also thank members of my thesis committee Prof. Tribikram Kundu (whose Finite Elements course I would strongly recommend to any mechanics graduate student) and Dr. Moe Momayez for their insights into my research and graduate life. Dr. Momayez, Prof. John Kemeny and Prof. Randy Richardson not only offered great courses, they had a wealth of grad school advice which has helped me in every stage of my life in Tucson. Geomechanics lab manager David Streeter has been an amazing and patient teacher every time I have asked him about working with his rock mechanics lab, and those few times I asked about his music collection.

My research would not have been possible without generous funding from the US Center for Disease Control and Prevention under Contract No. 200-2011-39886. I am also grateful for the laboratory and field geotechnical/geological data provided by the Xinwen Mining Company and Prof. Fuxing Jiang and Dr. Zhengxing Yu of University of Science and Technology Beijing.

I would also like to thank my lab group colleagues Yan, Pengfei, Hadi and Taghi for all of our discussions related to research, coursework, life after grad school and everything else. Yan and Hadi - you have been great office space neighbors, lab partners and fellow coffee connoisseurs and I have greatly benefited from every conversation with you. All the conversations with Taghi on rock bolt formulations gave me great momentum during the initial dull months of my research. I hope I have proved to be as useful a resource as you guys have been to me.

Dolores Fajardo, Rose Evans and Sherri Raskin have helped me greatly in their administrative roles have never shied from answering my questions on university procedures and guidelines.

My undergraduate mentors – Dr. Harsha Vardhan and Dr. Ram Chandar exposed me to high quality research early on, bringing out the best I had to offer, and pushed me to apply to grad school. I would not be here if not for them.

I thank Daniel and Anna for being there for me in general and during my finals week tantrums and breakdowns in particular. Special thanks to Anna for your important research question of whether 600 elephants, standing on one leg, stacked on top of each other, would destabilize the tunnels I was working on. Since this increases my numerical model's overburden stress by nearly 90 MPa, on average, I would have to say that 600 such elephants on my tunnels would indeed be incredibly inconvenient.

Finally, I would like to thank my family for the support and encouragement they have shown through this particularly rewarding and draining stage of my life.

To my late grandparents

Ambujavalli

and

Krishnaswamy

TABLE OF CONTENTS

LIST OF TABLES

LIST OF FIGURES

ABSTRACT

An imperative task for successful underground mining is to ensure the stability of underground structures, since it influences the safety, and in turn, the production capacity and economic performance of the mine. This is more so for deep excavations in soft rock which may be under significantly high stresses. In this thesis, stability studies on two tunnels, a horseshoe-shaped and an inverted arch-shaped tunnel, have been presented. The tunnels, running at a depth of 1325 m, are part of the Xiezhuang Coal Mine, in the Xinwen mining area, in China. Using the available information on stratigraphy, geological structures, in-situ stress measurements and geo-mechanical properties of intact rock and discontinuity interfaces, a three-dimensional numerical model has been built using the 3DEC 3-Dimensional Distinct Element Code to simulate the stress conditions around the tunnels. Based on available discontinuity geometry constraints, the rock mass has been modelled as a mixture of a discontinuum medium close to the tunnels and as an equivalent-continuum in the far field. Due to the unavailability of field measurements for rock mass mechanical parameters, the parameters have been estimated by incorporating the available intact rock mechanical properties and field deformation monitoring data into a strength reduction model calibration procedure. This back-analysis (calibration) has been carried out through a pseudo-time dependent support installation routine which incorporates the effect of time through a stress-relaxation mechanism.

The results from the back-analysis indicate that the rock mass cohesion, tensile strength, uniaxial compressive strength, and elastic modulus values are about 35–45 % of

the corresponding intact rock property values. Additionally, the importance of incorporating stress relaxation before support installation in numerical modeling has been illustrated, for the first time in literature, through the increased support factors of safety and reduced grout failures. The calibrated models have been analyzed for different supported and unsupported cases in an attempt to quantify the effect of supports in stabilizing the tunnels and to estimate the adequacy of the existing supports being used in the mine. A direct outcome is that the findings indicate that longer supports may be better suited for the existing geo-mining conditions around the tunnels since they have fractured zones that are larger than the supports currently in use at the mine. The effects of supports have been demonstrated using changes in deformations and yield zones around the tunnels, and changes in the average factors of safety and grout failures of the supports. The use of longer supports and floor bolting has provided greater stability for the rock masses around the tunnels. A comparison between the closure strains in the two differently shaped tunnels indicates that the inverted arch tunnel may be more efficient in reducing roof sag and floor heave for the existing geo-mining conditions.

Additional analyses focusing on parametric sensitivity studies on the rock and joint mechanical properties show that the tunnel stability is highly sensitive to changes in cohesion and internal friction angle of the intact rock, and changes in joint basic friction angle. Tunnel stability is seen to not be very sensitive to changes in intact rock tensile strength and joint shear stiffness for the tunnels being studied. Finally, support optimization studies conducted by studying the effect of changing cable diameters and grout uniaxial compressive strengths on support factors of safety and grout failures show the trade-off that is necessary in selecting cable strength vis-à-vis grout strength. The

results indicate that simply increasing either one of cable or grout strength parameters without considering their interactions and compatibilities could be detrimental to the stability of the support system.

KEYWORDS:

Tunnel stability; Numerical modeling; Back-analysis; Stress-relaxation; Discrete Element Method; High in-situ stress

CHAPTER 1: INTRODUCTION

1.1. Motivation and scope of study

Underground mining regularly requires the excavation of tunnels in a wide range of geological conditions including, but not limited to soft strata, high number of fractures, great depths, water bearing strata etc. This requires significant planning and stability analyses at every stage of the project. This thesis explores two tunnels in a very deep (>1000 m) coal mine in China, by employing a suite of state-of-the-art numerical modeling methods in an attempt to better characterize the stability of the tunnels. The studies have done in collaboration with the University of Science and Technology, Beijing, and the Xinwen Mining Company, that owns the coal mine (Xiezhuang coal mine).

One of the reasons for why the Chinese mining scenario provides the perfect setting and the most opportune moment to conduct the research is the history and record of coal mining safety in China. Underground mining in itself presents risks usually unseen in surface mining. This is more so in China because most of their (~95%) coal workings are underground (China Coal Society Open Pit Mine Committee, 2010). As their energy needs continue to increase, the country looks to its coal industry to satiate the demand and the industry is, in turn, forced to search deeper within the earth (He and Song, 2012). However, deep mining of coal comes with exacerbated problems in the ground control department, in the form of increased roof falls, coal bumps, water inrush etc. Statistics until 2008 hold roof falls responsible for the highest number of coal fatalities in China,

with about 1200 deaths in 2008 alone (The Compiling Committee of China, 2010). According to estimates by Chen et al. (2012a), China has had nearly 48000 reported coal fatalities since 2001. To put this in perspective, this figure is significantly higher than corresponding figures for the next nine highest producers of coal put together. This calls for a concentrated effort focused on characterizing and minimizing coal mine fatalities especially in deep mines in China and in the rest of the world.

Keeping this in mind, this thesis has attempted to focus on two tunnels of different shapes, their stability in the context of rock mass stability, local failures, floor heaving, deformation reduction and support stability. Since support stability can elegantly function as a proxy for tunnel stability (for instance, a given support system can be expected to be less stable in highly fractured rock masses than in more massive formations), it has been given due importance. The scope of the thesis extends to a holistic static analysis of the stability of the two tunnels through the study of tunnel deformations, damage zone in the rock mass around the excavation and support failures. This has been achieved through the use of a 3-dimensional discrete element method code which has been used to create accurate models of the geological system. Lithological, in-situ stress, intact rock mechanical property values, bedding plane orientations, and tunnel and support geometries have been explicitly incorporated with as much accuracy and reliability as possible in light of available information. Back-analysis studies have been performed using the available field deformation data to determine the rock mass mechanical property values in the region. The calibrated numerical models have been subsequently employed in analyses aimed at gathering more insights into the behavior of the supports used in the system, their efficacy and scope for improvement. New procedures have been

established to incorporate the effect of stress redistribution in the tunnel during the stand-up period between excavation and supporting, and for the calculation of support factors of safety and grout failures in the discrete element code. The tunnel shapes have been studied and the suitability of the tunnels in the existing geo-mining conditions has been discussed. Parametric studies have also been performed to understand the behavior of the rock mass to changes in rock and discontinuity properties and to understand the behavior of the supports to changes in cable and grout mechanical properties.

1.2. Objectives

The global objective of this thesis is to describe the stability of the tunnels in a deep soft rock excavation. This can be broken down into some more specific objectives as follows:

- To calibrate the models and estimate rock mass mechanical property values through a back-analysis involving the field deformation monitoring data
- To quantify the effect of explicitly modeling the stress redistribution during the stand-up time between excavation and support
- To assess the performance and adequacy of the support systems in the context of tunnel stability
- To assess the suitability of the two tunnel shapes for the given site
- To study the sensitivity of rock mass to variability in intact rock and discontinuity mechanical and frictional parameters
- To study the support behavior through a parametric analysis of cable and grout strengths

1.3. Research highlights

The outcomes of the research discussed in this thesis have been disseminated to the wider scientific community through publication in an international journal. Part of the work has also been accepted for presentation in an international geomechanics conference. Some of the highlights/novelties of the research are:

- The rock mass strength has been estimated through a back-analysis exercise for one of the deepest soft rock excavations in the world
- New procedures to incorporate stress relaxation and to study its effect on tunnel and support stability have been introduced
- Procedures to calculate cable factors of safety and grout bond failures in the discrete element code have been introduced as a way to quantify the support stability
- Tunnel stability has been quantified through tunnel deformations, cable factor of safety and grout failures
- Sensitivity of the rock mass to fluctuations in intact rock and joint mechanical properties has been quantified
- Support ‘slip’ or ‘snap’ analyses through numerical modeling have been introduced as a way to optimize support mechanical properties

1.4. Layout of the thesis

The thesis has a classical layout and starts off with an introduction to the research (Chapter 1). This is followed by Chapter 2 - a literature review focusing on various methods to quantify tunnel stability, with a focus on numerical modeling as applied to deep excavations in soft rock. The site of the study is subsequently introduced to the

reader in Chapter 3, with insights into the stratigraphy, geology and state of stress in the region, and a background to the mine. Chapter 4 introduces the discrete element code and its relevant mathematical formulations used in the study, with Chapter 5 building up on this by explaining the modeling set up and the procedures adopted to perform the actual analyses. Chapter 6 includes extensive discussions on the results from the analyses and the thesis concludes with Chapter 7 which also provides some new areas for future research focus. For a complete experience, the reader is advised to go through chapters sequentially. Readers interested in the mining region are directed to Chapter 3, those interested in the modeling procedures are directed to Chapters 5-7 and readers focusing on the physics behind the discrete element method are advised to go through Chapter 4.

CHAPTER 2: LITERATURE REVIEW

2.1. Introduction

This chapter discusses and reviews the existing literature pertaining to the use of three broad qualitative and quantitative methods (Rock mass classification, field instrumentation and numerical modeling) for describing the stability of underground structures. The past use of numerical modeling in studies on excavations in high in-situ stress conditions is reviewed, with a focus on the use of 3-dimensional discrete element methods. This chapter attempts to set up a justification for the psyche behind selecting the methodology used for assessing tunnel stability in this thesis.

2.2. Rock mass classification systems

One of the earliest documented rock mass classification systems aimed at attempting to assess tunnel stability was the rock load method proposed by Terzaghi et al. (1946). This method gained popularity in the United States and was found to be useful for designing steel supports for tunnels. However, it has found little use in modern tunneling which makes extensive use of shotcrete and rock bolts. According to Bieniawski (1989), the rock load system may be too qualitative and general to be used for quantitative rock strength and tunnel stability studies. The system makes use of qualitative and broad descriptions of the level of jointing and depth (eg. “massive”, “ moderately jointed”, “moderate depth”) to design the type of support required and the loading on the rock.

A seminal work of its time, on excavation stability, came from Lauffer (1958) as the Stand-Up time classification. This work provided a chart which could be used to estimate the length of time for which an excavated span of any size would stay stable without collapsing as this is a function of the rock mass strength and the area and shape of the excavation. However, it has been found to provide excessively conservative design estimates for modern tunnels.

A common rating system introduced by Deere et al. (1966) being used in most core logging applications around the world is the Rock Quality Designation (RQD). The RQD is based on a 0-100 scale with quality designations ranging from Very Poor to Excellent based on the numerical value of the RQD. It is simply the ratio of the sum of rock core lengths of cores greater than 10 cm in length to the total core run length, expressed as a percentage, as shown in equation 2.1.

$$RQD = \frac{\sum Length\ of\ core\ pieces > 10\ cm}{Total\ length\ of\ core\ run} \tag{2.1}$$

Note that equation 2.1 is based on the core size of 50.8 mm diameter. When drill core is unavailable, the RQD has also been estimated using Palmstrom's (1982) formula (equation 2.2), relating the joint volume (number of joints per cubic meter of rock block, J_v) to RQD.

$$RQD = 115 - 3.3J_v \tag{2.2}$$

This is particularly useful for tunnels. The RQD has been used as a reasonable proxy for tunnel quality and stability (Deere et al., 1970; Cecil, 1970; Cording and Deere, 1972; Merritt, 1972). While the RQD forms a basic parameter in the more popular classifications used at present, i.e., the Rock Mass Rating (RMR) and the Q- system, due to its simplicity, it is not a good standalone measure of rock mass quality due to its

disregarding for the other factors that affect rock mass strength – fracture orientation and size, infilling, roughness etc.

The Rock Structure Rating (RSR), introduced in the USA by Wickham et al. (1972), paved way for the two most commonly used rock mass classification systems for tunneling – RMR and Q. The RSR consists of three parameters designated as Parameters A, B and C, and the actual rating is the sum of these three parameters. Parameter A is the geology parameter and accounts for the rock type, hardness and the structure (faulting, folding etc.). Parameter B is the geometry parameter, taking care of the discontinuity spacing, orientation and tunnel orientation. Parameter C accounts for the effect of groundwater flow, joint condition and the rock mass quality as discerned from parameters A and B. While the RSR in its initial form is not used anymore, it paved way for the improved rock mass classification systems being used in different parts of world today, as discussed in subsequent paragraphs.

The most popular rock mass classification system, the Rock Mass Rating (RMR), was developed by Bieniawski (1974) as an empirical system based on field data from South African projects. It has, since, evolved through the contributions from Bieniawski and other scientists who have modified it or extended it to suit new data sets or other site or region specific criteria. The most established "first" version is by Bieniawski (1989) which estimates a rating for the rock mass as a function of intact rock strength (point load or uniaxial compressive strength), RQD, discontinuity spacing, joint alteration and groundwater flow. The initially estimated rating is then corrected for joint orientations. The discontinuity condition is judged as a function of persistence, fracture aperture, joint roughness, infill and weathering. Based on the estimated RMR, Bieniawski (1989)

provided guidelines for rock support as a combination of one or more of bolts, shotcrete and steel sets. The original RMR was modified by Laubscher (1977) to create the Modified RMR (MRMR) for mining, which accounts for high in-situ stresses, blast loading and weathering. It may be noted that the MRMR was formed from data sets primarily sourced from block caving operations. Cummings et al. (1982) and Kendorski et al. (1983) modified the MRMR for applications to block caving operations in the USA.

The Q-system, introduced by Barton et al. (1974), for the design of Scandinavian tunnels, factors in the RQD, a joint set number (J_n), joint roughness number (J_r), joint alteration number (J_a), joint water reduction factor (J_w) and a stress reduction factor (SRF). The equation to calculate the value of Q is given in equation 2.3. The Q value ranges from 0.001 (very squeezing ground) to 1000 (massive intact rock). The stress reduction factor attempts to quantify the effect of the intact rock strength and the in-situ stress on the rock mass quality. Essentially, the rock mass quality in the Q system is a function of the block size, shear strength between blocks and the effect of the in-situ stress field. Based on the values of Q and the span of the excavation, Barton et al. (1974) provide charts to estimate the quantity and quality of supports required.

$$Q = \frac{RQD}{J_n}\frac{J_r}{J_a}\frac{J_w}{SRF} \tag{2.3}$$

The Geological Strength index, introduced by Hoek (1994) and modified by Hoek and Brown (1997) attempts to characterize rocks based on the joint orientation, frequency and alteration, all judged from physical appearance. The GSI ranges from 0-100 and is used as an important input parameter for the Hoek-Brown failure criterion. Both the RMR and the GSI systems have been used as empirical proxies to relate and estimate other rock

properties such as strength, elastic modulus (Chun et al., 2009; Hamidi et al., 2010; Singh and Rao, 2005; Cai et al., 2004) etc.

Although the rock mass classification systems have established themselves as an important aspect of tunnel design either through their direct use or in probabilistic analyses (Hamidi et al., 2010; Cai, 2011; Delisio et al., 2013; Celada et al., 2014; Aydan et al., 2015), they are not without drawbacks. Due to the qualitative and highly subjective nature of their description, it is not possible to use them to fully describe the behavior of a tunnel in a jointed rock mass, to estimate its deformations, effects of blasting, staged tunneling, time-dependent weakening, seismic effects etc. The rock mass classification systems provide field engineers and technicians with a quick and simple estimate of the rock quality but they are far from a full description of the rock mass. Hence, there is a need for instrumentation and other forms of stability estimation such as modeling to record and process the full spectra of rock mass behavior over varying periods of time and in real-time.

2.3. Assessing tunnel stability through field instrumentation

The various uncertainties inherent in the different geological formations makes it a necessity to instrument tunnels and other underground and surface structures in rock, especially for gathering useful data that could serve as inputs for numerical modeling. Back-analyses, as described in this thesis, is an important application and extension of field monitoring. Sakurai (1997) reviews the different measurement techniques adopted in tunneling to quantify and monitor stability. The review stressed on the need for establishing hazard warning levels, similar to a safety factor, for the instrumentation

based measurements. This would establish an allowable threshold for various values measured from these equipments and alert an operator when the threshold is met or surpassed. For this, the author introduces the concept of critical strain, as calculated using deformation measurements in tunnels, to be used as a proxy for tunnel stability.

The Underground Research Laboratory (URL) in Canada has been home to significant advances and case-studies in rock mechanics for over two decades. Read (2004) documents the monitoring and instrumentation that has gone into the excavation response studies at the URL, which is under medium in-situ stress conditions (15-26 MPa stress fields). The studies conducted in the shafts include installation and monitoring of triaxial strain cells, extensometers, convergence pins, microseismic sensor arrays and hydraulic borehole packers. This was in addition to core logging and Colorado School of Mines (CSM) dilatometer tests (Ladanyi, 1982) for measuring rock mass deformation measurements. Tunnel deformations were measured through convergence arrays, extensometers and micrometers installed through parallel tunnels. Monitoring of stress changes was done through CSIRO Hollow inclusion (HI) triaxial strain cells (Fairhurst, 2003). Instrumentation for hydraulic pressure measurement included pneumatic straddle packers and vibrating-wire piezometers, with thermistors for temperature measurements. Through such extensive monitoring and field observations, the studies managed to document the failure progress in their tunnels, simulate these processes in numerical models and predict possible future failure paths. The microseismic monitoring showed acoustic emissions ahead of tunnel face advance in tunnels with breakouts, and the instrumentations were successful in characterizing the excavation damage zone (EDZ). The author also stresses on the need for numerical modeling as a compliment to the field

instrumentation and of the usefulness of the discrete element method for the case of modeling the URL. Martino and Chandler (2004) explain the usefulness of field instrumentation, specifically for stress and deformation measurements for characterizing the EDZ.

Bizjak and Petkovšek (2004) performed displacement analyses for a highway tunnel in Slovenia through instrumentation such as extensometers and pressure cells, and subsequently modeled the tunnel-support response through numerical modeling. The EDZ in the Mont Terri URL in Switzerland was monitored and characterized for the purpose of assessing the host rock as a waste disposal site through long term monitoring of pore pressures, breakouts and deformations in the microtunnel (Marschall et al., 2006). Other in-situ and laboratory instrumentation focused on the estimation of rock mass strength parameters. Delayed failure at the Messochora tunnel in Greece was analyzed through data gathered on tunnel deformation and accumulated strains in an attempt to better understand the pre- and post-failure behaviors of the tunnel and the reasons for the failure (Kontogianni et al., 2008). Cardarelli et al. (2003) used geophysical methods such as ground penetrating radar, seismic refraction and seismic tomography to evaluate the tunnel stability in a water tunnel where rock fracturing caused landslides.

In summary, monitoring and data acquisition is a useful tool in the process of evaluating tunnel stability, since it can be used as a standalone tool from which significant useful information can be inferred as to the state of the tunnel, and the data gathered can also be gainfully used in numerical modeling exercises. However, much of the data acquisition in tunneling is usually focused on research tunnels, pilot tunnels and shallow tunnels in the context of nuclear waste repositories and civil infrastructure (eg.

Lizhong et al., 2003; Jun et al., 2004; Liu et al., 2007; Gengye et al., 2005) and significantly fewer monitoring routines or monitored data sets are available for mining projects worldwide (eg. Szostak-Chrzanowski et al., 2005). Additionally, since monitoring can only provide the past and present statuses, the trends would have to be extrapolated to predict future behavior. Due to these limitations, it is also important to perform numerical simulation exercises, especially in situations with little monitoring data and for better predicting future trends in the stability of tunnels in complex geologic media.

2.4. Numerical modeling

Discontinuities are planes where a change in physical, mechanical or chemical properties of the rock mass can be observed (Price, 2008). Discontinuities may be fractures, fissures, joints, faults, folds, dykes or bedding planes. While discontinuities are of many types, they generally occur as planes of weakness where the likelihood of fracture is highest, when subjected to a stress. Hence, they are of significance when the stability of an underground excavation is to be estimated. The most commonly observed discontinuity type in underground excavations is a joint or joint set(s) and is usually characterized by parameters such as joint set number, joint orientation, joint spacing, joint frequency, joint size, joint roughness, joint stiffness, joint friction angle etc.

With the advent of powerful computers in tandem with advances in mathematics, several numerical modeling methods have been introduced to compute the stability of excavations. The methods can be broadly categorized as being continuum methods, discontinuum methods or hybrid methods (Elmo, 2006).

In continuum methods, the discontinuities are treated as elements which divide a continuous intact rock. The displacements can be estimated at the nodes but the fact that discontinuities behave differently from the intact rock is discounted. In other words, discontinuities are merely treated as interface elements and their stiffness and frictional properties are not considered. Hence, continuum methods are appropriate when modeling intact rock and highly fractured rock masses (equivalent continuum). The continuum methods are the Boundary Element Method (BEM), the Finite Difference Method (FDM) and the popular Finite Element Method (FEM) which has applications in wide ranging engineering problems.

The discontinuum approach builds upon and eliminates the elementary drawback of continuum methods by explicitly defining joints and assigning properties to them. Discontinuum methods are also known as the Discrete Element Methods (DEMs) as they fundamentally model a rock mass model as an assemblage of rigid or deformable intact rock blocks with explicit discontinuity interfaces separating them. In other words, discontinuum modeling allows the rock fabric to ‘tear’ and rupture, and is typically suitable for rock masses that have large and well defined joints. The popular discontinuum methods employed for modeling rock masses are the Distinct Element Method (DEM) and the Discontinuous Deformation Analysis (DDA).

Since both continuum and discontinuum methods have inherent strengths and weaknesses, researchers have attempted to mix them both to utilize efficiently, the advantages of both continuum and discontinuum methods, thus paving way for the hybrid methods. These relatively new techniques have been discussed in section 2.4.6.

The subsequent sections provide more insight into the common continuum, discontinuum and hybrid methods used in rock mechanics research, and some of the ways in which they have been applied to underground stability analyses.

2.4.1. Boundary Element Method (BEM)

The Boundary Element Method (BEM) solves those partial differential equations (PDE) which have been constructed as boundary integrals. The solution is achieved by fitting the problem's boundary values into the integral to provide approximate solutions.

The BEM has high computation speeds as it reduces the dimensions of the problem domain by one. It has been found to be particularly useful for solving problems in fracture mechanics which involve homogenous and linear elastic media. Ke et al. (2012) perform a 2D fracture mechanics analysis using the BEM and stress on its usefulness for the same. Liu and Li (2014) have performed a comparative study of the BEM and the Discontinuous Displacement Analysis (DDA) where they show that the two methods are equivalent for modeling crack propagation problems. Brady and Bray (1978) first used the BEM for rock mechanics applications, to determine stresses around and deformations undergone by excavations in a triaxial stress field. Prazeres et al. (2010) have used a modified BEM to perform a nonlinear analysis of a New Austrian Tunneling Method (NATM) tunnel construction and they report that the method proved to be computationally faster than and just as effective as the FEM. However, the model is an equivalent continuum and the presence of discontinuities has not been explicitly considered. Beer (2010) illustrated the modifications in BEM using which it can be successfully applied to heterogeneous geologic media, presence of rock reinforcements

such as shotcrete and for simulating sequential excavations. Cheng and Sun (2010) and Fraldi and Guarracino (2011) use the 2-dimensional BEM code Examine2D to carry out their respective analyses of brittle fracturing of rock mass due to an excavation and a study on the failure of a circular elastoplastic tunnel. Wu et al. (2015) performed a BEM study of the stress distribution in a mine roof. In this case, the mine roof was modeled as an assumed elastic medium and the behavior was compared with the results of a FLAC3D FDM simulation. The authors conclude that BEM proved to be a computationally superior method for modeling that specific case of mine tunnel roof. Maerten et al. (2014) use a 3-dimensional BEM code named iBem3D to model rock masses more accurately than was previously possible using the BEM. According to them iBem3D is capable of efficiently simulating discontinuities and fractures in heterogeneous media, without the assumption of elasticity.

2.4.2. Finite Difference Method (FDM)

The Finite Difference Method uses an explicit solution procedure using Lagrangian formulations for solving a system of Partial Differential Equations representing a model. Since the solution scheme is explicit, matrices are never formed. This allows modeling to be computationally efficient. The most popular commercial FDM packages used for rock mass evaluations are FLAC and its 3D counterpart FLAC3D. The FDM has been a popular go-to method for the analysis of slope stability in highly fractured and intact domains, and surface subsidence prediction due to underground structures. Xu et al. (2013) use FLAC3D to predict the surface subsidence in a coal mine and to select a mining scheme which would minimize the subsidence. A FLAC3D based subsidence

analysis for ground deformation caused by metro tunneling in shallow soft soils was undertaken by Chengping et al. (2010). Slope stability analyses for various ground conditions have been performed using the FDM, such as by Singh et al. (2013) for a fire-prone mine in India, by Shen and Karakus (2013) using shear strength reduction techniques, and by Porathur et al. (2013) for Highwall mining. Chen et al. (2011) modeled the stress redistribution and formation of a pressure arch around excavations during tunneling, using the FDM. An estimation of the post-peak strength of marble using a FLAC based simulation of the tri-axial compressive tests, for application to deep tunneling, was performed by Hsiao et al. (2012). Hasanpour (2014) and Hasanpour et al. (2014) simulated double shield TBM tunneling under high in-situ stress fields using FLAC 3D.

2.4.3. Finite Element Method (FEM)

The Finite Element Method was formulated and introduced by Clough (1958) and the name ‘finite elements’ first appeared in Clough (1960), where a plane stress problem was solved using the FEM. The FEM is a set of procedures to discretize a system into a finite number of elements and obtain approximate solutions for continuum based problems (Clough, 1990). Due to its wide ranging applicability, it has found popularity among engineers in all fields of structural, fluid and thermal and electromagnetic analyses. Since the method itself, and the available code packages, can deal with multiple conditions of material heterogeneity and complex boundary conditions in 2D as well as 3D, the FEM has been the most popular method for many years. However, its fundamental premise of continuum assumption is also its fundamental drawback for application in rock

mechanics, as it cannot realistically model the rock mass. Consequently, special joint elements are required to be used to incorporate discontinuities and fractures (Goodman et al., 1968). However, Deb and Das (2009) state that these joint elements cause numerical inconsistencies which seem to depend on the boundary conditions, problem geometry and the accuracy of the computer used, thus opening the doors for further research into developing better joint elements which can do away with these drawbacks. Despite its significant drawback in the context of rock engineering, the FEM is continued to be used in rock mechanics analyses, especially during calculations in intact rock and for highly fractured case studies which can be modeled as equivalent continuum media. Commonly used FEM codes in rock/soil mechanics are PLAXIS and PLAXIS3D, although ANSYS and ABAQUS are also favored by researchers who look to study crack and fracture growth. This is especially appropriate in case of soft rocks where the joints and rock mass have similar stiffness values. An example of this scenario is detailed in Klopčič and Logar (2014) where the authors explore the effect that the orientation of anisotropy planes with the tunnel axis has on the displacements experienced during tunneling. This has been done using PLAXIS3D.

2.4.4. Discrete Element Method (DEM)

The DEM was first introduced in a revolutionary paper published by Cundall (1971), which proposed an algorithm for a computer model which could accurately simulate large displacements in rock masses. This initial method was further developed by Cundall (1988), thus paving way for the DEM modeling software package Universal Distinct Element Code (UDEC) and its 3-dimensional version 3DEC. The DEM models rock

masses as a cluster of blocks which may be rigid or deformable and an explicit solution procedure is employed wherein the joints are modeled as having specific properties. Essentially, the DEM allows the blocks to behave as continuum media and the block and joint interactions are modeled by the Newton's laws of motion. This eliminates the need for a large stiffness matrix unlike in the case of FEM modeling. The superiority of DEM for modeling discontinuous rock masses has been explained by Fairhurst and Pei (1990), where the authors compare the results obtained by an FEM and a UDEC model of an excavation in a joined rock mass. Barla and Barla (2000) also compare the continuum and discontinuum approaches and conclude that, despite its relatively unproven nature at the time of publication, 3DEC and other DEM based packages perform a better job of accurately simulating jointed rock masses. They stress that the only constraint to its widespread use would be the requirement for superior computer hardware. Yuyong and Jian (2004) have successfully employed UDEC and 3DEC to perform a dynamic study on the response of discontinuous rocks to explosions underground. Hao and Azzam (2005) and Vardakos et al. (2007) have performed 2D discontinuum modeling of tunnels in different rock types, using UDEC. A 3D stress analysis using 3DEC, coupled with an equivalent continuum analysis, for a mine tunnel in an underground iron ore mine was performed by Wang et al. (2012), with encouraging results which correlated well with observed field deformations. Kulatilake et al. (2013) investigated the stability of a tunnel in an underground coal mine in China, using 3DEC and field deformation data, where the modeling results were found to be in good agreement with field observations. 3DEC has also been employed to perform a structural stability analysis of theoretical designs of a sculpture in an underground cavern in the Canary Islands (Macklin et al., 2012). This is a

classic example of the usefulness of numerical modeling before the actual commencement of the project as it helped eliminate structurally unsafe designs.

An approach similar to the DEM is the Discrete Fracture Network (DFN) approach which simply models the fracture networks for the purpose of fluid flow and permeability studies. It functions with the inherent assumption that the intact rock is insignificantly permeable when compared with the fractures and hence only the fracture networks are explicitly modeled (Wang et al., 2002; Jing, 2003). While a coupled deployment of DFN and DEM would be attractive for tunnel stability studies in areas with water inrush, the DFN technique has not seen widespread usage in the underground mining sector.

2.4.5. Discontinuous Deformation Analysis (DDA)

The DDA is a Discrete Element Method which was originally published by Shi and Goodman (1985) and further refined by Goodman and Shi (1988) and Shi (1992). It is essentially a method used to simulate and study the blocky rock masses. It can be used to model large displacements and block failure in deformable systems. The method, similar to the FEM, is derived using the principle of minimum potential energy. This is the fundamental difference between the DDA, which uses implicit energy based solution schemes, and the DEM code which uses explicit force based procedures. Wu et al. (2005) most recently proposed a code for 3D DDA analysis and demonstrated its usefulness for analyzing a rock slope's stability against toppling in Japan.

According to MacLaughlin and Doolin (2006), the DDA has been popularly used by rock mechanics experts for analysis of rock structure stability, especially in cases of slope and dam stability, and for underground caverns. Much study on the seismic response of

slopes, using DDA, has been observed in literature, such as those by Irie et al. (2009), Wu (2010), Wu and Chen (2011), Wu et al. (2011), Cai et al. (2013) and Zhang et al. (2013a). Shi (2014) has also used the DDA for the stability analysis of underground caverns, in addition to the stability of slopes, using 2D DDA and a simplified 3D DDA (only slope stability). Its usefulness for the analysis of toppling of slopes has been stressed upon by Shi (2007). Jian-ping et al. (2011) modified the original DDA code to include the potential energy due to rock bolts for optimizing the support requirements for the large deformations observed in a mine tunnel. The primary arguments in favor of the use of DDA, as put forth by Cheng (1998), are that the DEM method requires artificial springs to absorb the energy generated, to achieve equilibrium, and that the explicit time marching algorithm used by the DEM can cause numerical instability if very small time steps are not used. In addition, due to its non-commercialization, DDA is available as a freeware. In contrast, the DDA has a multitude of drawbacks of its own. Scheldt (2002) discovered that, if a model geometry is such that there is a large ratio between rock blocks, or if joints have nearly zero angle between them, the computation fails. Also, stresses within a block are assumed to be constant, blocks cannot undergo fracture, pore pressure has not been considered and the post-processing capabilities of the available DDA code is limited, as opposed to a wide variety of options available in the UDEC/3DEC code for DEM. An important limitation of the DDA, which has been repetitive throughout literature, is the problem of numerical truncation and loss of significant effective digits (Ma, 1999; Zhao et al., 2011; Ohnishi et al., 2014). Hence, while the DDA essentially guarantees numerical stability, it may not necessarily provide accuracy.

2.4.6. Hybrid methods

While there is no well-defined definition of a hybrid method or code, any code which employs two or more of the continuum and discontinuum methods in any combination can essentially be classified as a hybrid method. The Particle Manifold Method (PMM) (Sun et al., 2013) and Numerical Manifold Method (NMM) (Zheng et al., 2014) are two commonly implemented continuum-discontinuum numerical modeling methods. Two of the popular hybrid codes incorporating FEM/DEM, used for rock mass simulations, are ELFEN (Rockfield, 2011) and YGeo (Mahabadi et al., 2012). Munjiza et al. (1995) elucidated on the inherent issues in computing power which could be a deterrent for the FEM/DEM methods from gaining popularity. Progressive failure in rock slopes was modeled using a 2D hybrid FEM/DEM approach by Eberhardt et al. (2003). Elmo (2006) used the ELFEN code to determine the strength of a fractured rock mass. The modeling was further carried out on a 3D version of ELFEN. While the author reports satisfactory results, it has also been stressed that the code is still in development and multiple aspects of rock mass modeling are, as yet, not available in the code, such as ability to incorporate fluid pressures and tunneling in stages. The author stresses on the need for more efficient algorithms and to use the parallel processing capabilities of modern computers. However, recent versions of Elfen have been used to study fractured rock pillars in a limestone mine and surface subsidence due to block caving (Elmo and Stead 2010; Vyazmensky et al. 2010). Elmo et al. (2013) and Hamdi et al. (2014) use ELFEN to model further fractures in laboratory testing of specimens. Lisjak et al. (2014) present a 2D FEM/DEM analysis exploring the failure mechanisms of unsupported circular tunnels in clay shales.

2.4.7. Summary

A detailed analysis of the advantages and drawbacks of different numerical methods is tabulated in Coggan et al. (2012) and reproduced in Table 2.1. The authors also perform a comparative study between the results of ELFEN and UDEC in simulating the roof behavior of an underground coal mine roadway. In addition, they state that much of the existing work on numerical modeling of roof stability in coal mines have been performed without providing sufficient attention to the existence of fractures in intact rock. Jing (2003) and Lisjak and Grasselli (2014) have carried out a detailed literature review of the different DEM and hybrid FEM/DEM methods that have recently been fruitfully used in the realm of rock mass stability. Lisjak and Grasselli (2014) note that the hybrid FEM/DEM is not the same as a coupled continuum-discontinuum approach suggested by Pan and Reed (1991).

Table 2.1: Different numerical computational methods with their known advantages and drawbacks (Reproduced from Coggan et al., 2012)

Analysis method	Input assumptions	Advantages	Limitations
Continuum: Boundary element	Representative tunnel geometry, usually adopt simple constitutive criteria	Elastic analysis, capability of three-dimensional modelling, rapid assessment of designs and stress concentrations	Normally elastic analysis only, (non-linear and time dependent options are available.)
Continuum: Finite-element and finite-difference	Representative tunnel geometry, wide range of constitutive criteria, including weakness plane, groundwater, shear strength/stiffness of discrete interfaces, in-situ stress, support properties	Allow for material deformation and failure, can model complex behaviour, capability of three-dimensional modelling, able to assess simulate both saturated and unsaturated (multiphase) flow/water pressures, recent advances in hardware mean that complicated models can now be PC-based and run in reasonable time periods, can incorporate coupled dynamic/groundwater analysis, suitable for soil, rock or mixed soil rock analysis, time dependent deformation readily simulated	Must be aware of model/software limitations including effects of mesh size, boundaries, symmetry and hardware restrictions (i.e. memory and time constraints) and data input limitations (such as effects of variation of critical input parameters etc.); simple structures can be simulated with interfaces, but not suitable for highly jointed-blocky media; well trained and experience users and familiarity with numerical analysis methods essential; validation through surface/subsurface instrumentation important
Discontinuum: Discrete element	Representative tunnel and discontinuity	Able to model complex behaviour; including both block deformation and	As above. Scale effects: simulate representative discontinuity

Analysis method	Input assumptions	Advantages	Limitations
	geometry, rock mass constitutive criteria, discontinuity shear strength and stiffness, groundwater, in-situ stress, support properties	relative movement of blocks (translation/rotation); three-dimensional models possible; effect of parameter variations on instability can be investigated easily; dynamic loading, creep and groundwater simulated; can incorporate synthetic rock masses to represent the fracture network; use of Voronoi polygonal blocks allows simulation of rock fracture between blocks	geometry (spacing, persistence); limited data on joint stiffness available; predominantly used for jointed rock; validation through surface/subsurface instrumentation important
Hybrid codes incorporating intact rock fracture capability (finite–discrete element)	As above. Use fracture mechanics criteria or particle flow code (parallel/shear bonds) to simulate intact rock fracture	Able to allow for extension of existing fractures and creation of new fractures through intact rock, capable of three-dimensional modelling (although limited application to-date), can incorporate dynamic effects	Limited use and validation, state-of-the art codes requiring in-depth knowledge/experience of modelling methods/mechanics, must incorporate realistic rock fracture network, little data available for contact properties and fracture mechanics properties, limited capability to simulate effects of groundwater, extremely long run times will require use of parallel processing for large models

In conclusion, while FEM principles can only be applied to rock masses in specific cases of continua or equivalent continuum assumptions (Fig. 2.1), it is tempting to explore the new FEM/DEM techniques which are suggestive of good results.

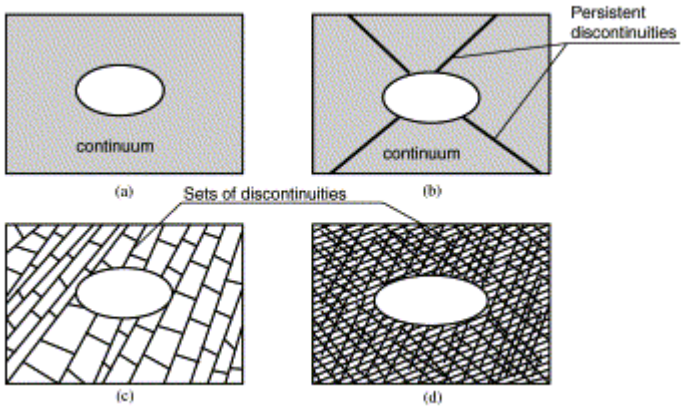

Figure 2.1: Typical rock masses which can be suitably modeled using (a) Continuum techniques (b) Discontinuum or continuum mechanics (c) Discrete methods (d) Continuum methods as an equivalent continuum (Source: Jing, 2003)

However, the hybrid techniques may be used cautiously. In theory, these techniques exist as a means to eliminate the inherent drawbacks of the various individual methods. Since the hybrid methods implemented as numerical modeling codes are relatively new and not as established or popular as the FEM or DEM codes, they may not have all the toolkits required for geomechanical modeling of excavations. This includes features such as prior extensive validation, support definitions, explicit rock-support interactions, capacity to model complex block or excavation geometries in three dimensions and the ability to manipulate data structures at the source (as opposed to a Graphical User Interface scheme).

While none of the methods can be said to be absolutely perfect or flawed (Jing, 2003), the choice of a numerical method rests with the researcher, and may be dependent on numerous factors which may be functions of the case at hand and the resources available at the researcher's disposal. Numerical modeling is a powerful toolkit in rock mechanics and can serve as a useful assistant at the design phase and as an important redundancy – as a risk assessment mechanism, during the life of a project.

2.5. Prior studies on stability of deep excavations in soft rock

Since 'deep' can be very subjective depending on the country of use, for the purpose of this thesis, deep mining refers to mining at depths exceeding 800 m. The presence of roadways, tunnels and shafts at such depths pose unique geotechnical challenges. Typically, higher humidity, water inrush, tectonic activities, rockbursts, gas explosions and significantly higher horizontal in-situ stresses, as compared to vertical stresses are some of the common problems that have to be dealt with while studying deep coal mines, as each of these may prove to be life threatening at various levels. The stability of deep mine roadways is of special interest as they are prone to roof falls and floor heaves at such high confining pressures and in the presence of discontinuities in the soft strata. Deep coal seams being operated for CO_2 sequestration have not been included in the discussion as they do not have significant safety threats associated with them, since miners do not physically works in such seams.

The popular AlpTransit system in Switzerland, of tunnel lengths running at up to 57 km, has overburden stresses equivalent to up to 2500 m. Vogel and Rast (2000) write about the safety considerations including stability of the tunneling in fractured rocks,

temperature and ventilation being some of the prime safety and stability factors. Schweitzer and Johnson (1997) comment on the geotechnical classification of the deep mining areas in South Africa, drawing attention to the gold mines driven at depths exceeding 3500 m. At these depths, rock bursts have been found to have exaggerated effects, as do seismicity and mining induced fracturing. The authors stress on the need for better understanding of the behavior of excavations at great depths through improved numerical modeling studies. Cichowicz et al. (2000) and Guler et al. (2000) study the rock mass stability in deep gold mines in South Africa placing impetus on seismicity and stope supports respectively.

In terms of sheer numbers of deep coal mines, China leads the world by a distance. Simultaneously, significant research efforts aimed at better characterizing deep tunneling has been seen out of China. For instance, He et al. (2005) and He (2006) review the existing methodologies and common instrumentation techniques in deep mining in China, and comment on the validity, or lack thereof, of using classical rock mechanics in soft, squeezing strata subjected to high stresses. Most research conducted by scholars has been practical in nature, with immediate and tangible results.

Wang et al. (2006) attempt to define deep rock engineering and discuss the mechanism of zonal disintegration in the rock mass around excavations in deep tunnels (> 1000 m) through the analysis of stress state, tunnel deformation and rock mass failures at different stages of tunnel advance. They also observe the post-peak behavior of the rock mass and look at its residual mechanical parameters. Based on this, they propose empirical cutoffs to classify excavations as shallow or deep within a Chinese context. Zhou and Qian (2007) argue that tunneling at depth is a dynamic problem. They approach the tunnel

stability issue by coupling strain localization, support interactions and fracture mechanics theories to estimate failure onset and residual behaviors. They reported that the size and quality of the fractured zone is a direct function of the tunnel advance rate and inversely related to the rock mass strength. Sun et al. (2011) treat the tunnel stability problem as a dynamic problem and attempt to establish the physics behind the rock mass instability. They propose analytical solutions for the time-history based tunnel response during the excavation of deep tunnels.

Yang et al. (2007) and Chen et al. (2012b) apply microseismics to monitor the state of stability in a deep copper mine and a hydropower project respectively. They find strong correlations between rock bursts and acoustic emissions and fracturing, and show that microseismic monitoring systems in deep mines can be a significant part of hazard prediction systems. Yaodong et al. (2004) study floor heaving in a deep coal mine through field investigations and physical modeling, and identify four unique classes of floor heaves through case studies in China. Zhang et al. (2009a) and Wu et al. (2011), through field observations introduce indices and classification systems for supports in roadways and failure modes of the roadway walls for deep mining in different mines. Zhang et al. (2009b) introduces the high strength, high pretension and high stiffness philosophy for deep roadway bolting, which has since been adopted in the Huainan coal mining district. Wu et al. (2011) divide roadway failure into three categories and identify nine unique failure modes and further go on to provide guidelines to prevent or localize these failures. Ma et al. (2008) perform experiments to study clays under high stresses typical of deep mining scenarios. Specifically, they look at the unloading behavior of the clays and study the lateral earth pressure coefficients that would evolve during this

scenario. They show that the behavior of clays is dependent on the unloading path taken. Wang et al. (2008) perform laboratory and field pilot tests to introduce steel fiber reinforced concrete as a support for deep excavations and show that it can withstand the large deformations typical of deep structures.

Extensive numerical modeling has also been performed to understand the behavior of deep excavations in China. Fault activation in the floor of a deep coal mine and the associated implications were studied by Wang and Miao (2006) using FEM. Xiao-Guang and Xiao-Hong (2007) modeled the stress fields in a deep tunnel in three dimensions, using accurate measurements of in-situ stress values and stress orientations. Gao and Kang (2008) study the effect of pre-tensioned bolts in on the stress redistributions in a roadway modeled as a continuum using the FDM. They studied models with different support patterns and unsupported cases and found that the introduction of pre-tensioning increased rock mass strength and capacity for load bearing on the roof and walls of the tunnel. Sun et al. (2009) used a coupling methodology to integrate the effects of bolting, meshing and anchoring in their FDM numerical model of a deep tunnel. They compared their model results with field observations to find good agreements with the modeling procedures. They stress on the need for introducing the bolt/support at an optimum time during tunnel excavation so as to optimize the best coupling effect. Zhang et al. (2009b) studied zonal disintegrations in a deep tunnel in the Huainan mining district through three dimensional modeling, and established failure laws for zonal disintegration and non-linear deformations. Zhou et al. (2009) analyzed tunnel stability for a hydropower project through the use of a Mohr-Coulomb elastoplastic and a strain-softening model. They discovered that the walls of the tunnels in the main cavern and junctions or tunnel

crossings undergo significant plastic strains and recommend support frameworks to adequately protect these structures.

2.6. Summary

This chapter reviews literature pertinent to numerical modeling of stability in deep tunneling. Commonly used tunnel stability evaluation techniques have been introduced with an attempt to objectively evaluate their strengths and weaknesses. The state of the art in rock mechanics research related to deep excavations in soft rock, with a focus on deep tunneling in coal-measure strata in China is also discussed in some detail. Based on available monitoring data and geomechanical data for the intact rock and discontinuities, the 3-D DEM has been selected as an appropriate methodology for the current study. This is due to the partial availability of joint data which calls for a mixed stability evaluation, incorporating concepts of discontinuum and continuum modeling for which the DEM is appropriate. Subsequent chapters will introduce the reader to the mine site and the numerical code used for the DEM analyses.

CHAPTER 3: INTRODUCTION TO THE SITE

3.1. Introduction

The mining site in China, on which the case study discussed in this thesis is based, is introduced in this chapter. Some of the geological and geomechanical features of the region are discussed.

The Xiezhuang coal mine, located in the Xinwen coal mining area (Fig. 3.1) is one of the deepest coal mines in China, with average excavation depths of 1000 m and the deepest tunnels running at 1400 m. Due to the great depth and development of high tectonic stresses, this mine is one of the most hazard prone mining operations in China, with the main hazards being related to ground control and thermal issues (Kang et al., 2010; Yuan et al., 2010).

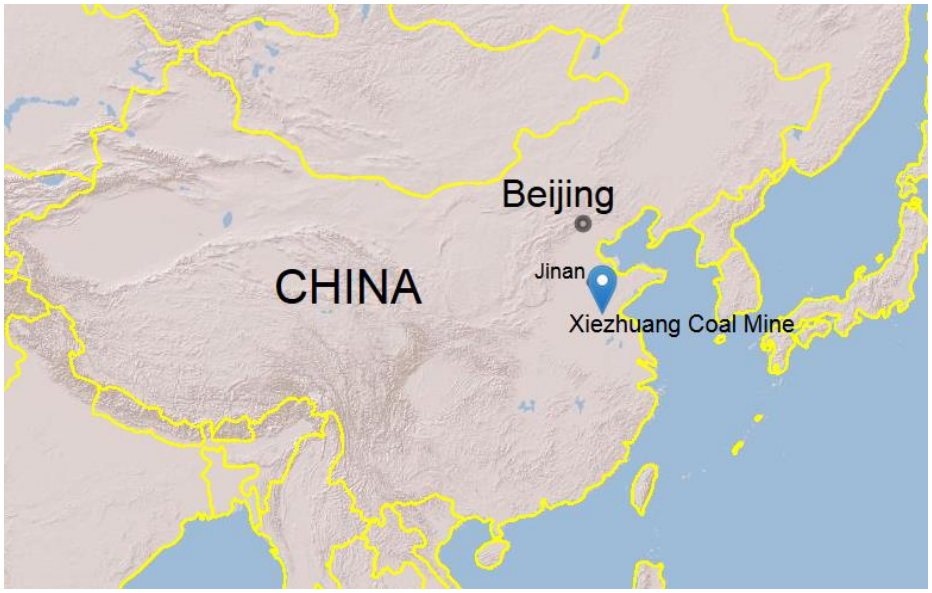

Figure 3.1: Geographic location of the Xiezhuang coal mine in China

3.2. In-situ stress measurements

In-situ stress measurements were undertaken by the Xinwen mining group for their various mining districts in collaboration with China University of Mining and Technology (Zhang et al., 2013b). Based on data reported by University of Science and Technology Beijing (USTB) in connection with this thesis, in-situ stress measurements for the Xiezhuang coal mine have been compiled and given in Table 3.1.

Table 3.1: In-situ stress measurements for the Xiezhuang coal mine

Depth (m)	Vertical stress (MPa)	Maximum horizontal principal stress (MPa)	Minimum horizontal principal stress (MPa)	Direction of maximum horizontal principal stress (MPa)
790	20.9	32.4	16.6	N33.5^{o}E
1071	28.4	39.8	20.6	N39.7^{o}E
1150	30.5	34.6	17.9	N12.5^{o}E

These values are consistent with another survey conducted by Kang et al. (2010). As can be seen from the values in Table 3.1, the vertical stress values are approximately consistent with the expected vertical stress gradient. However, the horizontal stress measurements are skewed in that there is a stress drop at 1150 m for the maximum and minimum horizontal principal stresses. This, based on communications with the mine and USTB, has been attributed to the presence of faults in this region due to which a stress relaxation may have occurred (for further reading on the tectonic stress states in northern China, the reader is referred to Xie et al., 2009 and Jing et al., 2013).

In an attempt to gather more in-situ stress measurements from this region, the World Stress Map Project (Zoback, 1992) was used to determine whether the mining region contains any useful information regarding the state of stress. The result of this approach is shown in Fig. 3.2 and indicates that the few stress measurements available from the region are of low-quality (C and D quality) from very shallow depths. Hence, the three available stress values were interpolated to estimate the stresses at 1300 m, as shown in Fig. 3.3. The figure shows a plot of the vertical section with stress variations expressed as a function of depth. It was decided to estimate the stresses without considering the stress measurement at 1150 m due to a two-fold consideration: (1) since the stress at 1071 m follows the expected stress gradient and a stress relaxation has occurred within a depth/distance of 80 m from this location (at 1150 m), the stress regime should readjust and stresses should start following the gradient within 80 m from 1150 m, i.e., by 1230 m. (2) In case the strength is not fully regained as hypothesized in (1), the analyses performed using values estimated from the first two points would be adequately conservative from an engineering standpoint.

Based on the vertical stress gradient, an average rock density of 2700 kg/m^3 was found to be appropriate for this site and the vertical stress at 1300 m was calculated to be 34.5 MPa according to equation 3.1. The lateral stress ratios as defined in equations 3.2 and 3.3 were used to calculate the two horizontal principal stresses.

$$\sigma_v = 0.0027\ gh\ (MPa) \tag{3.1}$$

Where,

g is the acceleration due to gravity (m/s^2)

h is the depth at which the vertical stress, σ_v, is being calculated (m)

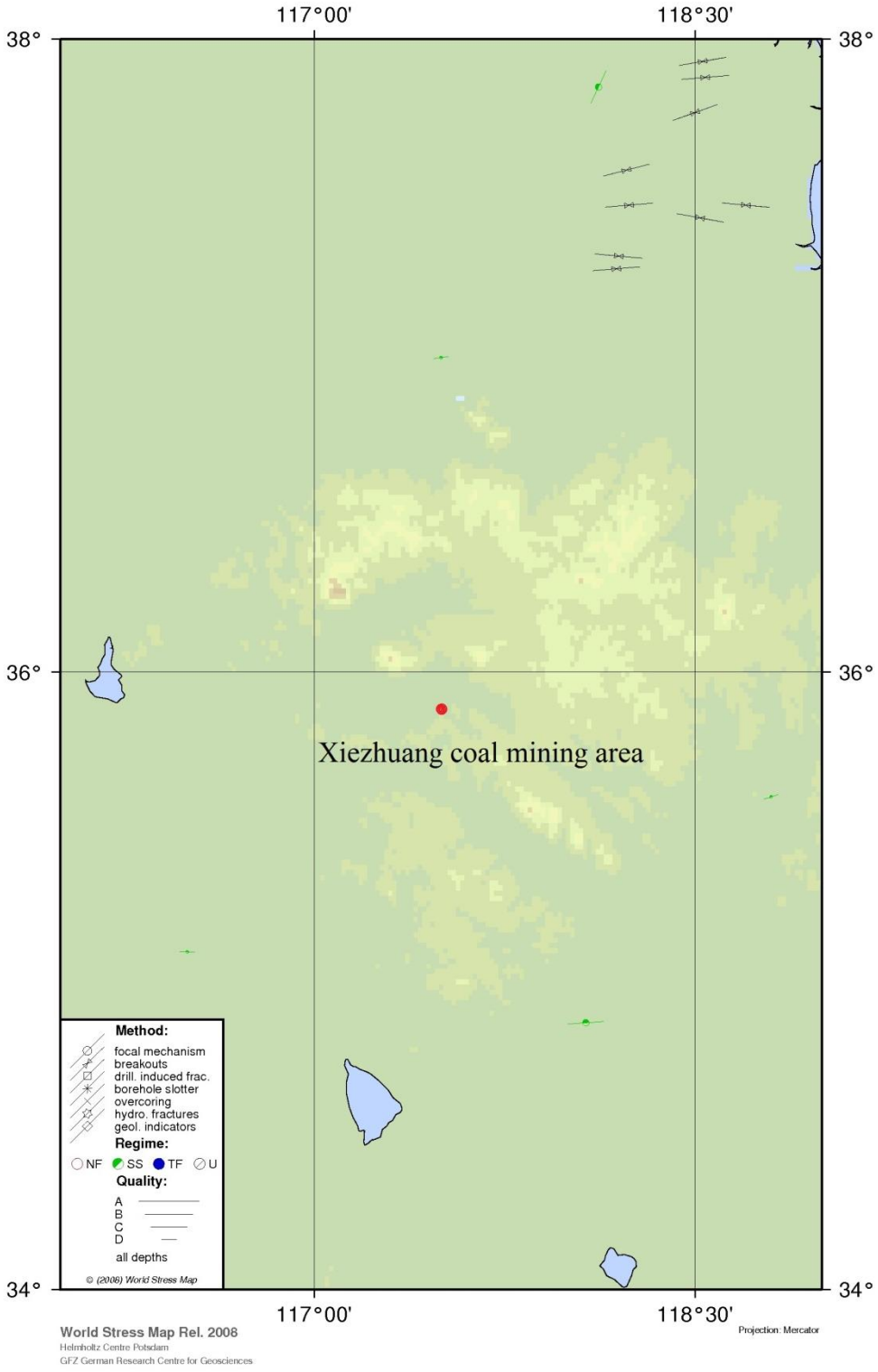

Figure 3.2: Regional tectonic stresses as available from the World Stress Map Project (Heidbach et al., 2008)

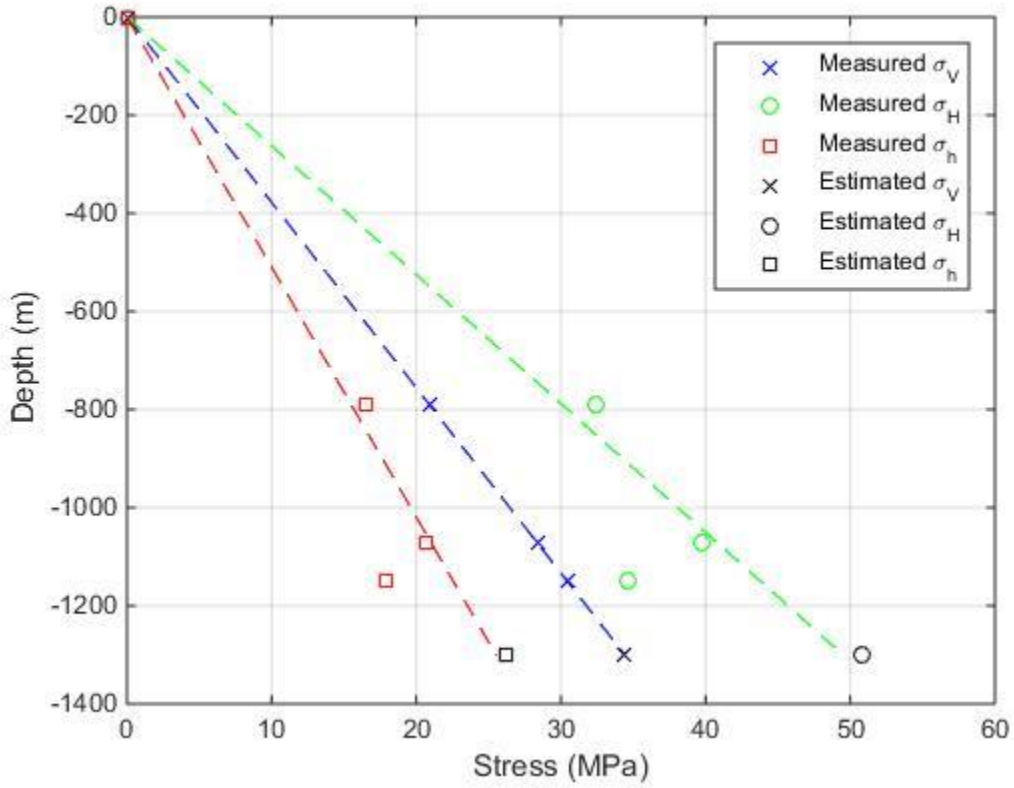

Figure 3.3: A plot of in-situ stress variations as a function of depth (σ_V – Vertical principal stress, σ_H – Maximum horizontal principal stress σ_h – Minimum horizontal principal stress)

$$K_{01} = \frac{\sigma_H}{\sigma_v} \tag{3.2}$$

$$K_{02} = \frac{\sigma_h}{\sigma_v} \tag{3.3}$$

Based on the stress ratios defined in equations 3.2 and 3.3, the maximum and minimum horizontal principal stresses, σ_H and σ_h, have been estimated to be 50.8 MPa and 26.2 MPa respectively.

3.3. Geological background

A comprehensive discussion of the structure and geological conditions which encouraged the formation of the coal in the Xinwen mining area has been discussed by Lu (2005). The Xinwen coalfields are located on the west side of the Mengyin trough in the Shandong province, with an east-west length of 30 km and north-south length of 10 km. Southern parts of the Xinwen coalfields have Carboniferous and Permian coal outcrops and contain high production mining facilities, with a total coal thickness of 248 m. The strata of the Mengyin formation formed in the upper Jurassic and Guanzhuang formation from the lower tertiary have a high thickness, unconformably overlying on Paleozoic lithology. Primary constituents include light red and brick red sandy mudstones, fine sandstones and conglomerates, collectively referred to as the red layer. The Jurassic formations are called the old red layer, while the lower tertiary stratum is referred to as the new red layer. The Carboniferous and Permian coal is thought to have been formed under isostatic conditions of shock, thus leading to the formation of a giant coal basin. Frequent and severe crustal movements in the Mesozoic and Cenozoic periods, along with erosion are thought to have separated this basin, thus scattering it throughout Shandong province. The Lotus Mountain fault is the most prominent, in addition to multiple minor faults in this region.

The region around the tunnels contains lithological units consisting of sandstone, coal and sandy-shales. Specifically around the tunnel systems, four different units have been identified, in increasing order of strengths as Coal, Sandy Shale #1, Sandy Shale #2 and Sandstone. The tunnels in the Xiezhuang mine are 57 m long and driven at a depth of about 1325 m in a soft sandy-shale stratum, Sandy-Shale #2. Based on primary

communications with USTB and secondary communications with the mine, intact rock mechanical property values for the lithological units around the tunnels as used in the numerical modeling experiments are given in Table 3.2. These values agree well with published literature on intact rock properties in this mine at depths greater than 1000 m (Kang et al., 2010; Kang, 2014; Wang et al., 2010; Zhang et al., 2013b). The primary joint set around the tunnel is a horizontal/near-horizontal bedding plane spaced at 1 m and running through the weak Sandy Shale #2 stratum.

Table 3.2: Physical and mechanical property values of the different intact rock types around the tunnel

Layer	Density (kg/m^3)	Elastic Modulus (GPa)	Poisson's Ratio	Cohesion (MPa)	Internal Friction Angle	Tensile Strength (MPa)	Uniaxial Compressive Strength (MPa)
Fine Sandstone (FS)	2670	35.6	0.17	28.0	36.5	7.0	111.6
Sandy Shale #1 (SS1)	2660	26.5	0.29	16.0	32.0	3.8	57.5
Sandy Shale #2 (SS2)	2500	25.4	0.32	13.0	27.0	3.2	49.0
Coal (C)	1392	3.0	0.36	2.8	24.0	1.0	8.5

3.4. Tunnel and support data

The two tunnels analyzed in the studies presented in this thesis are the conventional horseshoe shaped and an inverted arch shaped tunnel, as shown in Fig. 3.4 (a) and (b). The tunnels have the same width of 3.8 m, with the horseshoe tunnel having a height of 3.5 m and the inverted arch tunnel with a height of 4.5 m. The inverted-arch tunnel is approximately 30% larger by cross-sectional area.

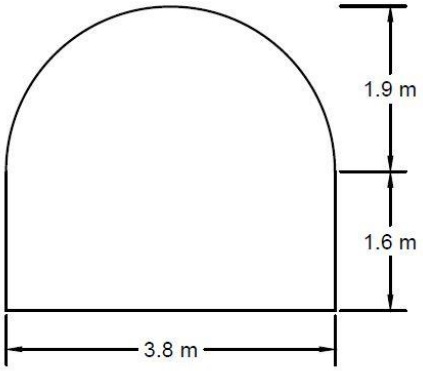

(a)

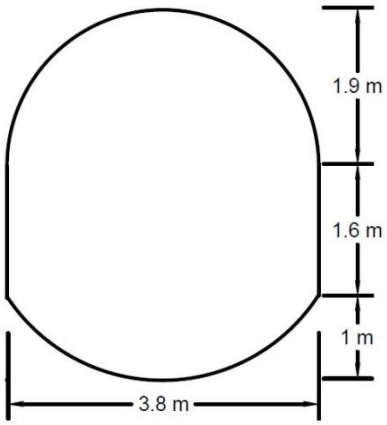

(b)

Figure 3.4: Dimensions of the (a) Horseshoe tunnel and (b) the inverted arch tunnel at the mine

A typical supported profile in the tunnels in the Xinwen mining district is given in Fig. 3.5. The supporting framework includes the use of rigid or cable bolts and wire mesh to protect against rock falls. Fig. 3.6 presents the status of failed and broken rock bolts from the mine, primarily due to the high in-situ stresses.

Figure 3.5: Profile of the main-gate including the rock bolts and wire mesh in a mine within the Xinwen mining area

Figure 3.6: Failed rock bolts used at depths greater than 1000 m in the Xinwen mining area

The bolts used in the tunnels being studied are two different steel cable bolts with mechanical specifications as listed in Table 3.3.

Table 3.3: Mechanical property values of supports in the mine

	First support	Second support
Young's Modulus of bolt (GPa)	98	98
Cable diameter (mm)	15.7	18.3
Cable cross-sectional area (mm^2)	193.5	262.9
Tensile yield capacity of bolt (MN)	0.28	0.35
Grout cohesive capacity per unit length (MN/m)	0.9	1.04
Grout stiffness per unit length (MN/m/m)	18674	19057

The tunnels are bolted on the roof and ribs but not on the floor. The inter-bolt spacing for each cable type, both in-plane and out-of-plane, is fixed at 0.8 m. The first support has a length of 2.2 m and the second support has a length of 2.5 m. The supports are installed in a staggered pattern and normal to the tunnel surface (except at edges/corners) as shown in Fig. 3.7 (a) and (b).

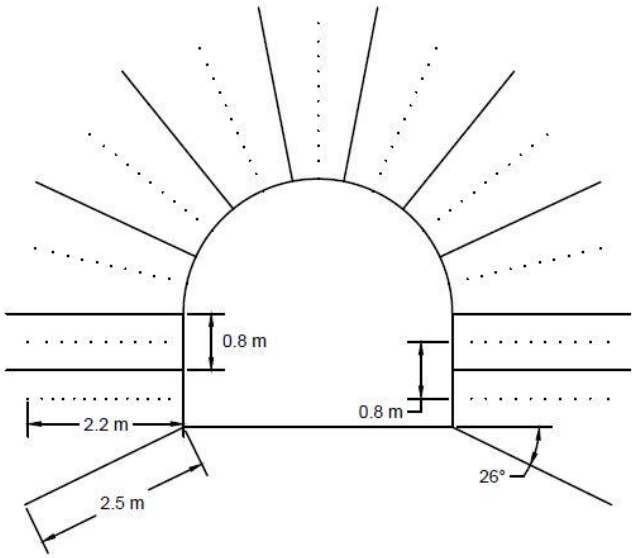

(a)

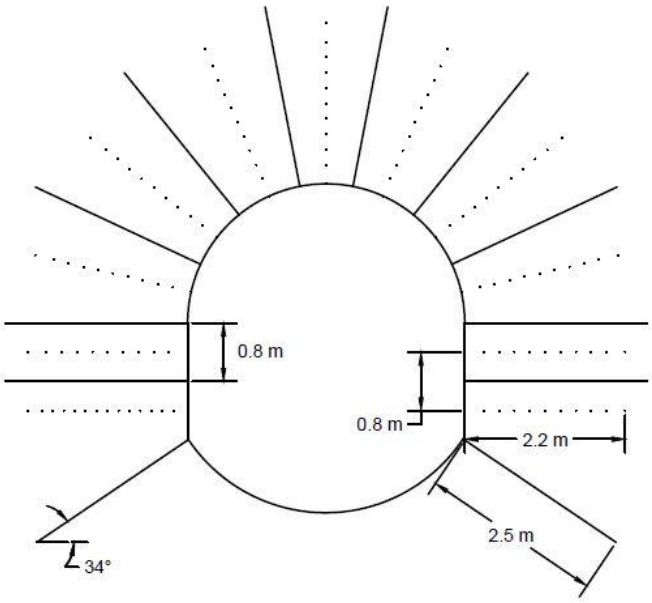

(b)

Figure 3.7: Dimensions and orientation of the roof and wall bolting in the (a) Horseshoe tunnel and (b) Inverted arch tunnel (Dotted lines-First support; Solid lines-Second support)

3.5. Tunnel deformation measurements

Tunnel deformation measurements at the two tunnels measured over a period of 350 days have been presented in Fig. 3.8 (a) and (b) as time series trends. Table 3.4 shows the final deformations used for the calibrations performed in this study. The deformations have been measured using tape extensometers at the mine at a halfway distance along the tunnel length for the two tunnels, on the roof, floor and wall. Wall deformations reported in this thesis are averaged to represent each wall's deformation. Raw deformation data used for generating the time series trends are presented in Appendix A.

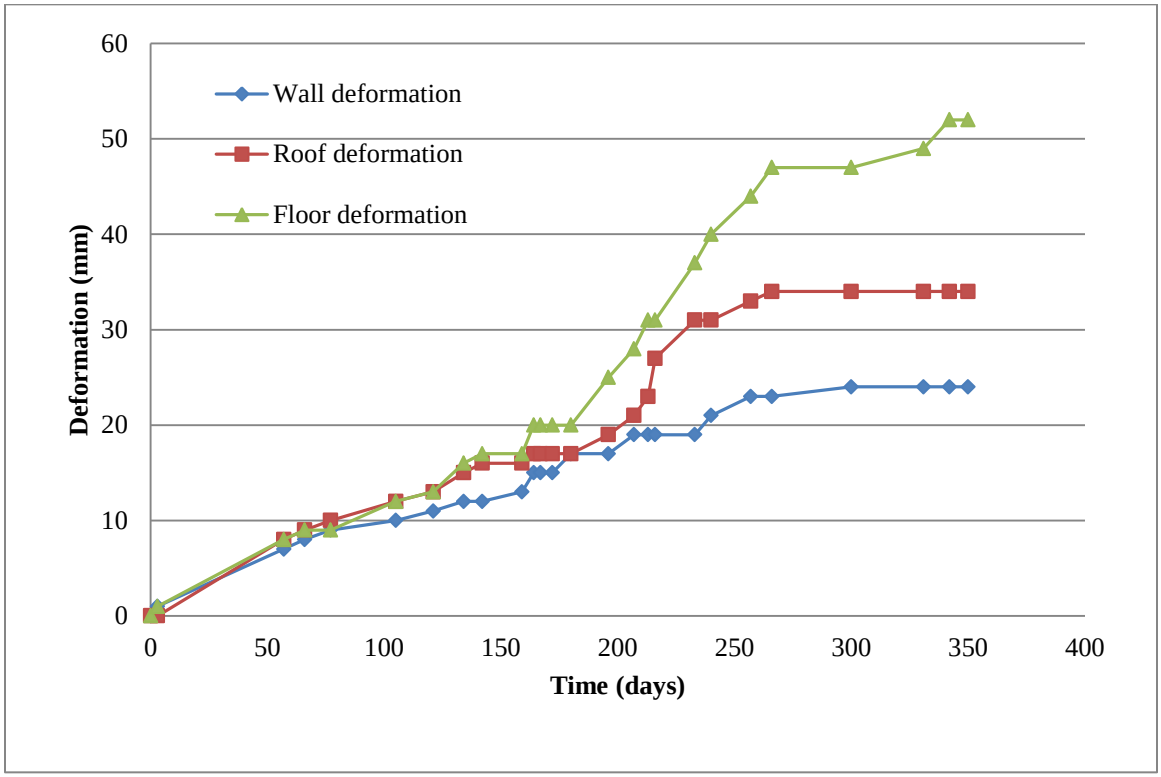

(a)

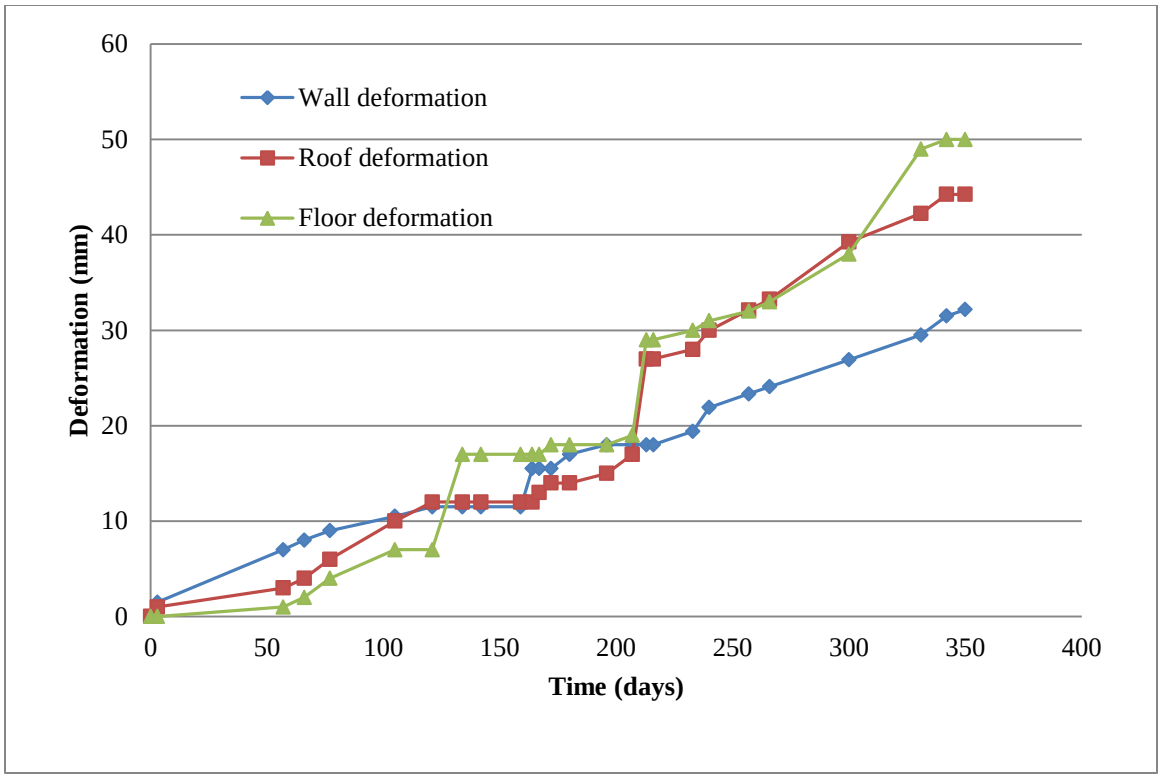

(b)

Figure 3.8: Deformations in the (a) Horseshoe and (b) Inverted-arch tunnel over a period of 350 days

Table 3.4: Deformation data at the monitoring point in the mine

Tunnel type	Roof (mm)	Wall (mm)	Floor (mm)
Horseshoe	34	24	52
Inverted arch	44	32	50

CHAPTER 4: NUMERICAL MODELING USING THE DISCRETE ELEMENT METHOD

4.1. Introduction

This chapter introduces numerical modeling using the discrete element method, in the 3DEC distinct element method environment (Itasca, 2008). The different theoretical aspects of rock block deformation, inter-block interactions and rock-support interactions with relevant mathematical and physical formulations are discussed in addition to some of the successful practical applications of the distinct element method.

Cundall and Hart (1992) define a discrete element method as one which allows for displacements, rotations and complete detachment (if applicable) of discrete bodies, and is capable of automatically recognizing new contacts as calculations progress. The distinct element method (usually used interchangeably with the term 'discrete element method' in literature) is a subset of the discrete element method, and uses explicit time-marching to solve equations of motion rather than through the formation of large matrices. While bodies may be rigid or deformable in the distinct element method, contacts are usually deformable. The subsequent sections discuss the numerical formulations in the 3DEC distinct element code.

4.2. Contact detection in 3DEC

A block's geometry can be described by vertices, edges and faces. To test for contact between any two blocks, all possible combinations (*n*) of edges (*e*), vertices (*v*) and faces (*f*) between two blocks A and B can be tested as in equation 4.1.

$$n = (v_A + e_A + f_A)(v_B + e_B + f_B) \tag{4.1}$$

However, such a brute force detection algorithm could prove to be excessively inefficient in complicated block geometries such as those required for the simulation of geologic structures. In 3DEC, a 'common plane' technique is used to reduce the number of iterations required to detect the presence and type of contacts between blocks. Here, a common plane is defined between any two blocks such that it takes up a position halfway between the blocks, at the maximum distance from both blocks, at an orientation defined by the sliding plane for the blocks. In this case, only a 'vertex to common plane test' is required to be carried out to determine whether (and how) the two blocks contact each other. This substantially reduces the number of tests (*n*) to

$$n = v_A + v_B \tag{4.2}$$

If the blocks are in contact with each other in any way, the common plane would have to touch both blocks, by definition. Alternately, if the blocks are not in contact, the common plane would not be touching either block. The common plane determination algorithm is simply to minimize the overlap (or maximize the distance) between the common plane and closest vertex. Fig. 4.1 shows some examples of the common plane (denoted as c-p) between blocks. The vertex-common plane contact detection is sufficient since edges are resolved as the contact of two vertices with the common plane and a face can be resolved

as the contact of more than two vertices with the common plane, for any given block. Face to face contacts are described as joints/discontinuities.

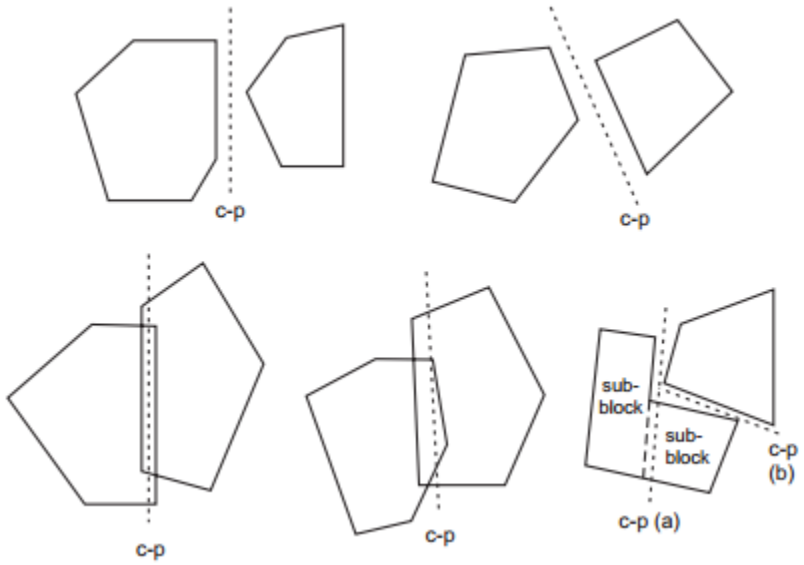

Figure 4.1: Common planes between blocks for different scenarios (Reproduced from Itasca, 2008)

4.3. Motion and interaction physics

This section describes the motion and interaction physics for blocks and the calculation cycles. This is based on work carried out by Cundall and Strack (1979) and Cundall and Hart (1985). Subsequent sections describe the internal calculation cycle, joint model (inter-block interaction physics), deformable block motion, discretization procedure and support physics. Rigid block motion formulations are not included in this chapter since the studies outlined in this work make use of fully deformable blocks.

4.3.1. Internal calculation cycle

The solution scheme in the distinct element method is an explicit finite difference based time-marching procedure that solves for equations of motion and block/joint constitutive equations at each time-step/cycle. This provides new block gridpoint positions and velocities, which are then used to determine sub-contact forces, which are subsequently applied to the whole block. This cycle is depicted in Fig. 4.2.

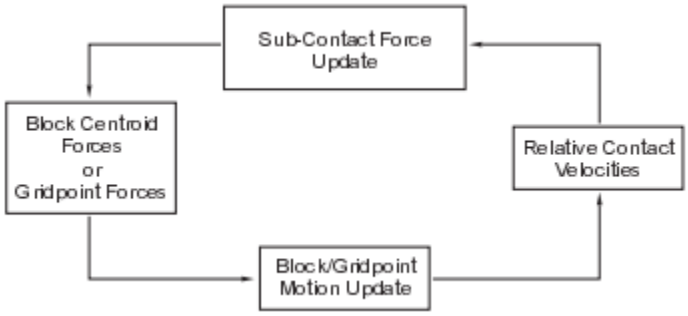

Figure 4.2: The calculation cycle in the distinct element method

4.3.2. Coulomb slip joint model

The Coulomb slip joint model is a constitutive law describing joint behavior as dictated by the Coulomb friction law. The spectrum of joint deformation includes elastic shear and normal deformations, as prescribed by shear and normal stiffnesses (Equations 4.3 and 4.4), and shear and tensile failure. Joint dilation is not considered for the scope of the current study.

$$\Delta F^n = -K_n \Delta U^n A_c \tag{4.3}$$

$$\Delta F^s = -K_s \Delta U^s A_c \tag{4.4}$$

Where ΔF^n and ΔF^s are the normal and shear force increments, K_n and K_s are the normal and shear stiffnesses across the discontinuity, ΔU^n and ΔU^s are the normal and

shear incremental deformation vectors, and A_c is the contact area. Equations 4.3 and 4.4 govern discontinuity movements in the elastic region, and the strength criterion defined in equation 4.5 governs the joint failure.

$$F^s_{max} = F^n \tan \varphi \tag{4.5}$$

$F^s{}_{max}$ is the maximum allowed shear force, and is determined by the Coulomb friction law as the product of the normal force across the joint, F^n, and the joint friction angle (φ). The contact forces are updated differently for tensile and shear failures as dictated by equations 4.6 and 4.7 respectively.

$$If\ |F^n| > |T_{max}|, then\ F^n = 0\ and\ F^s = 0 \tag{4.6}$$

$$If\ F^s > F^s_{max}, then\ F^s_i := F^s_{max} \frac{F^s_i}{F^s} \tag{4.7}$$

Where T_{max} is the maximum allowable joint tensile force (calculated as the directional product of the joint tensile strength and corresponding contact area), *i* and *:* represent the i^{th} component of a vector and updated values respectively. The shear force component in *i* and the total shear force are related as

$$F^s = (F^s_i F^s_i)^{1/2} \tag{4.8}$$

In the present study, the joint tensile strength and joint cohesion are assumed to be zero.

4.3.3. Deformable block mechanics

The deformable blocks used in this study are discretized into smaller finite-difference tetrahedral elements. The equation of motion/gridpoint acceleration ($\ddot{u}_i$) for the vertices of these tetrahedral elements (gridpoints) is

$$\ddot{u}_i = \frac{\int \sigma_{ij} n_j ds + F_i}{m} + g_i \tag{4.9}$$

Where s is the surface enclosing the body with mass m, σ_{ij} is the ij^{th} stress component, n_j is the unit normal to s, F_i is the resultant of external forces on the gridpoint, and g_i is the gravitational acceleration.

The gridpoint forces are obtained as a sum of external forces, sub-contact forces (for block boundaries) and internal forces in the block. Block deformation formulations, expressed in incremental form, are given in equation 4.10.

$$\Delta\sigma_{ij}^{e} = \lambda\Delta\epsilon_{v}\delta_{ij} + 2\mu\Delta\epsilon_{ij} \tag{4.10}$$

Where $\Delta\sigma_{ij}^{e}$ is the elastic increment of the stress tensor, λ and μ are the Lame constants, $\Delta\epsilon_{v}$ is the volumetric strain increment, $\Delta\epsilon_{ij}$ is the incremental strain and δ_{ij} is the Kronecker delta.

Rocks undergo elastic and plastic deformations. The elastic deformation in this study is governed by the Mohr-Coulomb failure criterion, and the plastic portion is modeled as a perfectly plastic behavior, as shown in Fig. 4.3.

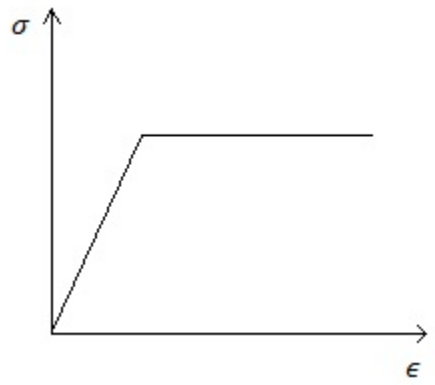

Figure 4.3: Elastic-perfectly plastic material behavior used in the numerical study (σ is the normal stress on the sample and ϵ is the corresponding strain)

The block constitutive model used in the current study, the Mohr-Coulomb model, is a conventional Mohr-Coulomb failure criterion (Equation 4.11) with tension cut-off, to accommodate for tensile failures through the explicit description of tensile strength.

$$\tau = c + \sigma \tan \varphi \tag{4.11}$$

Where τ represents the shear strength of the material, c is the material cohesion, σ is the normal stress and φ is the internal friction angle. The elastic (Hooke's law) formulations in the Mohr-Coulomb model can be expressed in incremental principal stresses (σ_1, σ_2, σ_3) and corresponding strains (ϵ_1, ϵ_2, ϵ_3) as

$$\begin{aligned} \Delta\sigma_1 &= \alpha_1 \Delta\epsilon_1^e + \alpha_2(\Delta\epsilon_2^e + \Delta\epsilon_3^e) \\ \Delta\sigma_2 &= \alpha_1 \Delta\epsilon_2^e + \alpha_2(\Delta\epsilon_3^e + \Delta\epsilon_1^e) \\ \Delta\sigma_3 &= \alpha_1 \Delta\epsilon_3^e + \alpha_2(\Delta\epsilon_1^e + \Delta\epsilon_2^e) \end{aligned} \tag{4.12}$$

Where the superscript e on the strains stands for elastic, signifying elastic strains. The total strain in an element is simply the sum of elastic and plastic parts of the strain. α_1 and α_2 are material constants related to the elastic constants-bulk modulus, K and shear modulus, G, as

$$\begin{aligned} \alpha_1 &= K + \frac{4}{3}G \\ \alpha_2 &= K - \frac{2}{3}G \end{aligned} \tag{4.13}$$

The failure criterion in equation 4.11 can be described in terms of the maximum and minimum principal stresses, σ_1 and σ_3, as a function of the shear failure criterion, $f^s=0$, as

$$f^s = \sigma_1 - \sigma_3 N_\varphi + 2c\sqrt{N_\varphi} \tag{4.14}$$

and the tensile failure can be defined by a criterion of the form $f_t=0$ such that

$$f_t = \sigma_3 - \sigma^t \tag{4.15}$$

Where σ^t is the tensile strength and

$$N_\varphi = \frac{1+\sin\varphi}{1-\sin\varphi} \tag{4.16}$$

It may be noted that the sign convention in 3DEC recognizes compressive stresses as negative stresses and tensile stresses as positive stresses. This is opposite to the conventional sign conventions used by the rock mechanics community at large.

4.3.4. Discretization in 3DEC

Discretization of blocks in 3DEC is achieved through the division of blocks into smaller elements. The elements can be tetrahedral (analogous to constant strain triangle) or quadrilateral/hexahedron. While the quadrilateral (*quad*) elements have more degrees of freedom and are suitable for plasticity calculations, the tetrahedral elements provide more flexibility in meshing irregular block geometries, and have been used for the present study. However, tetrahedral elements have the classical problem of mesh-locking due to the incompressibility of plastic flow (Nagtegaal et al., 1974). This problem can be eliminated by finer discretization in beams and in the layers around excavations, at the cost of computational efficiency. However, the concept of nodal mixed discretization (Marti and Cundall, 1982) does away with this stiffness locking problem by keeping order of elements low and by reducing the number of constraints on plastic flow. In this method, the isotropic and deviatoric components of the stress and strain tensors are discretized differently. The deviatoric behavior is described per tetrahedral element and the isotropic behavior is described over a zone (a cluster of tetrahedral elements forming a hexahedron). This method improves plasticity calculations without significantly

reducing computational efficiency or compromising the capacity to discretize complex block geometries. Hence, it has been used with tetrahedral elements in the study.

In nodal mixed discretization, the strain rate (ε_{ij}) obtained from nodal velocities is divided into deviatoric (e_{ij}) and volumetric (e) components as

$$\varepsilon_{ij} = e_{ij} + e\delta_{ij} \tag{4.17}$$

Where δ_{ij}, as usual, represents the Kronecker delta.

To calculate the volumetric strain across the zone, the mean elemental volumetric strain rate ($\bar{e}$) is calculated as a weighted average of values in surrounding elements (nodal volumetric strain rate) as shown in equation 4.18.

$$\bar{e} = \frac{1}{4}\sum_{n=1}^{4}\left(\frac{\sum_{k=1}^{m} e_k V_k}{\sum_{k=1}^{m} V_k}\right)_n \tag{4.18}$$

Where m is the number of elements surrounding a node, V_k is the volume of the kth element and the number '4' arises as a result of the four nodes in a tetrahedral element. The mean volumetric strain rate, $\bar{e}$, is then used to redefine the total strain rate defined in equation 4.17. The procedure is similar for stress tensors and is especially applicable for dilatant materials.

4.3.5. Cable support formulations

Cable elements are capable of normal and shear resistance, and are described through their constituent steel and grout physical and mechanical properties. The cables in 3DEC are divided into a finite number of segments of length L, with their segmental nodes at the end of each segment. Cable supports are defined by the cable cross-sectional area (A), Young's modulus of the cable (E), tensile strength of the cable, grout-rock interfacial shear stiffness per unit length (K_{bond}), grout-rock interfacial cohesive capacity per unit

length (S_{bond}) and yield strength of the cable. The axial behavior of the cable segment is described in incremental expressions, as the incremental axial force, ΔF^t, expressed as a function of the incremental cable axial displacement, Δu^t, in equation 4.19.

$$\Delta F^t = -\frac{EA}{L}\Delta u^t \tag{4.19}$$

The shear force per unit cable length, developed in the grout elements, F_s, is calculated as a function of the displacement difference between the cable axial displacement (u_c) and the rock axial displacement (u_m) as

$$F_s = K_{bond}(u_c - u_m) \tag{4.20}$$

The grout-rock interfacial shear stiffness and cohesive capacity are not easily obtained through field measurements and their descriptions are sometimes poorly understood. A reasonable estimate for their input in 3DEC (Itasca, 2008) is given in equations 4.21 and 4.22.

$$K_{bond} = \frac{2\pi G}{10\ln(1+2t/D)} \tag{4.21}$$

$$S_{bond} = \pi(D + 2t)\tau_I Q_B \tag{4.22}$$

G is the grout shear modulus, D is the reinforcing diameter, t is the grout annulus thickness, τ_I is an empirical constant (approximately half of the uniaxial compressive strength of the grout or rock, whichever is smaller) and Q_B is the bond quality index (0-1) between the grout and rock. In this study, Q_B is used as the bond efficiency between the grout and steel for reasons described in subsequent chapters.

4.4. Applications of the 3DEC distinct element code in rock engineering

The 3DEC distinct element code has been used in a wide range of rock mechanics analyses spanning the civil, mining and petroleum engineering sectors. This has ensured that the code remains refined and free of errors, and new physics for different analyses such as creep, discrete fracture networks, acoustic analyses etc. have been added from time to time. For instance, Stefanou et al. (2011) have used the code to perform dynamic analyses on a multi-drum masonry column with fractures to determine the effect of fractures and cracks on the overall structural stability of ancient monuments, especially during earthquakes. Similarly, Wang et al. (2006) studied the effect of presence of joints on wave propagation including the effect on attenuation and velocity of primary and secondary waves. The 3D distinct element code has been applied to study coupled hydromechanics of stimulated fractured systems using the discrete fracture network concept by Rachez and Gentier (2010). They concluded that the numerical simulations provided results similar to those obtained from borehole monitors and microseismic analyses in the geothermal system. Damjanac and Cundall (2016) detailed the methodology that can be used to apply 3DEC to study hydraulic fracturing in naturally fractured reservoirs through coupled hydro-mechanical codes. The model they created was found to able to evolve based on both intact rock fracturing and through the shearing and opening of existing joints. Studies on hard rock to potentially identify and analyze nuclear waste repository sites (Stephansson and Shen, 1991) and underground powerhouse caverns (Dasgupta et al., 1995), considering effects of joints, earthquakes and fluid flow, are some of the less conventional applications where the 3D distinct element code has been successfully applied. In mining, 3DEC has been applied to both

surface and underground analyses. Firpo et al. (2011) used 3DEC in a rock slope stability analysis in tandem with digital photogrammetry. Remote fracture mapping and 3DEC modeling were integrated in a slope stability analysis of a gold mine in an area with complex fault geometries by Kulatilake and Shu (2015). A cavability assessment criterion to ascertain an excavation's proneness to caving was built by Vakili and Hebblewhite (2010), using numerical analyses of longwall panels mining using a Longwall Top Coal Caving (LTCC) method. Fundamental studies using the concepts of Representative Elementary Volume (REV) have been applied to rock tunnels to study scale effects during the modeling of fractures by Wu and Kulatilake (2012a, 2012b). Further studies have been performed to study the tunnel stability through the methods created.

4.5. Summary

The underlying numerical modeling formulations and block movement and interaction physics in the distinct element method used as part of the current study has been discussed in detail in this chapter. The most important concepts that figure in the background in subsequent chapters have been provided in an attempt to make the thesis as standalone as possible and to enhance readability. This includes concepts such as contact detection, block translation and rotation, joint failure laws, discretization logic, support definitions and block-support interactions. Further, a discussion has been included to show the applicability of the code for solving common rock engineering problems in recent literature.

CHAPTER 5: MODELING THE TUNNELS

5.1. Introduction

The procedures adopted in modeling the tunnels are presented in this chapter. This begins with the process of creating accurate lithological sections, the boundary conditions, assigning in-situ stresses, joints and interface properties and discretization. The chapter also explores the stress relaxation and support stability quantification procedures introduced in the study. Further, the procedures adopted during the back-analysis of rock mass mechanical property values, installation of floor supports and parametric sensitivity analyses have been discussed.

5.2. Setting up the initial numerical models

The numerical model space is a polyhedron of dimensions 57 m along the tunnel length and a 50 m X 50 m square across the tunnel's cross-sectional profile. The model dimensions, along with lithological sections, for the horseshoe (HS) tunnel are provided in Fig. 5.1. Note that the orientation of the coordinate system is presented at the top-right corner of Fig. 5.1. The tunnel axis (and maximum principal stress direction) is the y-axis, and the vertical axis is the z-axis. The x-axis represents the direction of the minimum principal stress, which is the actual spatial orientation of the stresses in the tunnels/mine. Furthermore, the x-axis in the numerical model is set-up to go from x=-25 m to x=+25 m, the y-axis ranges from y=0 m to y=57 m and the z-axis ranges from z=-23 m to z=+27 m.

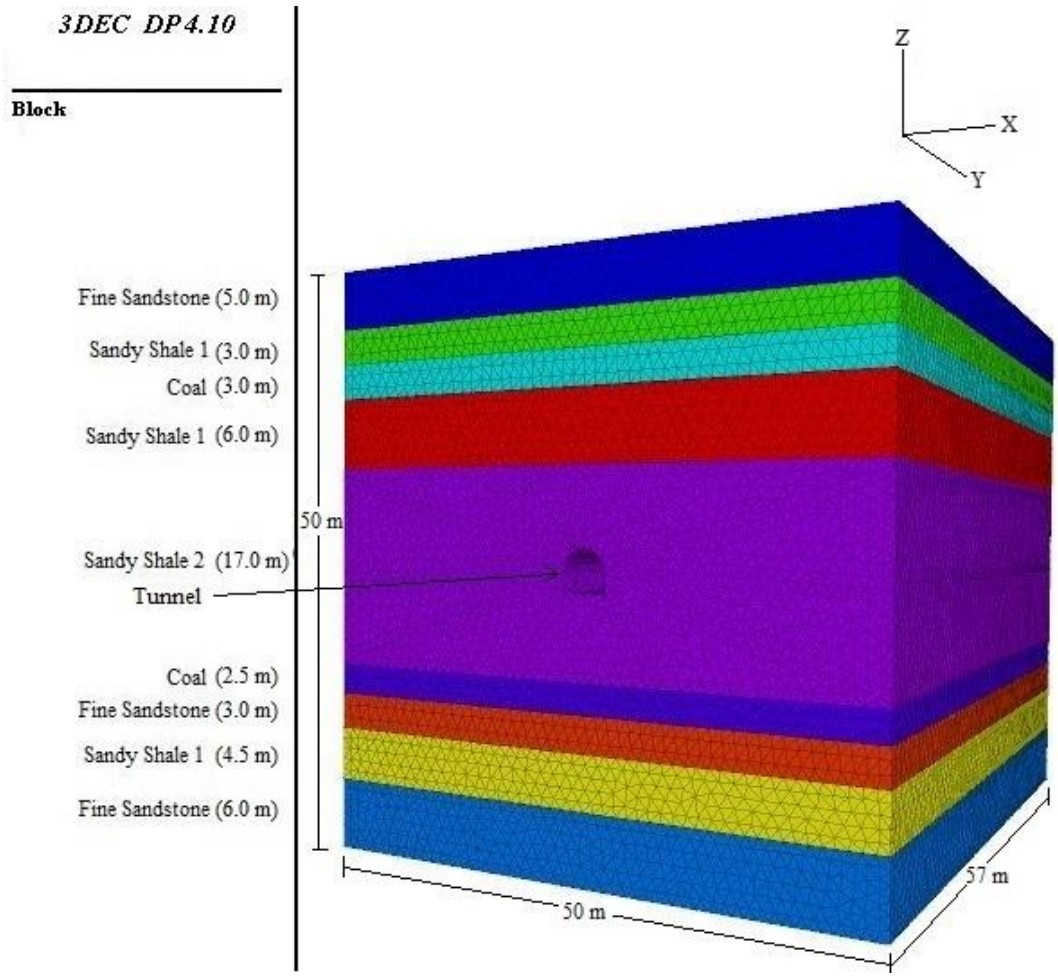

Figure 5.1: Set-up numerical model with different lithologies and model coordinate system

To ensure that the model boundary is not influenced by the tunnel boundaries, the model dimensions have been carefully selected such that they are at least five times larger than the tunnel width in any direction from the tunnel. The in-situ stresses in the model have been assigned in each zone based on the vertical stress at 1300 m, the stress gradient as dictated by gravity and the stress ratios (See equations 3.1, 3.2 and 3.3). The boundary conditions in the model have been selected as a combination of stress and velocity constraints to ensure model stability and physical accuracy. The model base has been

fixed in the vertical direction, and a vertical stress equal to overburden stress has been placed at z = 27 m (34.5 MPa). The four faces of the polyhedron have corresponding principal stresses and increasing stress gradients with depth. Fig. 5.2 shows the boundary conditions in the model in 2-dimensions. The out-of-paper boundary conditions are same as the stresses seen on the walls shown in figure.

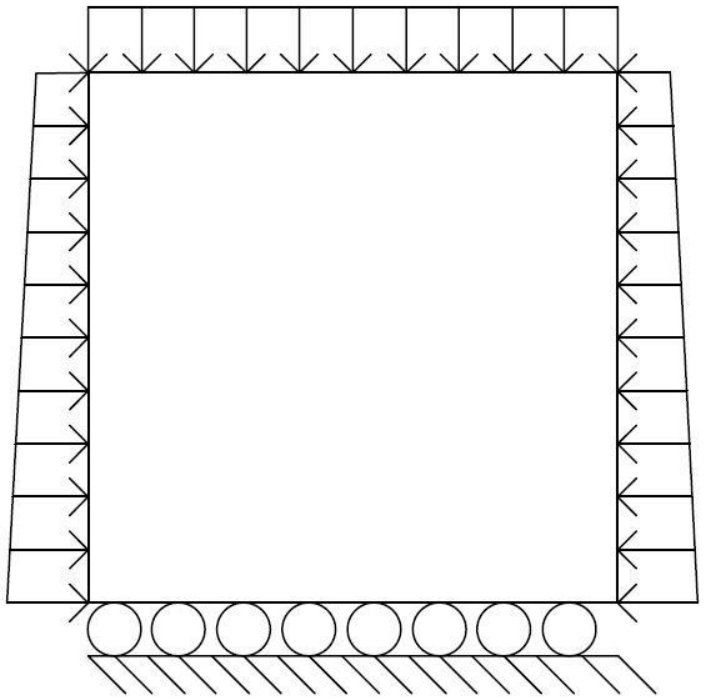

Figure 5.2: Boundary conditions used in the numerical modeling

The bedding planes of spacing 1 m defined explicitly in the Sandy Shale #2 stratum are shown in Fig. 5.3 (a) and (b) for the HS and inverted arch (IA) tunnels respectively. The interfaces between lithologies and the bedding planes have been defined using the Coulomb-Slip joint model (*jcons=1* in 3DEC) which is a derivative of the Coulomb friction law as explained in section 4.3.2. The intact part or the continuum in the model has been described using the elastic-perfectly plastic Mohr-Coulomb strength criterion

with tension cut-off (*cons=2* in 3DEC), as discussed in section 4.3.3. Hence, the numerical model is neither a pure continuum since it has explicit interfaces and bedding planes but is not completely discontinuous since it has included the minor fractures as part of the continuum. Due to this, it has been described as a 'mixed discontinuum-equivalent continuum' model. This is not to be confused with hybrid numerical models which incorporate concepts of both continuum and discontinuum mechanics.

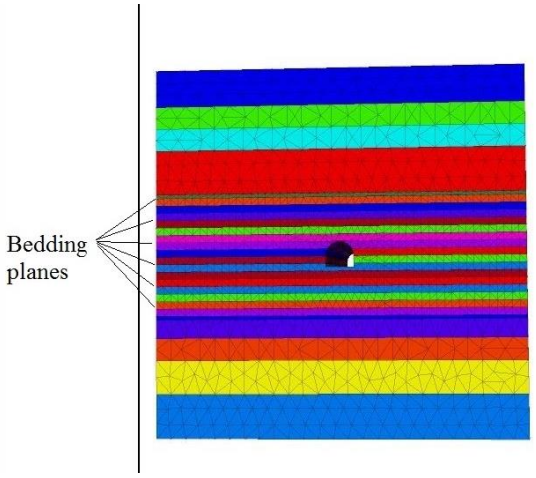

(a)

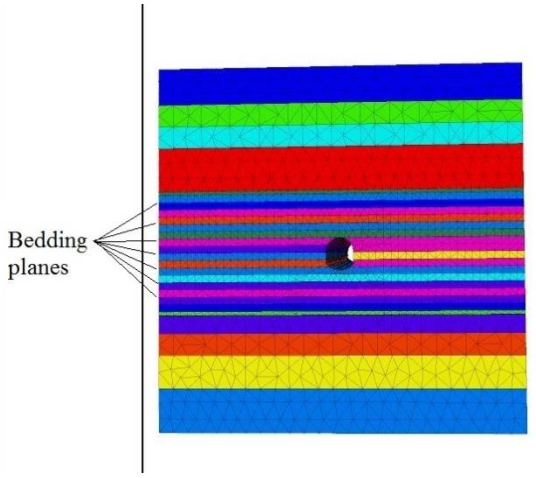

(b)

Figure 5.3: The bedding planes in the (a) HS tunnel and (b) IA tunnel

The interfaces between lithologies have been assigned parameters in such as a way as to provide a gradual change in strength between strata as is normally observed in the field. To do this, the framework suggested by Kulatilake et al. (1992) and Kulatilake et al. (1993) has been used to estimate the interface mechanical property values. The interface friction angle and cohesion have been selected as the average of the friction angles and cohesion values between the rock layers that they are sandwiched between. The joint shear stiffness (JKS) for the interface is estimated such that the ratio of the average shear modulus across the interface to the interface JKS is in the range 0.008-0.012 m. The joint normal stiffness (JKN) is then selected as being between 2-3 times the JKS. As a guideline, an appropriate value for coefficient may be the ratio of the average elastic modulus and average shear modulus across the interface. The interface mechanical property values and bedding plane mechanical property values used in the study are provided in Table 5.1.

Table 5.1: Interface and bedding plane mechanical property values used as input to the numerical model

Discontinuity	Type	Friction Angle (Degrees)	Cohesion (MPa)	Tensile Strength (MPa)	Joint Shear Stiffness, JKS (GPa/m)	Joint Normal Stiffness, JKN (GPa/m)
FS/SS1	I	34.3	16	0	1063	2736
SS1/SS2	I	29.5	13	0	828	2133
SS2/C	I	25.5	2.8	0	447	1150
FS/C	I	30.3	2.8	0	675	1738
SS1/C	I	28.0	2.8	0	474	1220
SS2	B	16.0	0	0	8	21

I=Interface, B=Bedding planes, FS= Fine Sandstone, SS1=Sandy Shale #1, SS2=Sandy Shale #2, C=Coal

The bond quality index, Q_B, introduced in equation 4.22 has been defined for the purpose of this study as the quality between the grout and cable rather than between the grout and rock. This has been done because the norm in many mines in Asia is to use discarded wire ropes from haulages and pulleys as cable bolts, in an attempt to save costs (Singh et al., 2001). These discarded ropes typically have grease and/or other forms of lubricants on them and have been subjected to significant cyclic loading during their operational life. Due to this, they typically have lower adhesion to the grout and it is a reasonable expectation, then, that the grout-rock interface would have a higher roughness than the grout-steel interface. Taking this into consideration, Q_B has been assumed to be 0.45. Physically, this means that the grout-rock interface (grout-steel interface for the

purpose of this study) has a cohesive efficiency of 45% of its maximum cohesive capacity (S_{bond}).

The discretization was done using tetrahedral zones of 2 m close to the model boundary and using 1 m zones close to the tunnels. Instead of adopting smaller discretization which would significantly impede solution runtime, the nodal mixed discretization (NMD, equations 4.17 and 4.18) was adopted to improve plasticity calculations.

One of the contributions of this study to the state-of-the-art is the treatment of support installation. For all analyses performed, an effort has been made to incorporate the effect of stress redistribution that occurs between excavation and supporting cycles. The difference between considering this effect (henceforth referred to as stress relaxation, SR, in this study) and using the conventional simulation scheme of simply installing supports after excavation (referred to as instantaneous, I, installation in this study) has also been studied. Stress relaxation or its variants (using density perturbation) has been previously adopted by Ghee et al. (2006) and Vardakos et al. (2007) in their two dimensional distinct element numerical studies but its effect on the rock supports has not been studied. To incorporate stress relaxation, the following procedure has been adopted, derived and modified from Vardakos et al. (2007):

- Immediately after excavation, before starting the mechanical calculations, external balancing stresses are installed on the tunnel boundary as if the tunnel were never excavated.
- These external stresses are gradually reduced quasi-statically in an ideal condition (but in decrements of 10% for realistic computational time in this

study) with mechanical calculations being performed after each stress reduction decrement.

- After sufficient stress redistribution, supports are installed normally, the balancing stresses are removed, and mechanical calculations run until equilibrium.

The amount of stress redistribution that needs to be undergone before supports are installed is a very site-specific measure and is a function of the rock mass strength and deformability parameters. This study uses a relaxation of 50% reduction from initial stresses as a reasonable estimate for excavations which may be left unsupported for 8-10 hours, which is the shift cycle for this mine. This is based on comparison of the rock mass strength in this case to the rock mass strengths in Ghee et al. (2006) and Vardakos et al. (2007), and the relaxation values used by them.

In addition to looking at the tunnel deformations and stability, cable stability has also been given due importance since it serves as a useful proxy for rock mass stability. This has been done through the calculation of cable factor of safety (FS) and grout failure. The cable FS has been calculated individually for both first and second supports and has not been combined since they are of different lengths. To calculate the FS, the highest axial force out of all segmental axial forces in each cable was taken as the cable axial force and averaged over all cables in the first and second supports to give a composite cable FS, as shown in equation 5.1.

$$FS = \frac{\sum_{c=1}^{N} Max(F_{seg})_c}{NT} \tag{5.1}$$

Where F_{seg} is the segment axial force for cable c, and N is the number of cables of a particular type and T is the yield capacity of the cable (unit N).

The grout failures in 3DEC are available as a list of segmental failure flags. In other words, each segment's grout bond will have a status assigned to it as intact or broken. The grout failures have been calculated as the number of broken bonds expressed as a percentage of the total number of grout bonds in the cable. The exercises of calculating the cable FS and grout failures have been performed in RStudio, an environment for the R programming language, after exporting the relevant lists from 3DEC as text files.

5.3. Back-analysis of rock mass mechanical property values

The rock mass property values have been estimated indirectly from the numerical modeling using a back-analysis procedure. In this procedure, a strength reduction using the binary search algorithm was applied to the numerical model until the model deformations matched the field deformation monitoring data. The density and intact rock internal friction angle were kept unchanged during the strength reduction procedure since they are a feature of the intact part of the rock (Kulatilake et al., 2004). The Poisson's ratio was increased as the strength of the rock mass was reduced, based on observations by Kulatilake et al. (2004). The increase was a function of the reduction in strength, with percentage increase in magnitude being half the percentage decrease in strength parameters. For instance, if the other strength parameters were reduced by 10%, the Poisson's ratio was increased by 5%, capping at the physical limit for rocks - 0.5.

The binary search method was adopted to actually perform the strength reduction based calibration. Here, a range of possible rock mass property values with upper and lower limits are specified which are updated at each iteration. The initial values for the upper and lower limits are the intact rock properties and zero respectively. During the

first iteration, the upper limit of the range, i.e., the intact rock properties are used as the initial estimates for the rock mass. In each subsequent iteration, the average of values in the range is used as the estimate for the rock mass property values. After each iteration, the model deformations are compared to the field deformation data sets and the range is updated based on whether the model deformations are larger or smaller than field deformations. If the model deformations are larger, the rock mass property value becomes the new lower limit and a new rock mass property estimate is made. If model deformations are smaller, the existing rock mass property values become the new upper limit for the range, and a new rock mass property value is estimated accordingly. In this way, the property values are averaged over the designated range at each iteration until the numerical model deformations matched the field deformation values within the range of acceptable error. At this point, the model was said to be calibrated and the corresponding rock mass property values have been used as the rock mass property values for subsequent analyses.

5.4. Modeling the effect of rock supports

The calibrated numerical model was used to perform subsequent analyses as detailed in Table 5.2, in an attempt to observe the effect of rock supports. A total of ten cases, spanning both HS and IA tunnel shapes were studied. Different combinations of supports – unsupported, roof and wall supports, and floor bolting were simulated to see the effect on tunnel stability. It may be noted that floor bolting, in this study, refers to floor bolting in addition to roof and wall bolting. The pattern of bolting, when floor bolting was

introduced, is shown in Fig. 5.4. Additionally, the effect of longer bolts (3.5 m long first support; 4.0 m long second support) was studied for reasons described in Chapter 6.

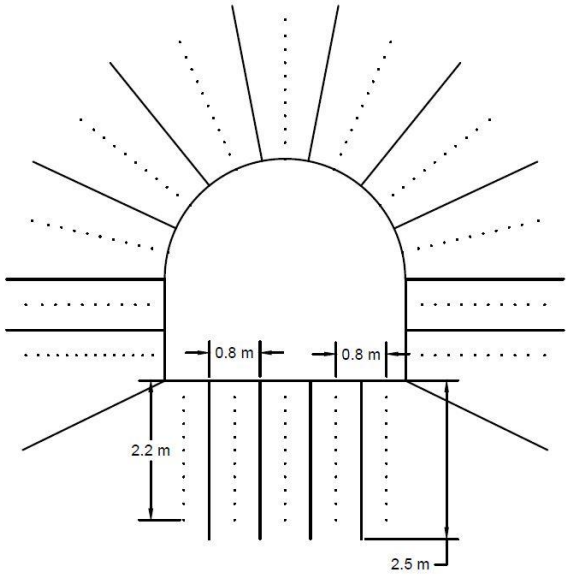

(a)

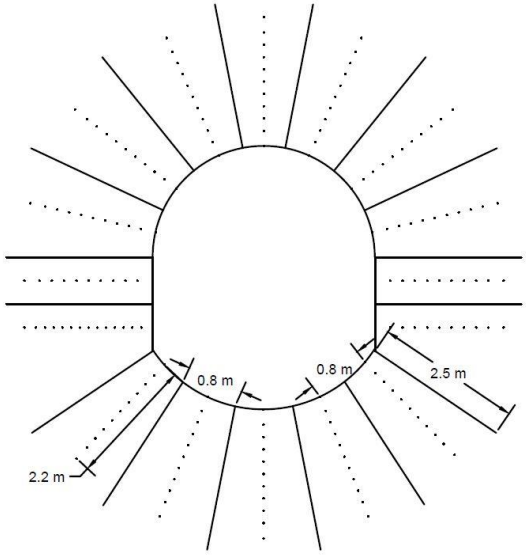

(b)

Figure 5.4: Floor bolting pattern in (a) HS tunnel and (b) IA tunnel

Table 5.2: The various cases simulated using the calibrated model

Case	Tunnel shape: Horseshoe (HS) / Inverted arch (IA)	Support installation routine: Instantaneous (I) / Stress-relaxation (SR)	Roof and wall bolting (Y/N)	Floor bolting (Y/N)
1	HS	Unsupported	Unsupported	Unsupported
2	HS	I	Y	N
3	HS	I	Y	Y
4	HS	SR	Y	N
5	HS	SR	Y	Y
6	IA	Unsupported	Unsupported	Unsupported
7	IA	I	Y	N
8	IA	I	Y	Y
9	IA	SR	Y	N
10	IA	SR	Y	Y

5.5. Parametric sensitivity analyses

A parametric study was carried out to determine the effect that different rock and discontinuity mechanical property values have on the tunnel deformations, so as to better understand which properties need to be estimated with higher accuracy in future strength measurement routines at the mine.

The properties that were parameterized for the intact rock include the cohesion, internal friction angle, tensile strength and elastic modulus. Each parameter was varied by +/-15% and +/-30% from their mean calibrated values. Similarly, the bedding plane JKN, JKS and basic friction angles were varied from -30% to +30% of their mean calibrated values in increments of 15%.

In an attempt to ascertain whether the cable configuration could be optimized, the cable diameters and grout compressive strengths were varied in specific ranges. These two properties were selected since they are the most easily modifiable parameters in the field. The cable diameters were changed in diameter pairs for the first and second supports as shown in Table 5.3 (Default pair is configuration 1). These pairs are based on manufacturer specifications for some commonly available cable diameters in China. The grout compressive strengths have been varied between 25 MPa and 55 MPa in increments of 10 MPa, and are also based on the uniaxial compressive strengths of commercially available grout compounds. The default grout compressive strength for the study is 55 MPa.

Table 5.3: Different support diameter pairs studied

Configuration	First support diameter (mm)	Second support diameter (mm)
1	16	19
2	19	22
3	22	26
4	26	29

CHAPTER 6: ANALYSIS AND RESULTS

6.1. Introduction

The analyses set up in Chapter 5 and their corresponding results are discussed at length in this chapter. The created numerical model is first checked for correctness in applied boundary conditions and material properties, and the tunnel systems are calibrated to estimate the rock mass strengths around the tunnels. Then, the results from analyses focusing on support behavior and tunnel stability have been reported. The chapter concludes with results from parametric analyses focusing on continuum mechanical properties, bedding plane mechanical properties and support strength parameters. Unless explicitly stated, all results have been recorded at the tunnel cross-section y=28.5 m (the center of the tunnel), the vertical deformations on the roof and floor have been performed at x=0 m, and the wall deformation measurements at 1.6 m above floor level for the horseshoe (HS) tunnel and 2.6 m above floor level for the inverted arch (IA) tunnel.

6.2. Preliminary analyses on model behavior

To study the behavior and correctness of boundary conditions and in-situ stress fields, a HS tunnel model without any bedding planes was created. This was done since bedding planes running across the excavation can complicate the analysis of stress fields around it. Fig. 6.1 shows the vertical (ZZ) and horizontal (XX) stress fields around the HS tunnel in the case with no bedding planes.

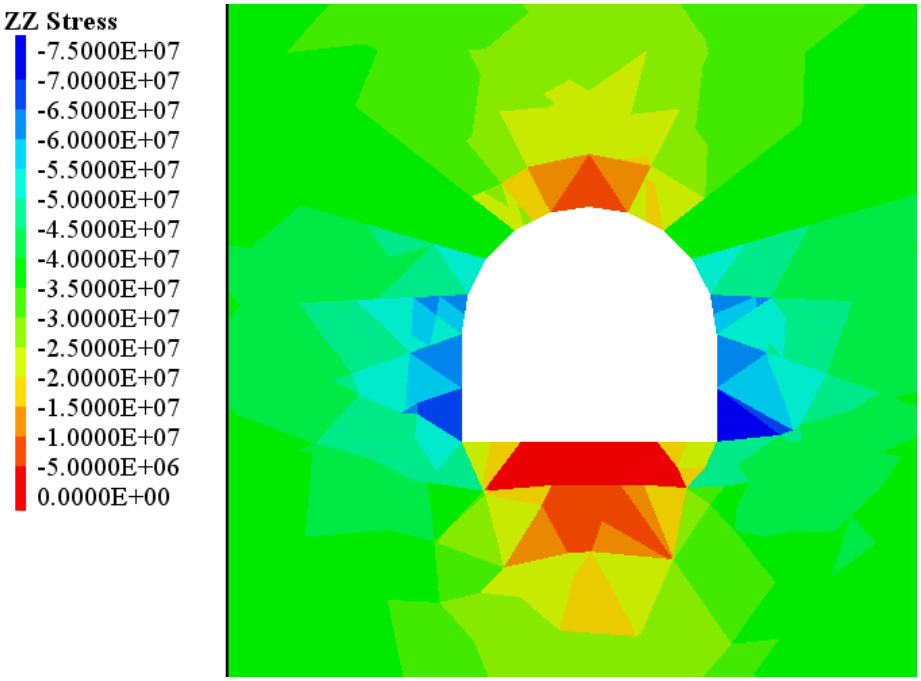

(a)

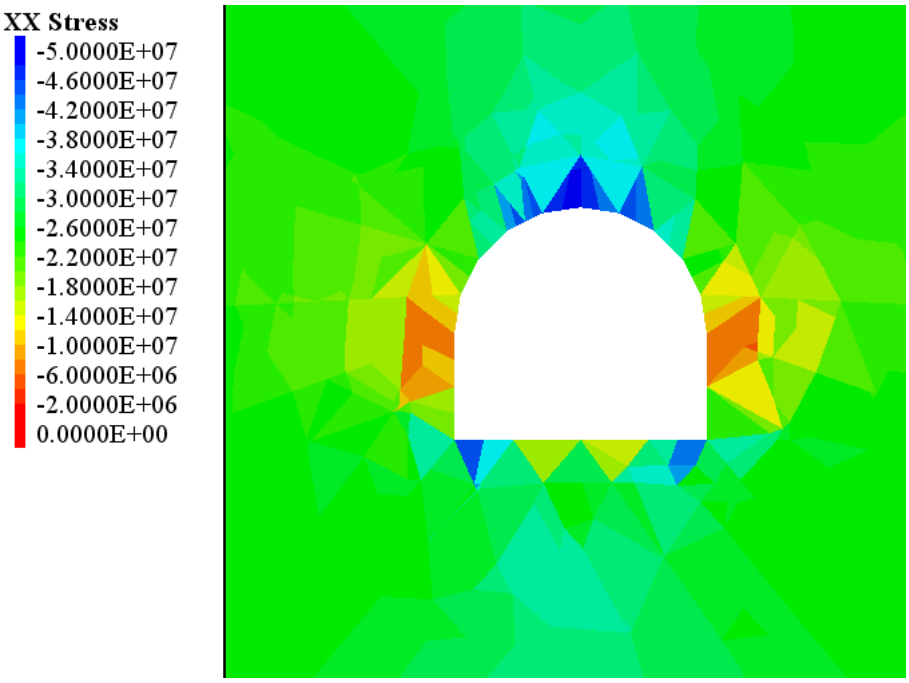

(b)

Figure 6.1: (a) ZZ stress distribution and (b) XX stress distribution in the HS tunnel modeled with no bedding planes

Fig. 6.1 shows that the ZZ stress approaches zero on the roof and floor, and is highest on the walls. Similarly, the XX stress approaches zero on the walls and is highest on the roof and floor. This shows that the stress fields are following the expected trends. It may be noted that the negative stress values on the legend indicates compressive stresses by convention, and tensile stresses are represented by a positive direction. The far field stress (green) in the ZZ direction is approximately 35 MPa, and the far field stress field in the XX direction is about 28 MPa, which are the approximate values used in the 3DEC numerical model. This shows that the numerical model is behaving as one would expect. The models in this study have been run till a force balance ratio of 10^{-5}, i.e., until the average unbalanced forces in the model became 10^{5} times smaller than the initial unbalanced forces in the model. This ensures that the numerical calculations have sufficiently progressed to stability. Fig. 6.2 shows a typical graph of the unbalanced forces in the numerical model versus the number of calculation cycles. Quantitatively, an unbalanced force value of about 500 N can be considered insignificant in a model of 50 m X 50 m X 57 m.

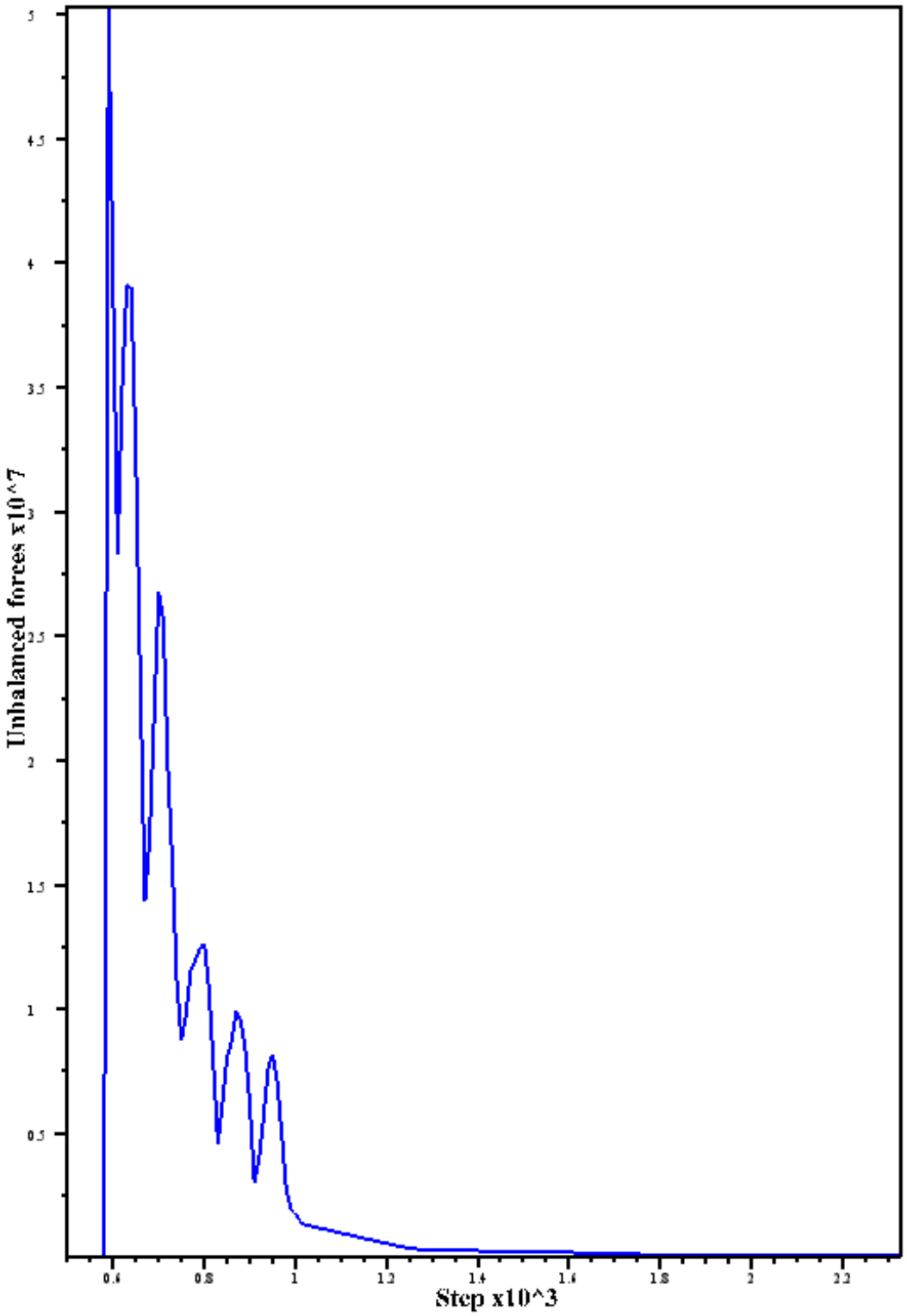

Figure 6.2: Unbalanced forces with calculation cycle progress in a typical model

6.3. Calibration of rock mass mechanical property values

Iterative calibration of the rock mass mechanical property values were carried out through both instantaneous excavation and support installation, and stress relaxation based techniques detailed in sections 5.2 and 5.3. Results of these analyses are presented for both tunnels in tables 6.1 through 6.4.

Table 6.1: Iterative calibration of the HS tunnel through instantaneous excavation and support

Iteration	Percentage of Intact	Deformations (mm)			Factor of safety		Grout bond failure (%)	
		Roof (mm)	Wall (mm)	Floor (mm)	First Support	Second Support	First Support	Second Support
1	100	8.9	4.7	11.8	3.67	2.79	2.02	3.58
2	50	26	20.5	33	1.18	1.27	11.11	10.39
3	25	74.5	79.5	93.4	1.02	1.05	19.11	13.67
4	37.5	41	37	51	1.02	1.11	11.86	9.57
5	43.75	32.5	27	41	1.04	1.16	11.22	10.10

Table 6.2: Iterative calibration of the HS tunnel through stress relaxation

Iteration	Percentage of Intact	Deformations (mm)			Factor of safety		Grout bond failure (%)	
		Roof (mm)	Wall (mm)	Floor (mm)	First Support	Second Support	First Support	Second Support
1	100	8.9	4.8	11.9	4.58	4.07	0.69	0.09
2	50	25.7	19.8	32.1	1.36	1.42	10.12	9.94
3	25	78.8	86.5	97	1.02	1.05	19.34	14.9
4	37.5	40.2	35.7	47.8	1.06	1.18	11.21	10.95
5	43.75	31.9	26.6	39.3	1.14	1.25	11.01	11.5

Table 6.3: Iterative calibration of the IA tunnel through instantaneous excavation and support

Iteration	Percentage of Intact	Deformations (mm)			Factor of safety		Grout bond failure (%)	
		Roof (mm)	Wall (mm)	Floor (mm)	First Support	Second Support	First Support	Second Support
1	100	8.7	5.5	9.3	3.77	2.68	2.02	2.58
2	50	26	22.5	31	1.22	1.24	12.34	10.99
3	25	78.5	88	98.8	1.01	1.06	17.39	17.95
4	37.5	42	41	50.5	1.01	1.11	12.73	11.31

Table 6.4: Iterative calibration of the IA tunnel through stress relaxation

Iteration	Percentage of Intact	Deformations (mm)			Factor of safety		Grout bond failure (%)	
		Roof (mm)	Wall (mm)	Floor (mm)	First Support	Second Support	First Support	Second Support
1	100	8.7	5.4	9.2	5.18	4.53	0	0.05
2	50	26.5	22.7	31.3	1.39	1.34	10.19	11.54
3	25	81.2	93	102.7	1.02	1.07	20.37	18.84
4	37.5	42.5	42	51	1.09	1.17	13.2	12.2

It was found through the comparison of model deformation data and field deformation monitoring data that the best-fit rock mass mechanical property values were approximately in the range of 37.5% - 43.75% of the intact rock strength, as seen from Fig. 6.3. It may be noted that the term normalized rock mass strength refers to the rock mass strength expressed as a percentage of the intact rock strength property values calculated using the procedure described in section 5.3.

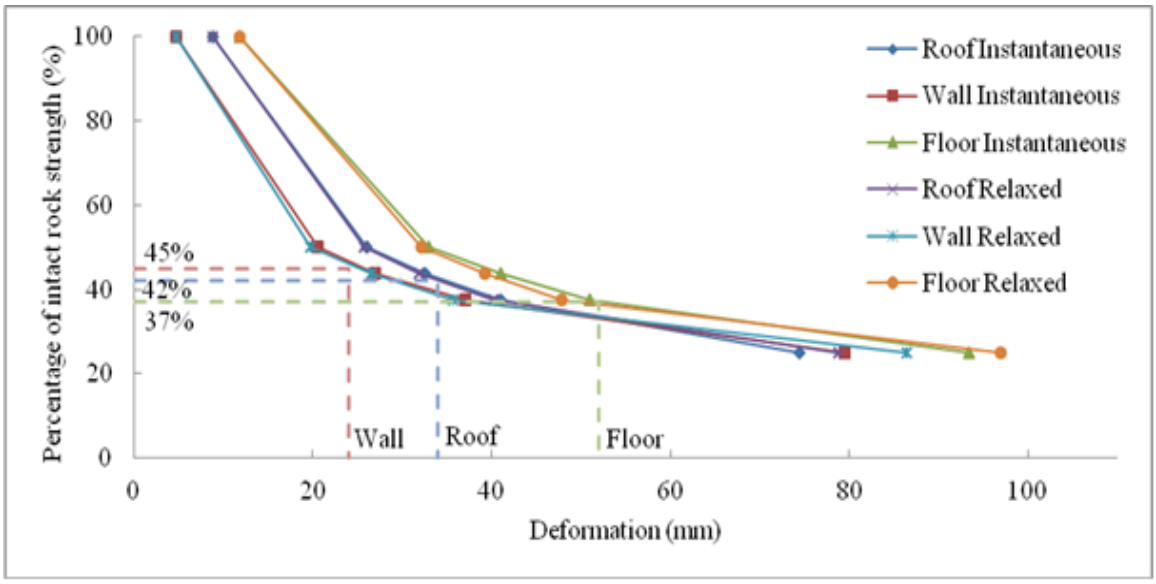

(a)

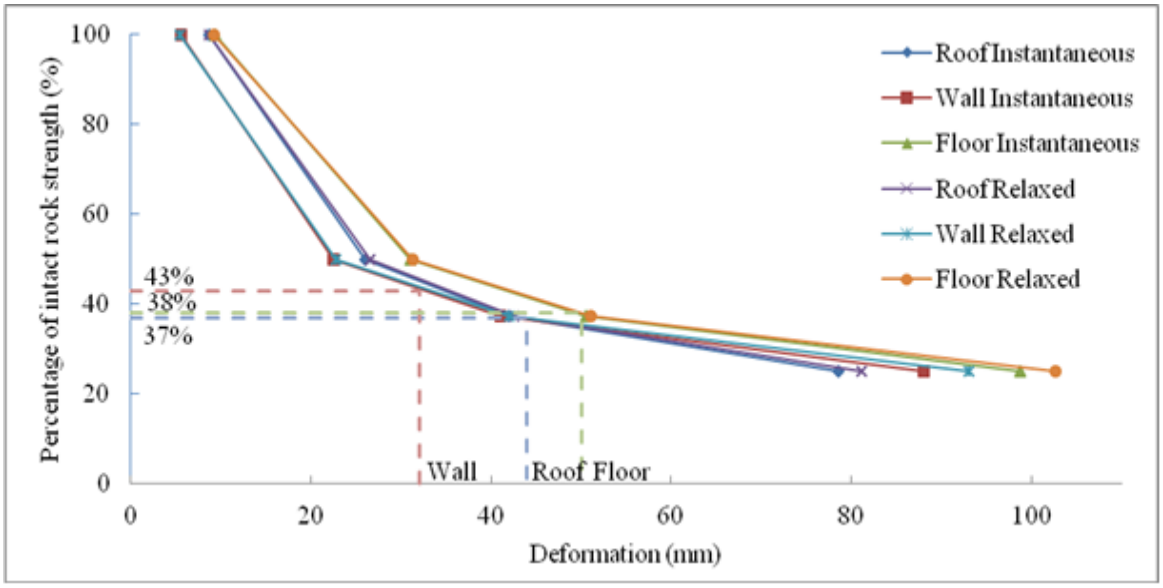

(b)

Figure 6.3: Tunnel deformations expressed as a function of normalized rock mass strength for (a) HS tunnel and (b) IA tunnel

Based on the results in Fig. 6.3, a range of 35% - 45% has been selected to describe the calibrated rock mass strength values in this mining region, accounting for possible variability in property values. The calibrated strength parameters at a normalized rock mass strength of 40% are given in Table 6.5.

Table 6.5: Calibrated rock mass mechanical property values

Layer	Density (kg/m^3)	Elastic Modulus (GPa)	Poisson's Ratio	Cohesion (MPa)	Internal Friction Angle	Tensile Strength (MPa)	Uniaxial Compressive Strength (MPa)
Fine Sandstone (FS)	2670	14.2	0.21	11.2	36.5	2.8	44.6
Sandy Shale 1 (SS1)	2660	10.6	0.36	6.4	32.0	1.5	23.0
Sandy Shale 2 (SS2)	2500	10.2	0.40	5.2	27.0	1.3	19.6
Coal (C)	1392	1.2	0.45	1.1	24.0	0.4	3.4

Figures 6.4 through 6.10 show the typical outputs from 3DEC for the HS and IA tunnels at the normalized rock mass strength parameter values of 37.5%. Figures 6.4 and 6.5 show the vertical (ZZ) and horizontal (XX) stresses respectively for the HS and IA tunnels. The effect of joints on the stress fields can be clearly seen. While the stresses follow intuitive trends, the peak values on the walls and, roof and floor for the ZZ and

XX stresses respectively occur at some distance from the tunnel boundary. This is due to the presence of bedding planes, causing a stress relief effect. Figures 6.6 and 6.7 show the vertical and horizontal deformation distributions respectively for the HS and IA tunnels. The effect of bedding planes is pronounced here too, in the form of discontinuous contours. Fig. 6.8 shows the failure states in the HS and IA tunnels. These failures states represent the area of failed region around the tunnels and the mode of failure. For instance, the suffix ‘p’ in shear-p indicates that the region corresponding to that color failed in shear in the past. The past here refers to the solution cycle and not a point in physical time. This suffix can be ‘p’ for past or ‘n’ for now, indicating current failures. Hence, shear-p and tension-n would indicate shear failures in the past and current tensile failures, and so on. Figures 6.9 and 6.10 show the cable axial force distributions and grout failure distributions respectively. Fig. 6.9 shows that the maximum axial force in some cable segments is 353.9 kN, which is close to the axial yield capacity of cables (354 kN). This, along with the values in tables 6.1 to 6.4, show that even when the average system factor of safety (FS) is above 1.0, local FS values could be 1.0 indicating local failures. Hence, an analysis of both average FS and the axial force contours is necessary to fully realize the status of a support system. Grouts are classified as intact bonds or broken bonds, as seen in Fig. 6.10. In interesting observation from Fig. 6.9 and Fig. 6.10 is that some of the locations of local failures in cable segments also correspond well with broken grout bonds. This is very similar to physical observations of cable and grout behaviors and shows the likelihood of failures in different cables in a system.

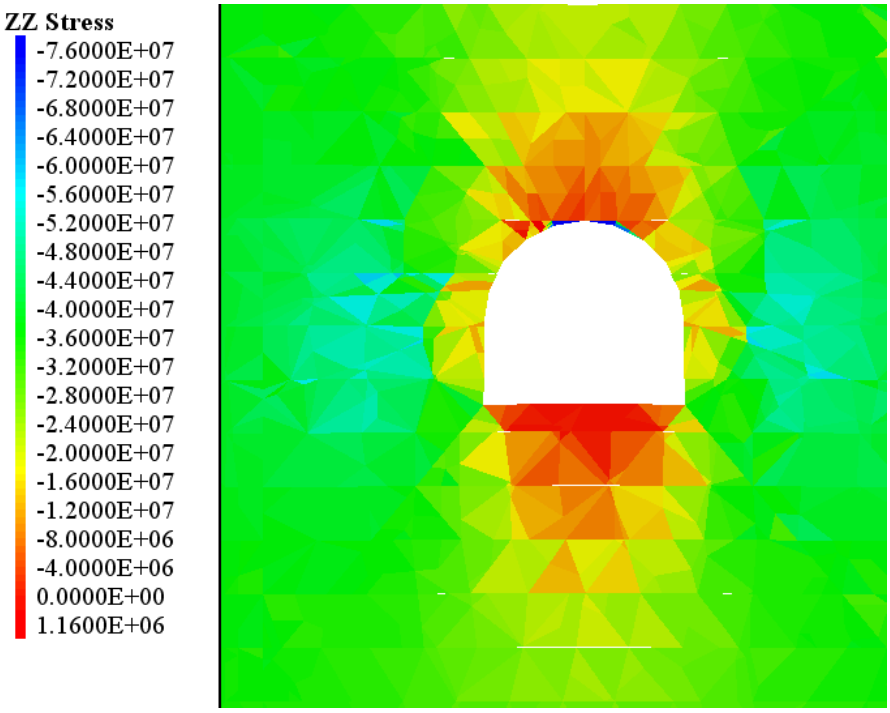

(a)

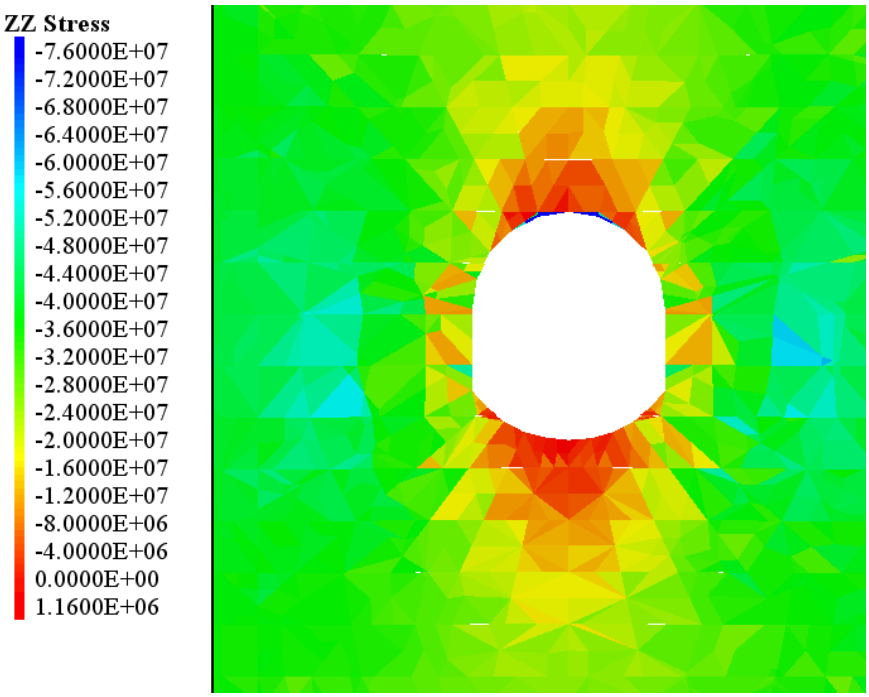

(b)

Figure 6.4: Vertical (ZZ) stress distribution contours around the excavations for (a) HS and (b) IA tunnels (unit: Pa)

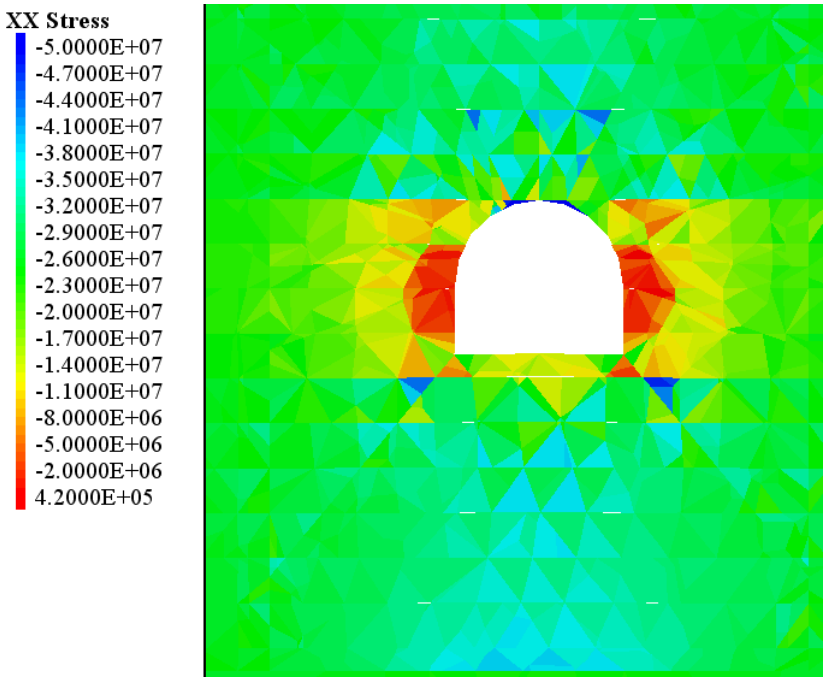

(a)

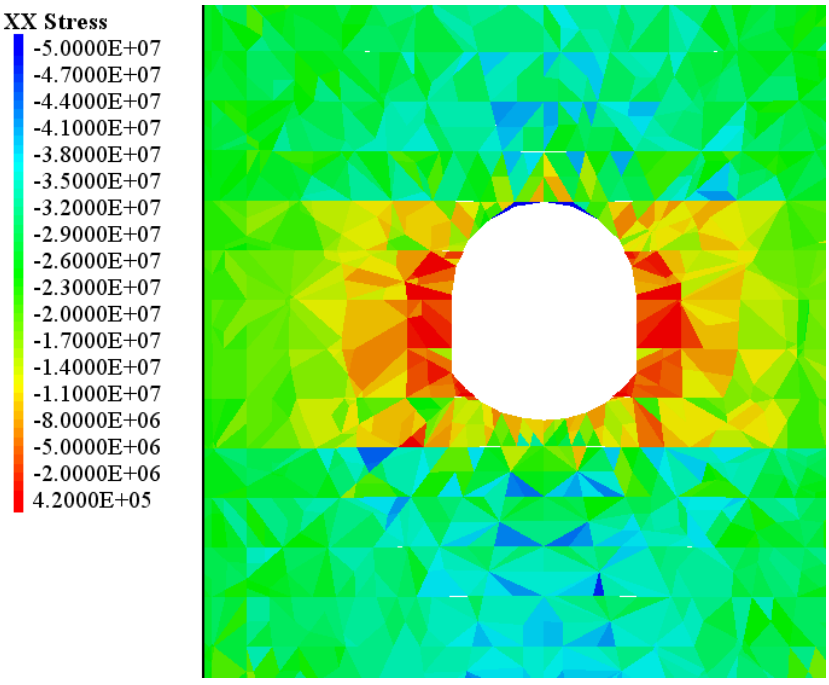

(b)

Figure 6.5: Horizontal (XX) stress distribution contours around the excavations for (a) HS and (b) IA tunnels (unit: Pa)

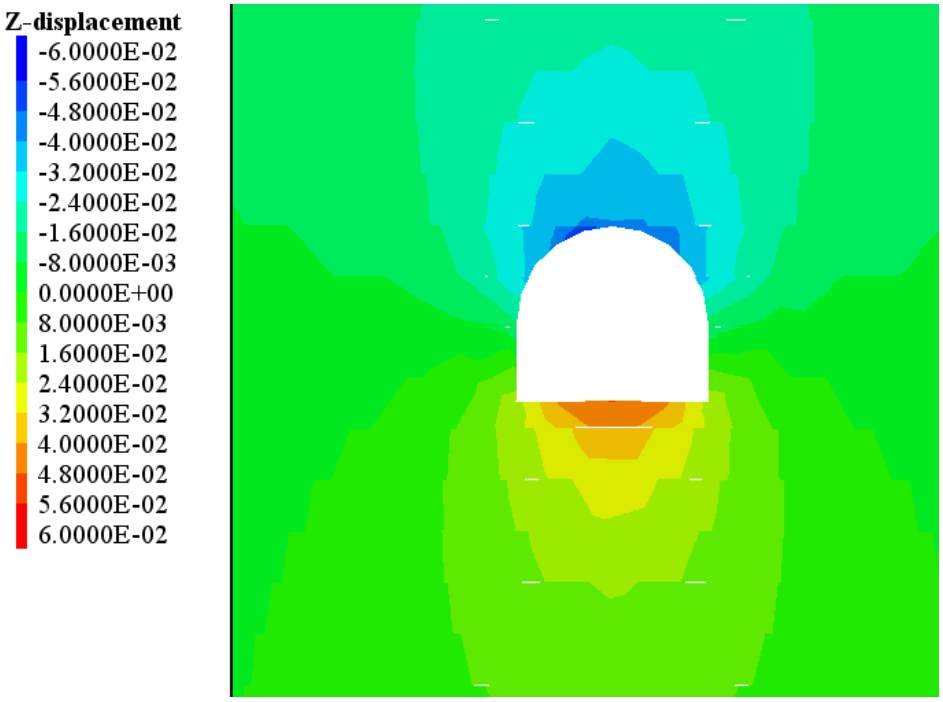

(a)

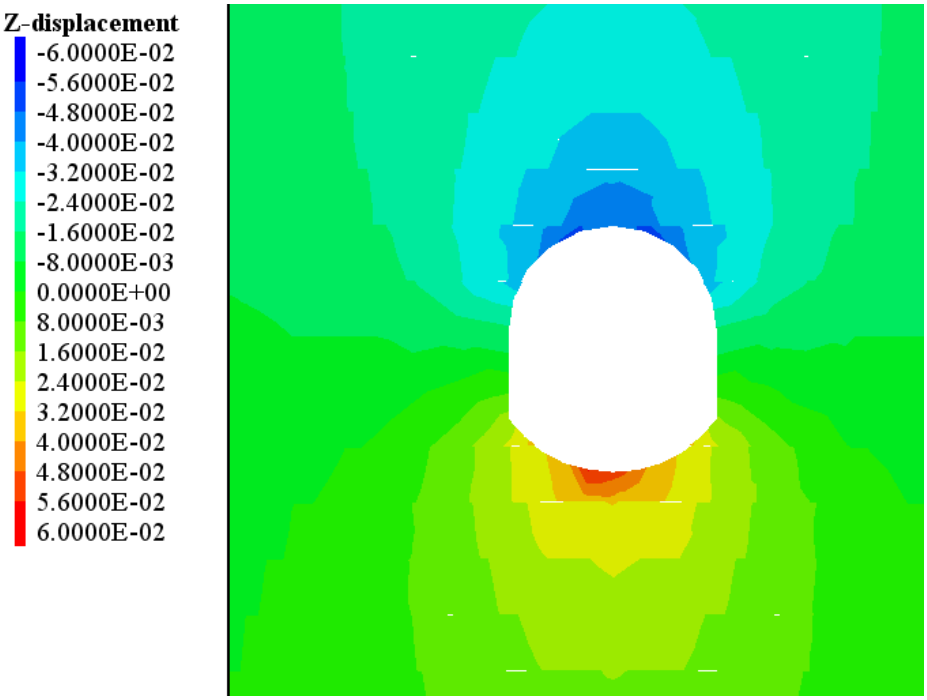

(b)

Figure 6.6: Vertical deformation distribution contours around the excavations for (a) HS and (b) IA tunnels (unit: m)

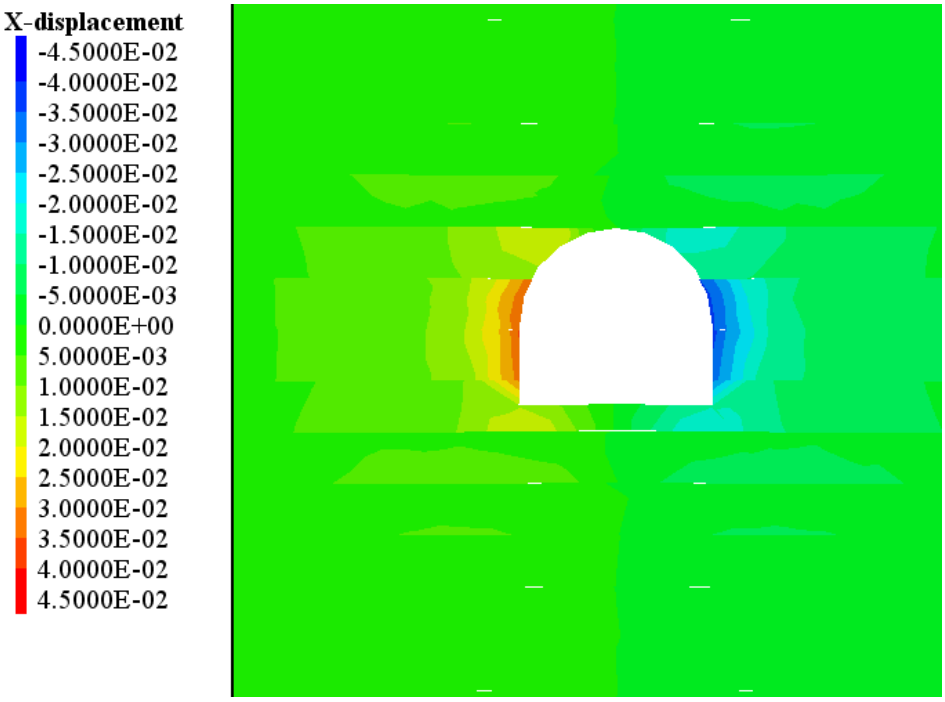

(a)

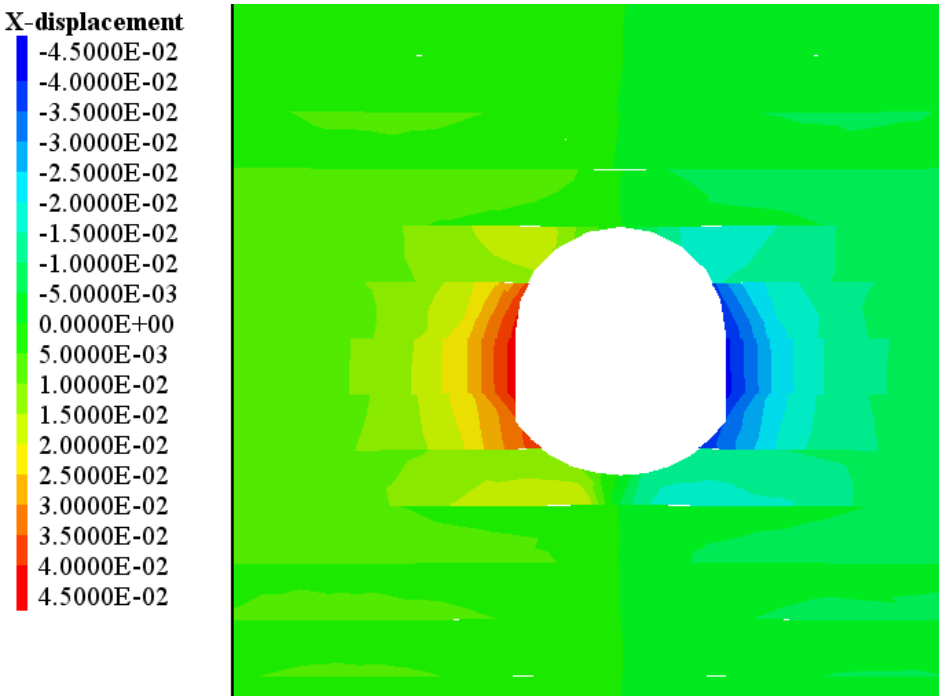

(b)

Figure 6.7: Horizontal deformation distribution contours around the excavations for (a) HS and (b) IA tunnels (unit: m)

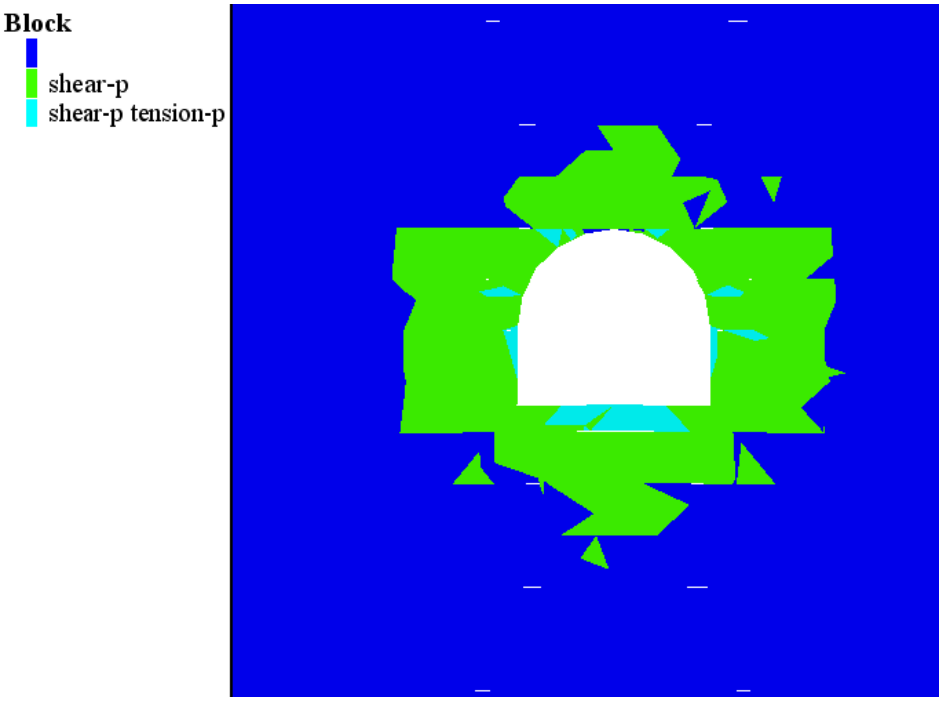

(a)

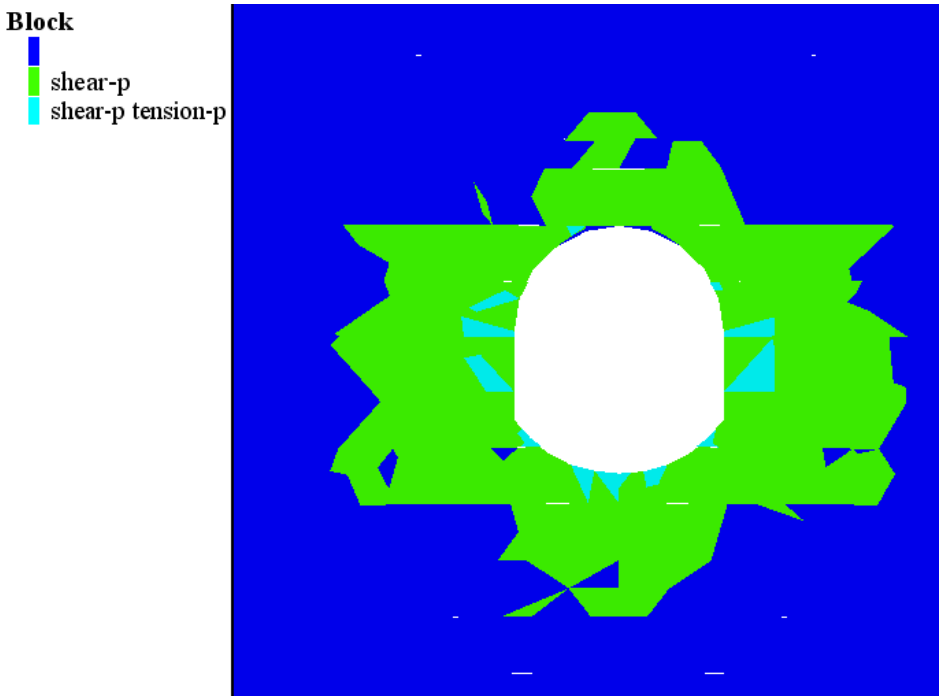

(b)

Figure 6.8: Failure flags around the excavations for (a) HS and (b) IA tunnels

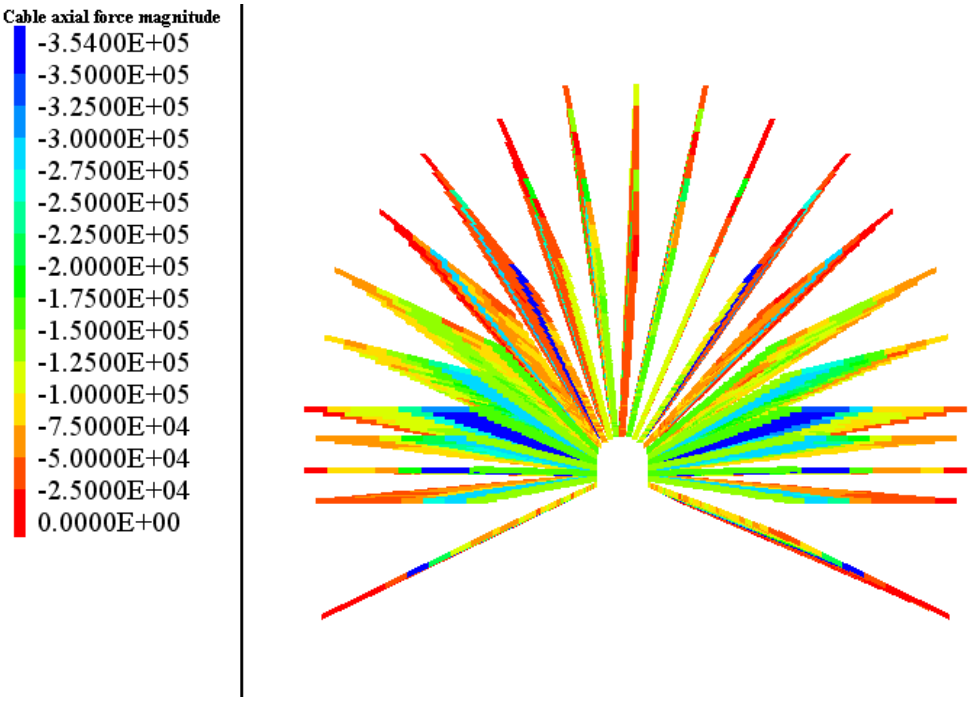

(a)

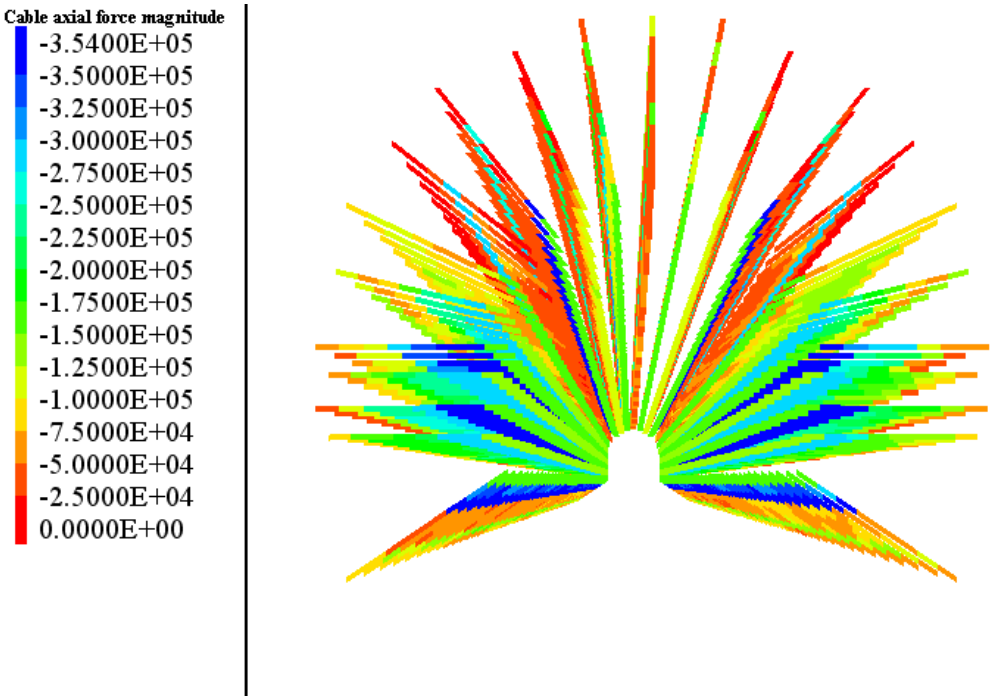

(b)

Figure 6.9: Axial force distributions for segments in the cables of (a) HS tunnel and (b) IA tunnel (unit: N)

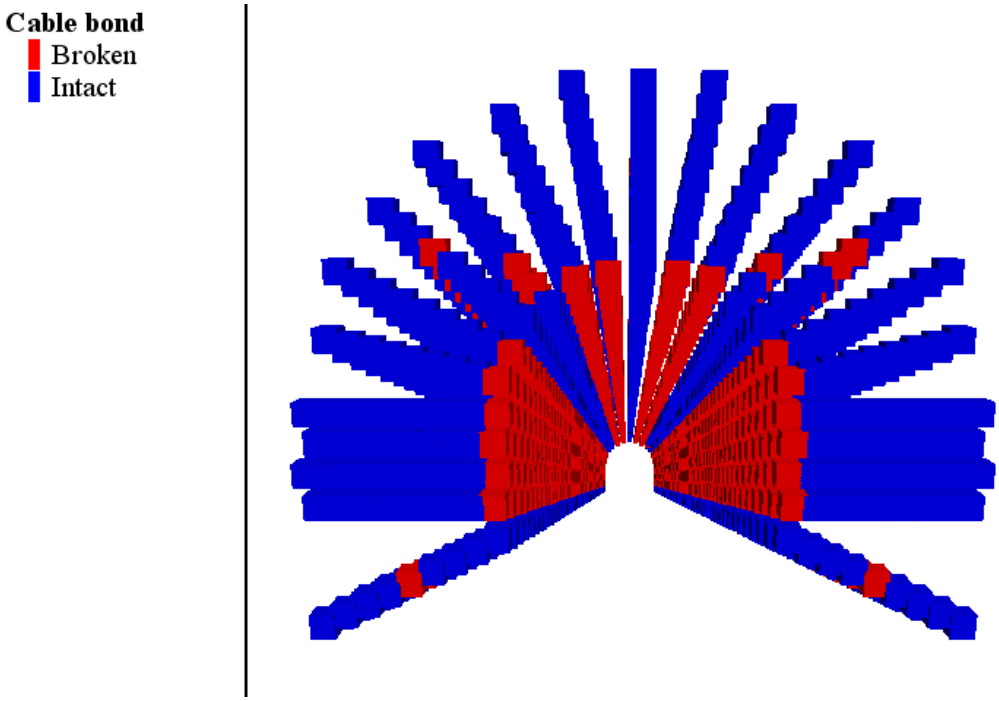

(a)

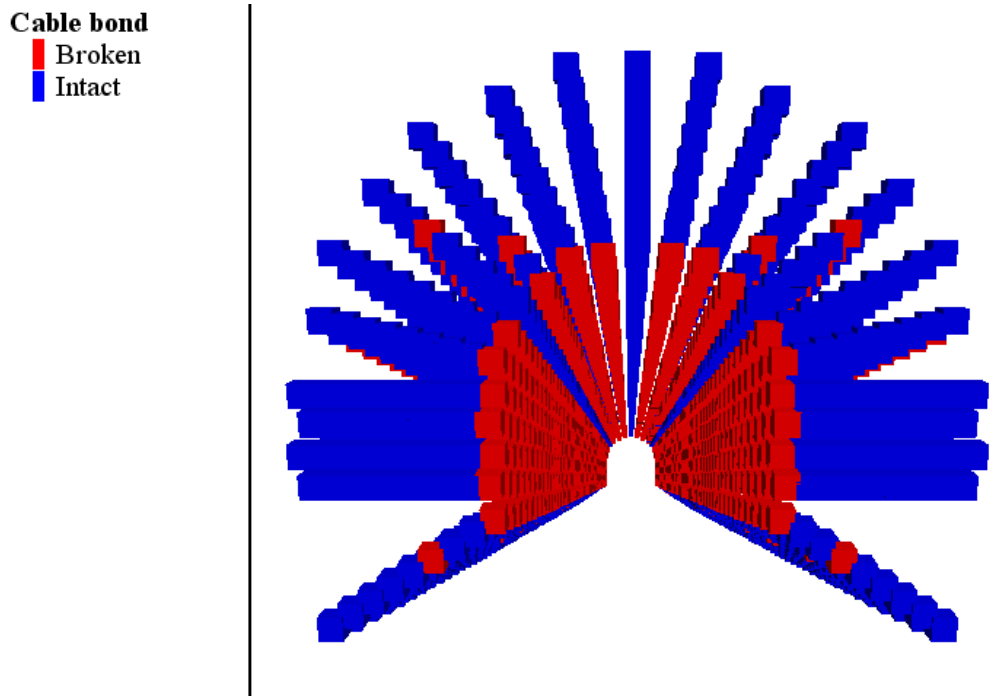

(b)

Figure 6.10: Grout bond failure statuses for segments in the cables of (a) HS tunnel and (b) IA tunnel

In addition to Fig. 6.3, figures 6.11 and 6.12 graphically present the information and trends seen in tables 6.1 to 6.4. The effect of method of support installation – instantaneous or stress relaxation is apparent from these figures. Figure 6.3 indicates that the method of support installation has little to no bearing on the deformations in the tunnels. However, the effect is significantly more pronounced in the behavior of the supports. Overall, the deformations are an inverse function of rock mass strength, as one would expect. As the rock mass strength decreases, the deformations increase. It can also be seen that the deformations follow the increasing trend of wall<roof<floor until about 37% normalized strength after which the wall and roof deformations are nearly the same at lower normalized strength values.

Figure 6.11 shows the cable FS expressed as a function of the normalized rock mass strength. It may be noted that some of the curves have been truncated to a FS of 3.0 to provide better resolution in the lower rock mass strength regions. The percentage values at the truncation represent the normalized rock mass strength at these values. The overall behavior between the first and second supports is similar for both support installation procedures. The support FS are direct functions of rock mass strength in that they increase as the rock mass strength increases. The first support has a lower FS than the second support until 50% normalized rock mass strength and the trend reverses after this. This indicates uneven load sharing between the two supports. The second support takes lesser loads until about 50% strength after which it starts taking more loading. For a given normalized rock mass strength, the instantaneous support procedure predicts lower FS than the stress relaxation. For instance, the instantaneous support predicts a FS of 1.0 for the first support for normalized strengths of 45% and below whereas the stress

relaxation procedure predicts FS of 1.0 for normalized strengths of 25% or lower. This is because the stress relaxation procedure accounts for the stress redistributions that the rock mass undergoes during its unsupported stand up time. Hence, the stress relaxation procedure estimates more plausible support FS and grout failure values, providing a better picture of the rock and support statuses.

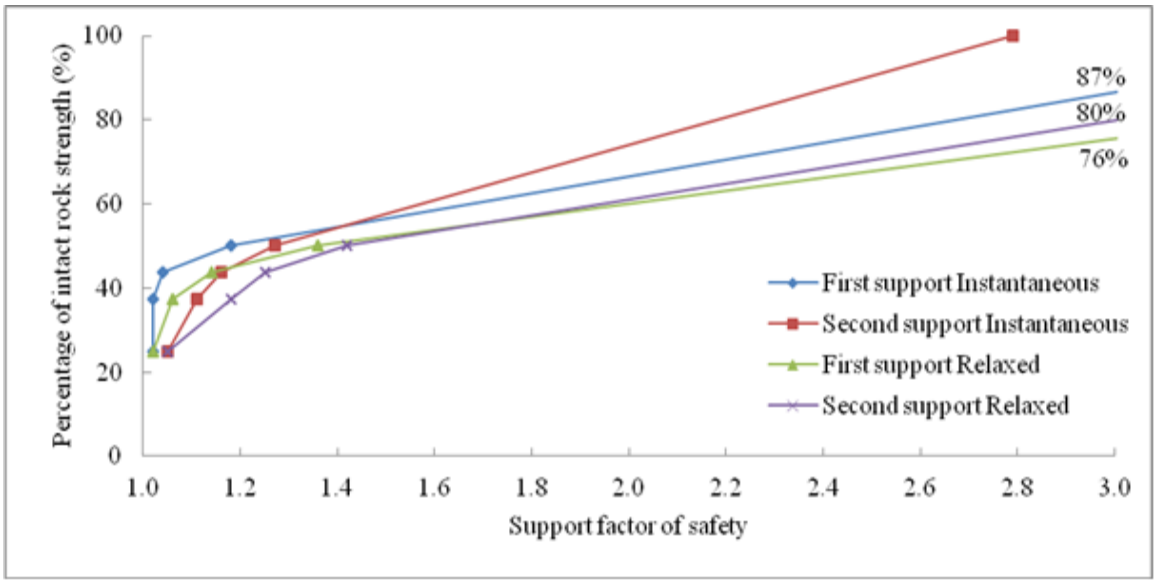

(a)

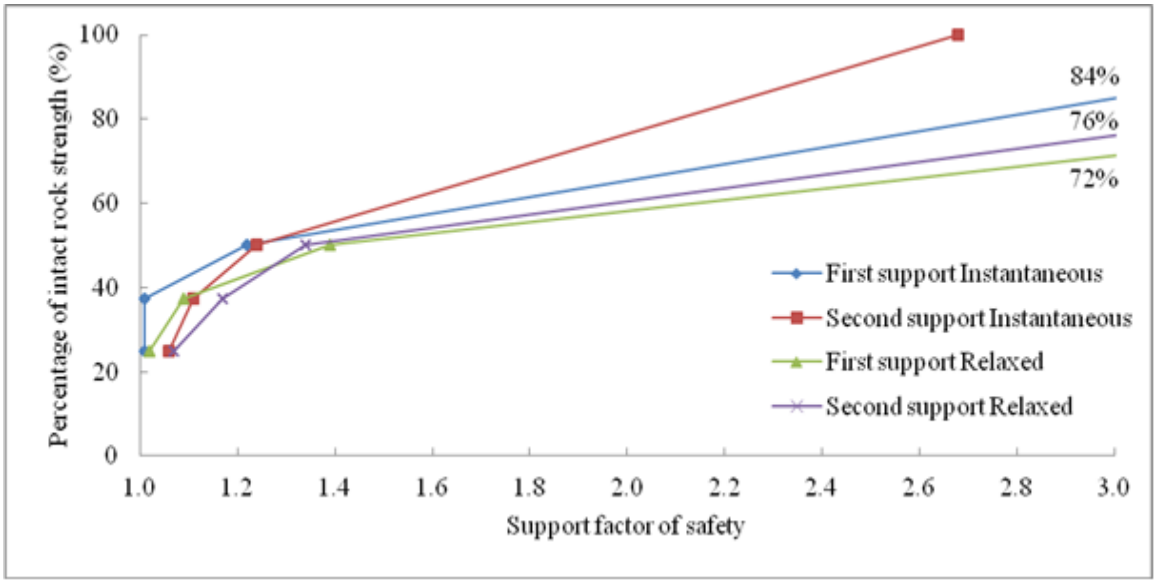

(b)

Figure 6.11: Cable FS expressed as a function of normalized rock mass strength for (a) HS tunnel and (b) IA tunnel

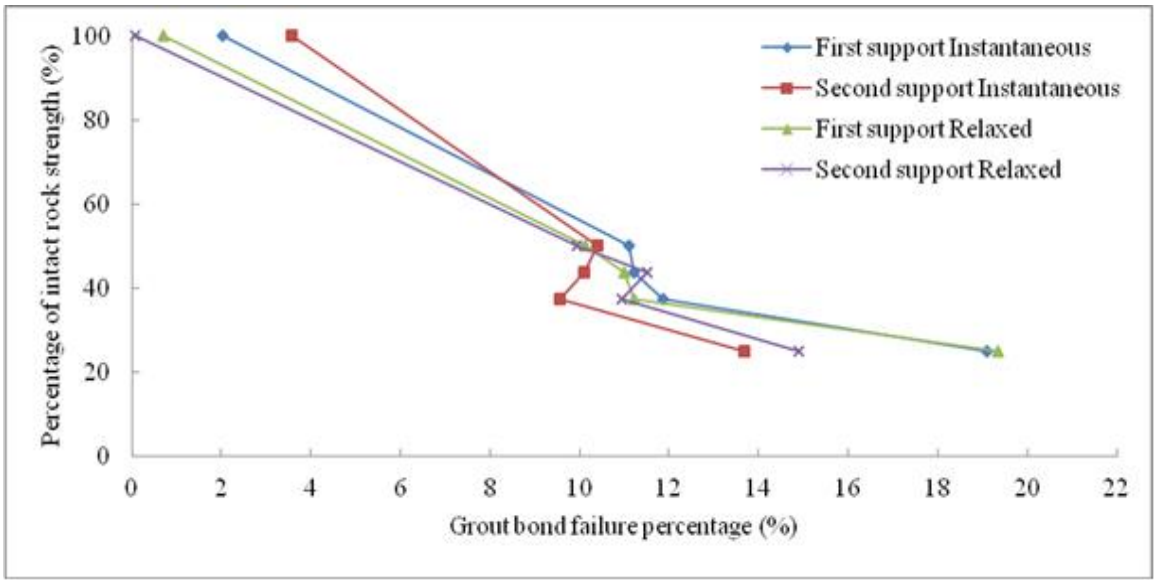

(a)

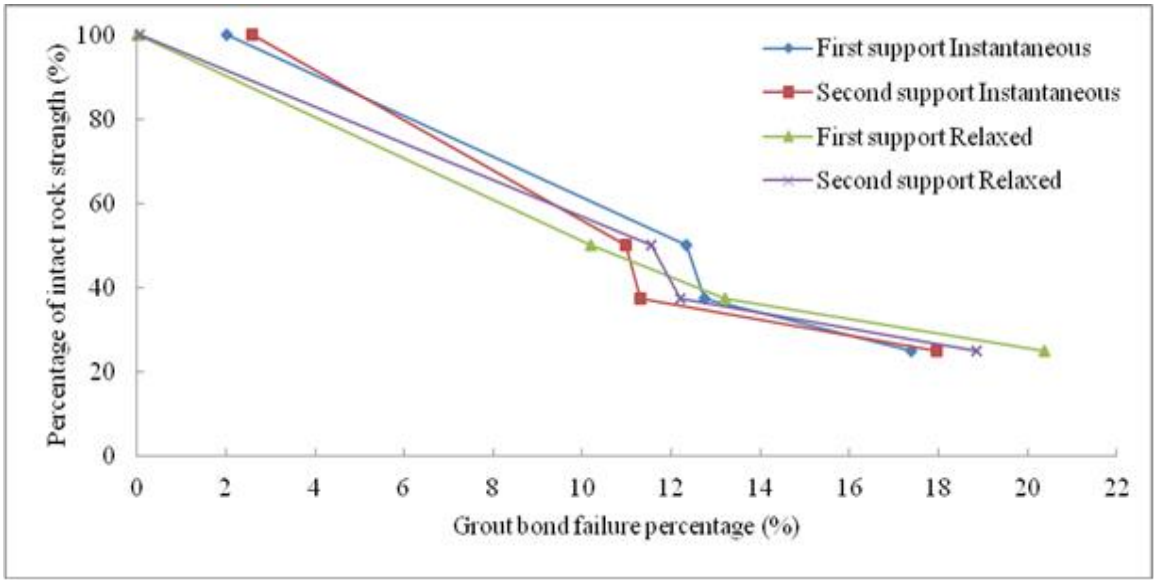

(b)

Figure 6.12: Grout bond failure percentages expressed as a function of normalized rock mass strength for (a) HS tunnel and (b) IA tunnel

Fig. 6.12 indicates inverse trends for the grout failures which increase with decreasing rock mass strengths. Similar to the FS, the grout failure estimates are higher and more conservative for the instantaneous support procedure as compared to the stress relaxation. Since the grouts have been divided as failures for the first and second supports, there exists a possibility that grout failure trends can depend on the load sharing between supports. While an overall decreasing trend can be observed, local trends may be distorted to reflect the uneven load sharing between the supports. This is also observed in the form of an anomaly in the trend between 50% and 37.5% rock mass strengths in Fig. 6.12. The calibrated HS and IA models have then been used to perform analyses listed in table 5.2 to study the effect of supporting on tunnel stability through tunnel deformation and support stability proxies.

6.4. Effect of rock supports on tunnel stability

The results from the analyses tabulated in table 5.2 are presented in table 6.6. Quickly browsing through the size of yield zones in table 6.6 reveals that the size of yield zones is very similar to the length of cables being used in the mine, and is even larger than the cable lengths in some cases. This opens up the possibility that the cables may not have sufficient surface area to ensure proper anchoring in the intact portion of the rock especially if most of the cable is coupled with failed/fractured rock. Hence, it was decided to carry out further analyses using longer bolts of 3.5 m and 4.0 m lengths for the first and second supports respectively. The comprehensive results are provided in table 6.7 and graphically expressed in figures 6.13 through 6.15.

Table 6.6: Results of analyses carried out on the calibrated model

Case	Deformation (mm)			Factor of safety		Grout bond failure (%)		Yield zone (m)		
	Roof	Wall	Floor	First support	Second support	First support	Second support	Roof	Wall	Floor
1-HS Unsupported	34.5	30	42.5					2.1	2.3	2.6
2-HS, I, Normal	32.5	27	41	1.04	1.16	11.22	10.10	2	2.3	2.6
3-HS, I, Floor	32	27	36.8	1.08	1.12	13.52	14.54	2	2.1	2.5
4-HS, SR, Normal	31.9	26.6	39.3	1.14	1.25	11.01	11.5	1.5	2	2.1
5-HS, SR, Floor	31.8	27	36.8	1.18	1.22	10.17	11.08	1.5	2	1.5
6-IA Unsupported	45	47	52					2.1	3.2	2.6
7-IA, I, Normal	42	41	50.5	1.01	1.11	12.73	11.31	2	3.2	2.7
8-IA, I, Floor	41.5	40	47	1.02	1.09	12.20	11.40	2	3	2.2
9-IA, SR, Normal	42.5	42	51	1.09	1.17	13.20	12.20	1.5	2.5	2.5
10-IA, SR, Floor	42.5	41.5	46.8	1.05	1.13	16.00	12.30	1.5	2.6	2

I-Instantaneous supporting, SR-Stress relaxation

Table 6.7: Results of analyses carried out using longer bolts of 3.5 m and 4.0 m as first and second supports

Case	Deformation (mm)			Factor of safety		Grout bond failure (%)		Yield zone (m)		
	Roof	Wall	Floor	First support	Second support	First support	Second support	Roof	Wall	Floor
HS, I	32	26.5	36	1.17	1.21	7.70	8.30	2	2.1	2.5
HS, SR	31.5	26	36.8	1.34	1.31	6.00	7.00	1.5	2	1.5
IA, I	41.4	39.7	46.4	1.07	1.09	7.78	8.35	1.9	2.8	2
IA, SR	42	41	46.6	1.12	1.12	7.62	7.15	1.2	2.5	1.7

I-Instantaneous supporting, SR-Stress relaxation

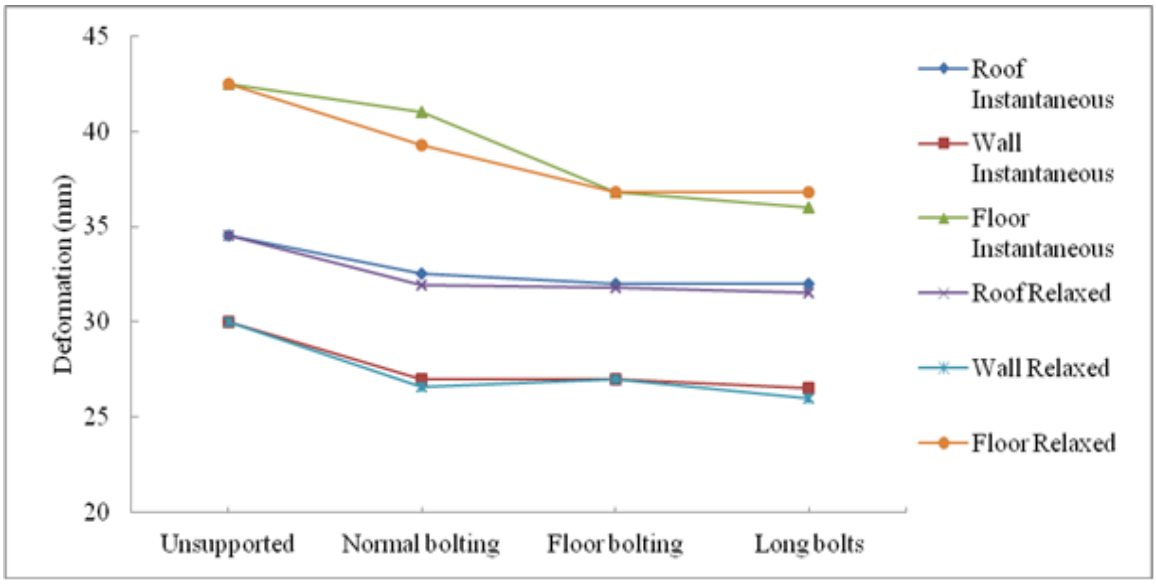

(a)

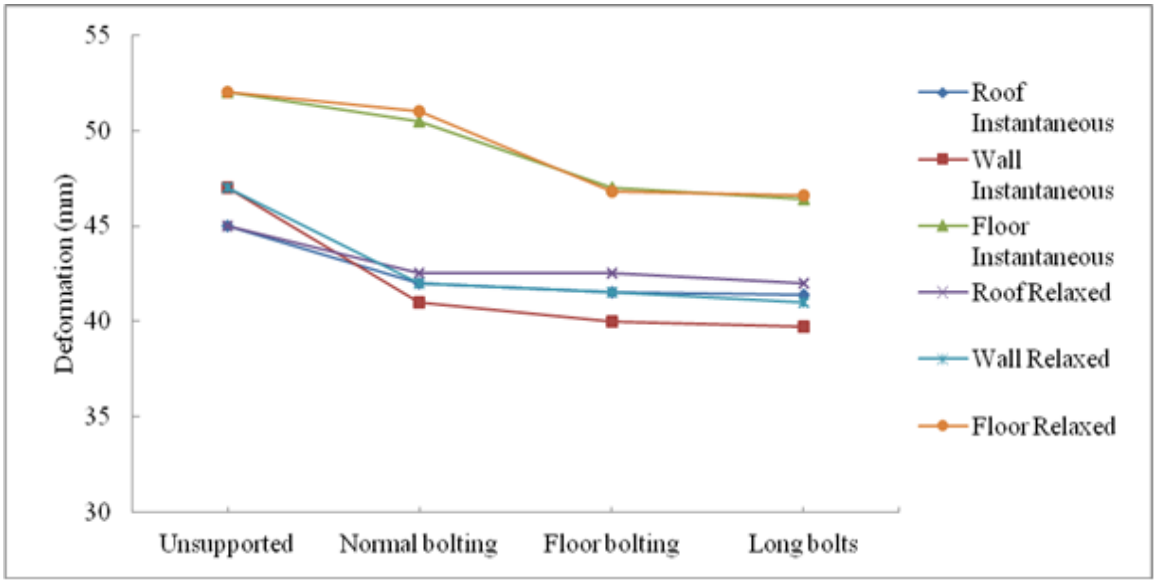

(b)

Figure 6.13: Effect of different bolting configurations on deformation for (a) HS tunnel and (b) IA tunnel deformations

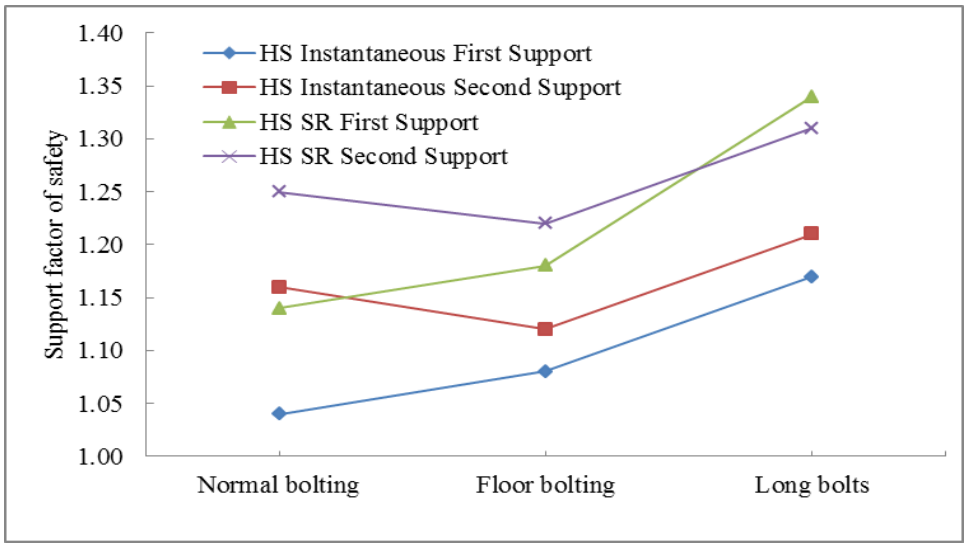

(a)

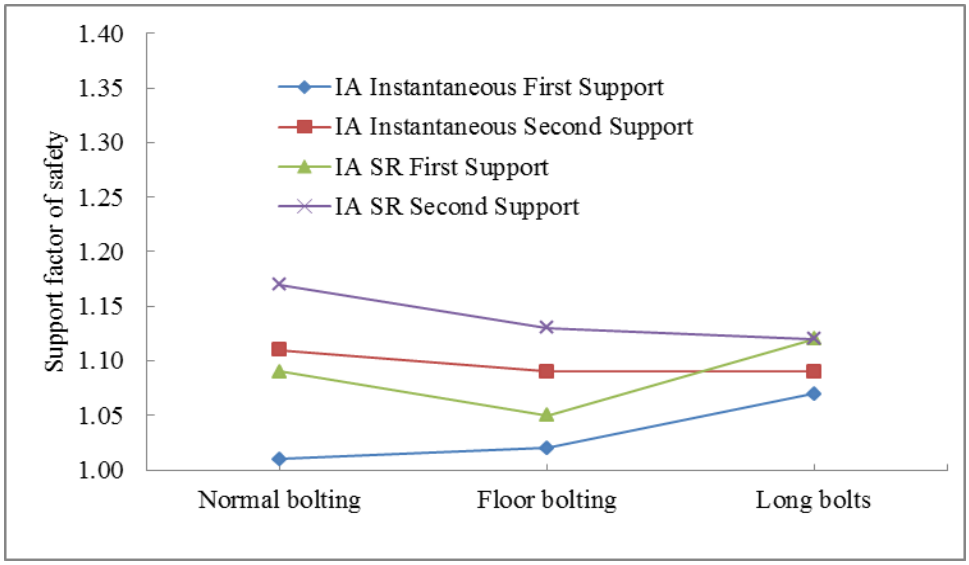

(b)

Figure 6.14: Effect of different bolting configurations on cable FS for (a) HS tunnel and (b) IA tunnel

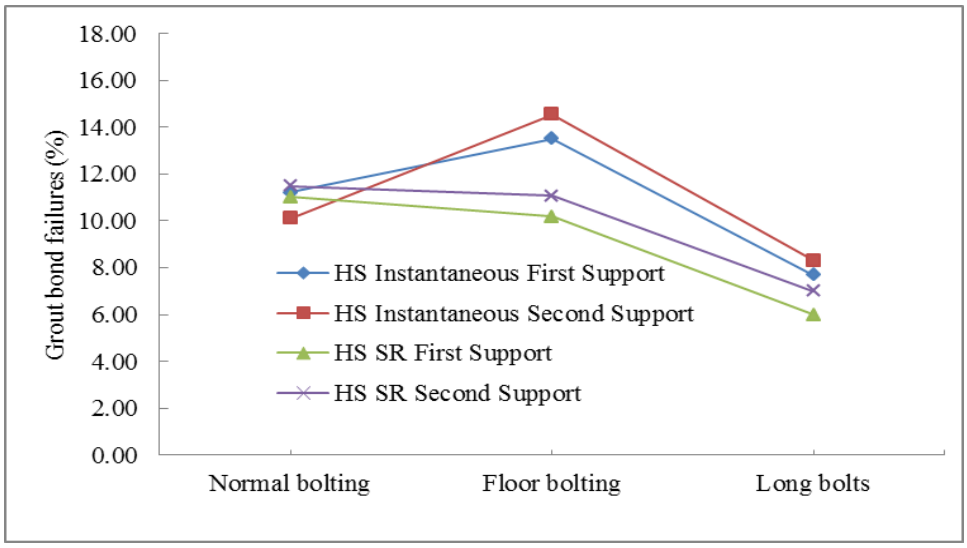

(a)

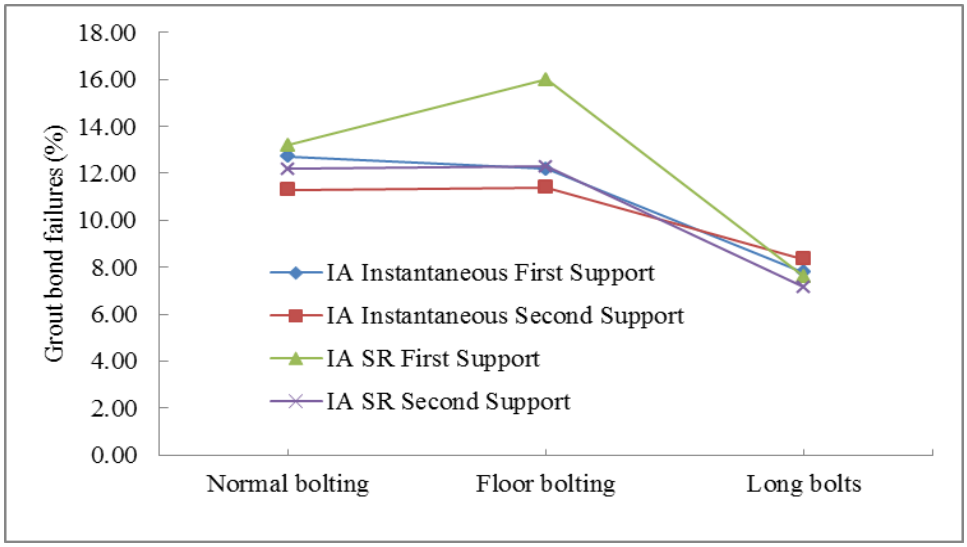

(b)

Figure 6.15: Effect of different bolting configurations on grout failures for (a) HS tunnel and (b) IA tunnel

It can be seen from Fig. 6.13 that the supports help reduce tunnel deformations. Compared to the unsupported condition, normal bolting on the roof and walls is seen to reduce deformations by up to 15%. However, it has moderate-low effect on the floor deformations. However, floor bolting along with roof and wall bolting is seen to reduce floor deformations by up to 12% in the HS and 10% in the IA tunnel. Longer bolts are seen to not affect the deformations significantly. It can, however, be seen from table 6.7 that longer bolts have helped reduce the size of the yield zone as compared to cases 3, 5, 8 and 10 in table 6.6. The effect of cable length is also pronounced in the increased cable FS, reduced grout failures and better load sharing as seen in figures 6.14 and 6.15. In the HS tunnel, the use of longer bolts has improved the support FS. The slightly lower FS for the second support, after floor bolting, as compared to normal bolting indicates possible instabilities in the floor. Another reason for this behavior could be the uneven load sharing between the supports. In the IA tunnel, floor bolting does not significantly change the support FS and the use of longer bolts is seen to greatly improve load sharing between the supports as seen from their similar FS values. As previously explained, the use of stress relaxation or delaying support installation provides more realistic FS numbers when compared with instantaneous supporting. This allows the user to estimate a range for the support FS values, between an average (stress relaxation) and a lower limit (instantaneous supporting) for the system FS.

In case of the grout failures in figure 6.15, floor bolting either causes no change in grout failures or increases the grout failures. This trend is observed in both tunnels. Using longer bolts, however, is seen to greatly improve (reduce) and localize grout failures. Similar to the FS, using both instantaneous and delayed support installation procedures

can provide useful ranges for grout failure values as between more likely and more conservative estimates. In subsequent analyses, only the stress relaxation procedure has been used since it provides more insight into the support behavior.

6.5. Tunnel closure strains

Since the two tunnels studied have different cross-sectional areas, their deformations cannot be compared directly. To normalize them, the closure strains have been estimated (Table 6.8) and plotted as a function of normalized rock mass strengths in figure 6.16. Since the two supporting methods provide similar deformations, the closure strains have not been separately plotted for them. Table 6.8 and figure 6.16 show that, for a given normalized rock mass strength, the HS tunnel has a slightly lower horizontal closure strain than the IA tunnel, with a difference of less than 0.25%. However, its vertical closure strain is significantly higher than that of the IA tunnel especially for the lower normalized rock mass strength values (~1% difference in closure strains). The fact that the mine experiences significant floor heaving and that the IA tunnel has lower vertical closure strain than the HS tunnel despite having a 30% higher cross-sectional area indicates that the IA tunnel may be a better performer under the existing geo-mining conditions at the site being studied.

Table 6.8: Closure strains for the HS and IA tunnels

Rock mass strength as a percentage of intact strength (%)	Horizontal closure strain (%)		Vertical closure strain (%)	
	Horseshoe	Inverted arch	Horseshoe	Inverted arch
100	0.25	0.28	0.59	0.40
50	1.04	1.19	1.65	1.28
37.5	1.89	2.21	2.53	2.09
25	4.55	4.89	5.02	4.09

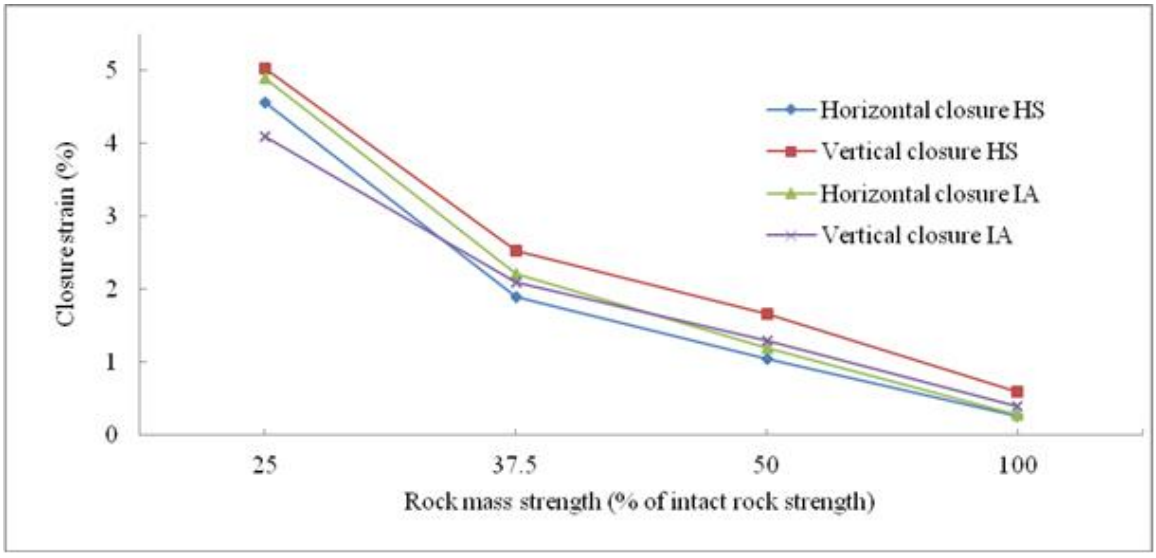

Figure 6.16: Closure strains for HS and IA tunnels expressed as a function of normalized rock mass strength

6.6. Parametric sensitivity studies

6.6.1. Variation of continuum mechanical parameters

The continuum mechanical properties that have been varied for the current study are the cohesion, internal friction angle, tensile strength and elastic modulus. Sensitivity studies have been performed to provide additional insights into the mechanical parameters of the rock mass and bedding planes. This has been done so as to direct the focus of future testing routines at the mine to concentrate on those parameters whose fluctuations most affect the rock mass stability. As described in section 5.5, the analyses have been done by varying the above mentioned parameters between +30% and -30% of their mean estimated values (Table 6.5), in increments of 15%. The results of this study have been expressed as variations in floor deformations and are given in figure 6.17.

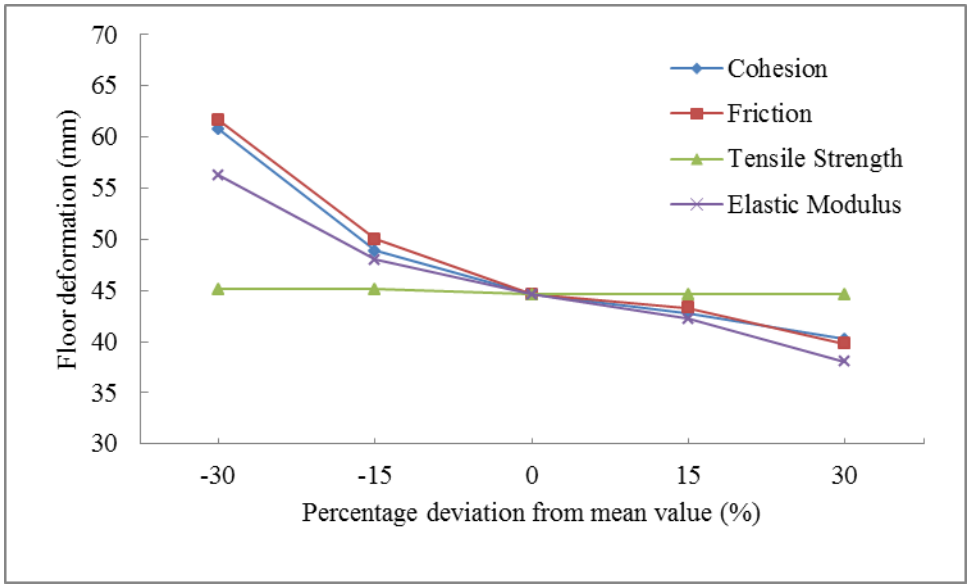

(a)

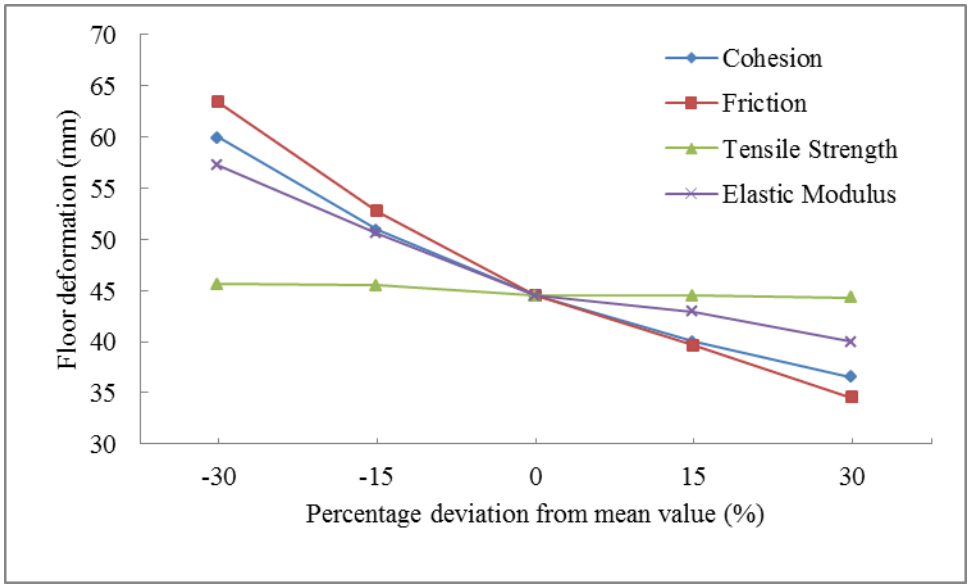

(b)

Figure 6.17: Floor deformation response to changes in continuum mechanical properties for (a) HS tunnel and (b) IA tunnel

It is seen from the figure that the tunnel floor for both HS and IA tunnels is most sensitive to changes in internal friction angle and closely followed by cohesion. When the cohesion and friction angle reduction is 30%, the deformations are seen to increase by up to 40%, and the deformations reduce by up to 12% when the values are increased by 30%. The plastic behavior of floor deformations is apparent from the non-linear nature of the curves in the -15% to -30% range. The elastic modulus is seen to also cause significant fluctuations in floor deformation. The overall trends show that an increase in cohesion, internal friction angle and/or elastic modulus stabilizes the rock mass and the deformations decrease. The tensile strength plays no overall role in the deformations. This makes sense since the tensile strength is a more important factor in the detection of failure rather than in the post-failure phase.

6.6.2. Variation of bedding plane mechanical parameters

Similar to the procedure for the continuum mechanical properties, the joint normal stiffness (JKN), joint shear stiffness (JKS) and the basic friction angle for the bedding plane have been varied from -30% to +30% in 15% increments. Figure 6.18 shows the response of floor deformation to changes in these parameters for the HS and IA tunnels.

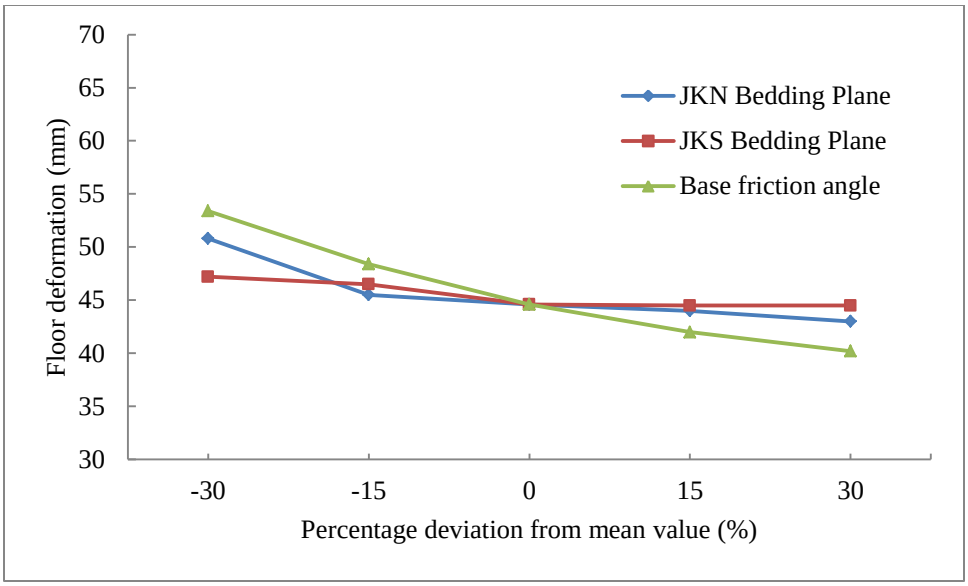

(a)

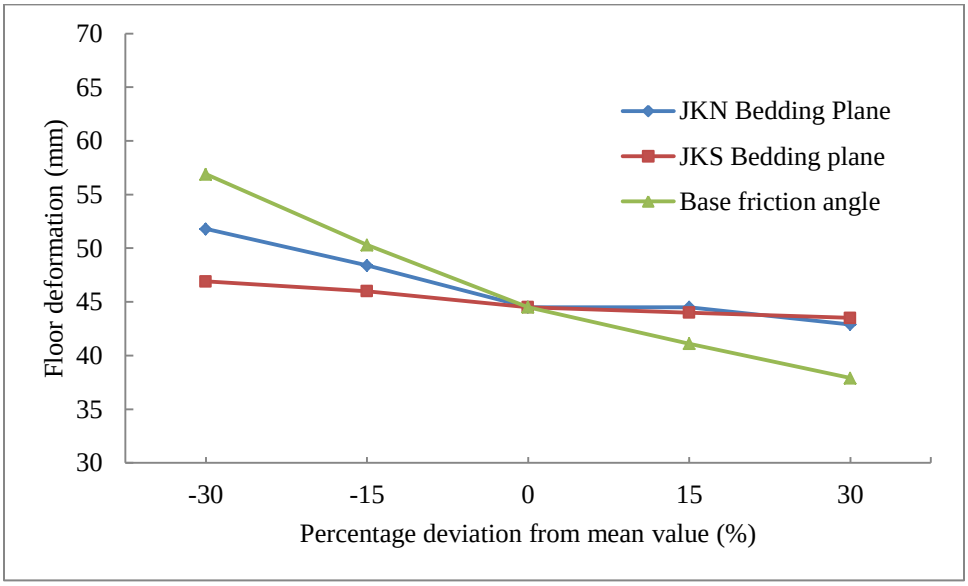

(b)

Figure 6.18: Floor deformation response to changes in bedding plane mechanical properties for (a) HS tunnel and (b) IA tunnel

It can be seen that the deformations are most sensitive to changes in the basic friction angle, followed by changes in joint normal stiffness. The joint shear stiffness is seen to not have much effect on the floor deformation. This is because the floor heave is principally governed by normal separation of the bedding plane and tensile beam bending. Wall deformations, on the other hand, can be expected to be significantly influenced by the shear stiffness. The effect of bedding plane friction angle is more prominent in the inverted arch tunnel floor deformation as compared to the horseshoe tunnel floor deformation, both for the strengthening and weakening cases. In the strengthening case, the deformation reduces more for the inverted arch tunnel (45 mm to 37 mm, 18%) than in horseshoe tunnel (45 mm to 41 mm, 9%). Conversely, in the weakening case, the inverted arch tunnel shows higher increase in deformation (45 mm to 57 mm, 27%) versus horseshoe tunnel (45 mm to 53 mm, 18%). The tables containing the actual data sets used to plot the figures shown in section 6.6.1 and 6.6.2 are given in Appendix B.

6.6.3. Variation of support mechanical parameters

The support response was studied by varying cable and grout strengths through the parameterization of cable diameter and grout uniaxial compressive strengths as discussed in section 5.5. In these analyses, the nominal support factor of safety (FS) for engineering design is taken to be 1.2 although this is subjective and may be site specific and regulated federally in various countries. Figures 6.19 through 6.22 show the variations of support FS and grout bond failures with changes in cable and grout strengths. The dotted horizontal line in figures 6.19 and 6.21 represents the nominal FS of 1.2.

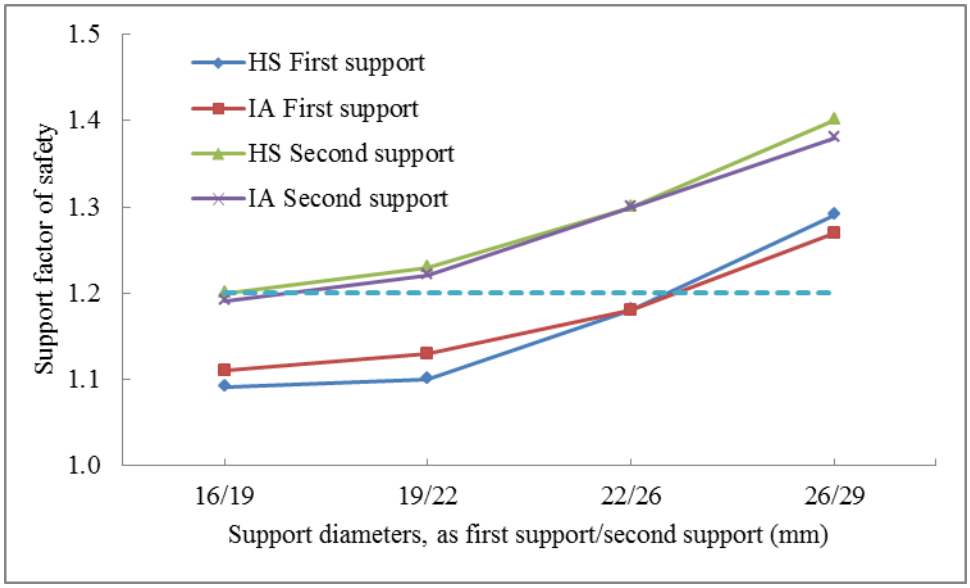

Figure 6.19: Support factors of safety as a function of cable diameters

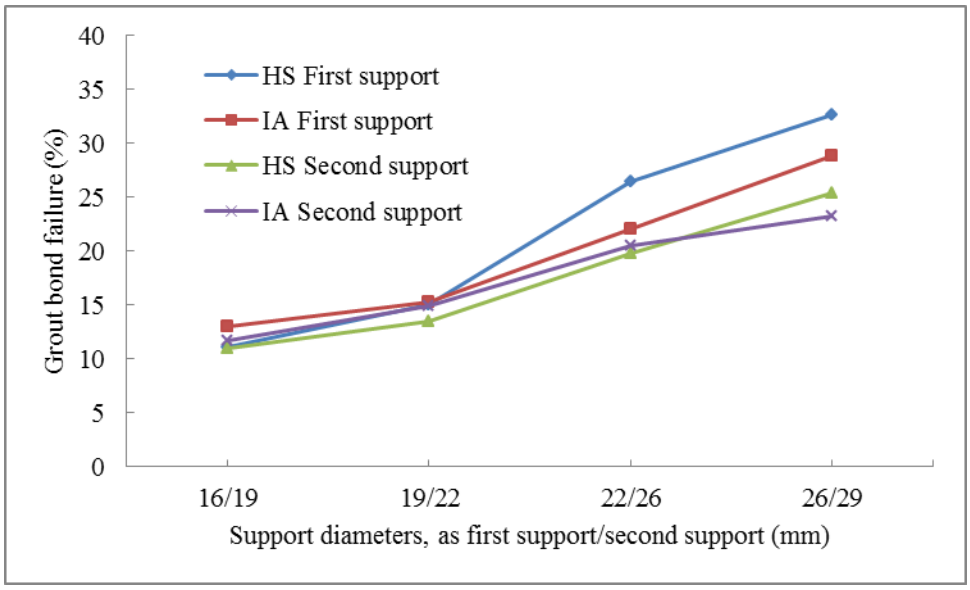

Figure 6.20: Grout bond failures as a function of cable diameters

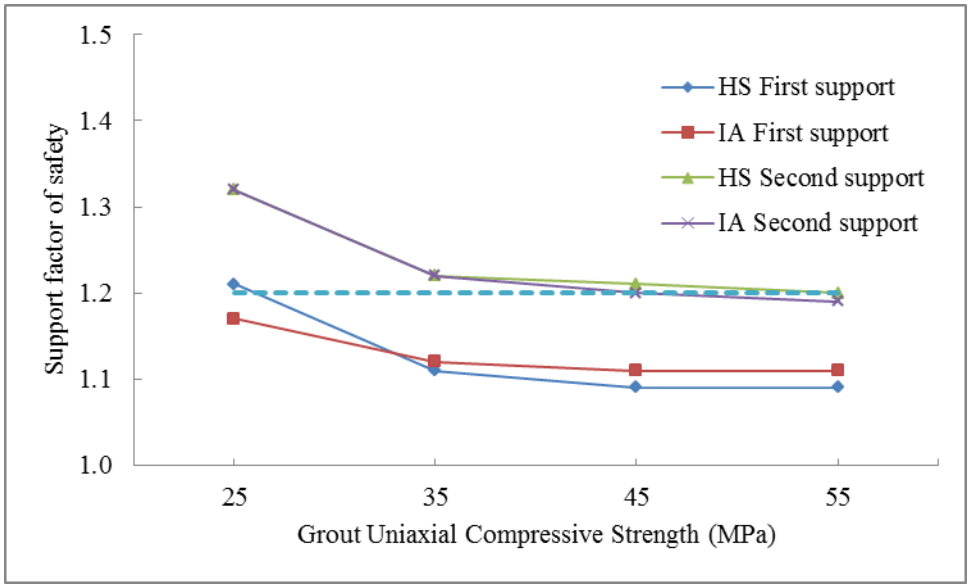

Figure 6.21: Support factors of safety as a function of grout uniaxial compressive strength

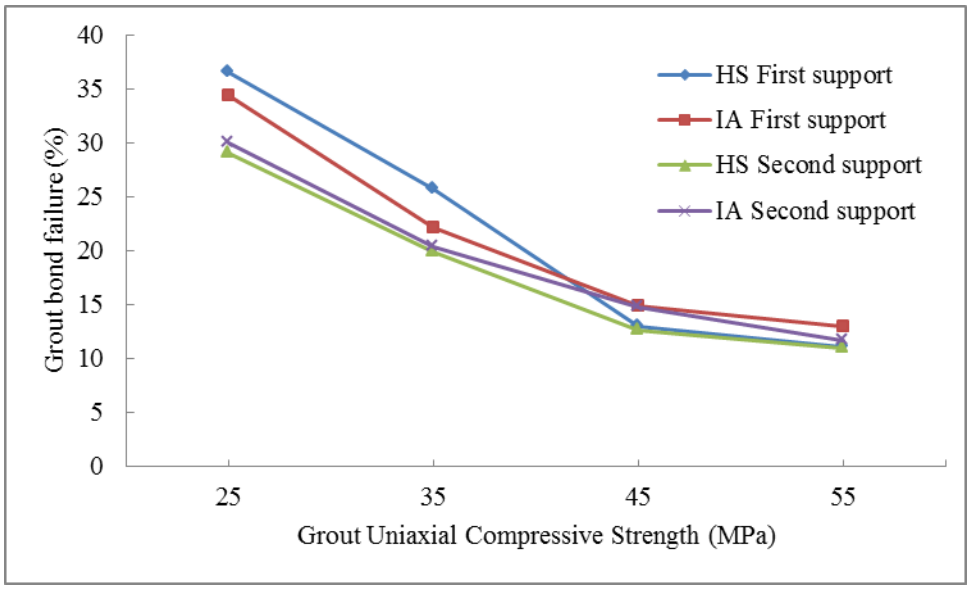

Figure 6.22: Grout bond failures as a function of grout uniaxial compressive strength

Since the support diameters were parameterized in pairs as first and second supports, the x-axis in figures 6.19 and 6.20 may be interpreted as the diameter of the first support/diameter of the second support. For instance, 16/19 indicates that the first support was 16 mm in diameter and the second support was 19 mm in diameter. Figure 6.19 shows that, for both HS and IA tunnels, as support diameters increase, the support FS increases. This is because thicker cables are stronger and less prone to tensile failures (snapping). It can also be seen that the support FS for the HS and IA tunnels are more or less similar across the spectrum of cable diameters. The support pair 22 mm/26 mm is seen to be the 'thinnest' pair with the FS for both supports being at least 1.2. Figure 6.20 shows the behavior of grout bonds with increasing cable strength/diameter. The grout bond failures are seen to increase as cable strength increases. This is because, as cables become stronger and less prone to tensile failures, the failures may occur through grout shear and slipping would emerge as the governing mode of support failure.

Figures 6.21 and 6.22 show the behavior of support FS and grout failures as functions of changing grout compressive strengths. These analyses have been carried out for the support pair 16 mm/19 mm. It can be seen that the trends reverse in this case. As grout compressive strength increases (Figure 6.21), the support FS decreases. Parallelly, the grout bond failures also decrease (Figure 6.22). This is because, as the grout is strengthened, the failure mode is now governed by the 'weaker' cables and cable tensile failures dominate. It can be seen from figure 6.21 that for the support pair 16 mm/19 mm, grout compressive strengths above 25 MPa reduce the FS to 1.2 or less. However, the reduction in support FS is very gradual and more or less constant. Hence, a trade-off between the slip (shear failure) and snap (tensile failure) of cable bolts is necessary to

arrive at an optimum compatibility system. Differential stiffnesses of the steel and grout can destabilize the system and increase proneness to one of the two modes of failures. Again, the overall trends are insignificantly different for the HS and IA tunnels. The raw numbers for the analyses carried out on the HS tunnel are presented in tables 6.9 and 6.10. Due to the similarity in results between HS and IA tunnels, the results are not presented for the IA tunnel. As one would expect, if either component of the support system – cable or grout, is strengthened, the deformations are seen to decrease across the roof, wall and floor of the tunnels. However, the size of yield zone is largely unaffected by the analyses.

Table 6.9: Results of variation of cable diameters for HS tunnel

Diameter (mm) – First/second support	Roof (mm)	Wall (mm)	Floor (mm)	Average FS		Grout bond failure (%)	
				1st Support	2nd Support	1st Support	2nd Support
16/19	36.5	32.1	44.6	1.09	1.2	11.11	10.92
19/22	36	31.1	44.1	1.1	1.23	15.03	13.42
22/26	35.4	30.4	43.8	1.18	1.3	26.4	19.77
26/29	34.9	29.1	43.5	1.29	1.4	32.63	25.42

Table 6.10: Results of variation of grout uniaxial compressive strengths for HS tunnel

Grout UCS (MPa)	Roof (mm)	Wall (mm)	Floor (mm)	Average FS		Grout bond failure (%)	
				1st Support	2nd Support	1st Support	2nd Support
25	37.1	32.5	44.6	1.21	1.32	36.6	29.08
35	36.8	32.3	44.5	1.11	1.22	25.7	19.87
45	36.7	32.1	44.3	1.09	1.21	12.98	12.57
55	36.5	32.1	44.6	1.09	1.2	11.11	10.92

CHAPTER 7: CONCLUSIONS AND RECOMMENDATIONS FOR FUTURE WORK

7.1. Conclusions

This thesis lays out numerical modeling studies performed on two tunnels, a horseshoe (HS) shaped and an inverted-arch (IA) shaped tunnel, driven in a coal-measure stratum in one of the deepest soft rock excavations in the world. Accurate 3-dimensional distinct element numerical models have been created using available data on the state of stress in the region, lithological and geological considerations, joint and intact rock properties, tunnel dimensions and support properties. The numerical models have been used to analyze the stability of the tunnels and supports in a variety of ways. Modeling has been carried out using two procedures – an instantaneous supporting method which installs the supports immediately after excavation, and a stress relaxation procedure developed in this research which accounts for the stress redistribution undergone by excavations during the stand-up time between tunnel drivage and support installation. A new procedure has also been developed to describe the state of the cable and grout for each support type, and all models are accompanied by these support status descriptions. The cable has been described through a factor of safety (FS) definition and the grout has been described through the calculation of failed grout bonds as a percentage of total grout bonds.

The created numerical models have been tested and validated for correctness of applied input parameters, and have been subsequently used in a back-analysis routine to calibrate the rock mass mechanical property values. This has been achieved through a

binary search based strength reduction approach using baseline intact rock and bedding plane mechanical property values, and a comparison against available field deformation monitoring datasets. The rock mass was found to have strength parameter values of approximately 35%-45% of intact rock strength in the region, using both excavation-support procedures. It was also found that, while the stress relaxation and instantaneous support procedures predict similar tunnel deformation values, they predict largely different values for the support parameters – the cable FS and grout bond failures. This allows a user to employ both methods to get a range of descriptive/quantitative values for the support behavior.

The calibrated models have further been analyzed by changing support configurations and lengths, to better understand the response of the tunnels to the existence (and a lack) of supports. It has been found that the tunnels undergo higher deformations and have larger fractured zones in the absence of supports and had the lowest overall deformation and size of fractured zones in the presence of supports in the roof, wall and floor. It was also found that the existing supports (2.2 m, 2.5 m) were approximately as long as the size of the fractured zone around the tunnels, indicating insufficient room for proper rock-support coupling. Hence, analyses have been carried out using longer bolts (3.5 m, 4.0 m) to study their effect on the tunnel stability. It has been found that while the longer supports did not significantly change the tunnel deformations, they helped reduce the size of the failed/fractured zone, and they also had ‘safer’ cable FS and lower grout failures.

In the next stage, a comparative study between the two tunnel shapes was performed through the analyses of normalized deformations in the form of closure strains. It was found that, for the existing geo-mining conditions where the tunnels at the site are

undergoing significant floor heaving, the IA tunnel had lower vertical closure strains than the HS tunnel. This, despite the IA tunnel having a 30% higher cross-sectional area, appeared to indicate that the IA tunnel may be better suited to handle the floor instabilities which are part of the existing geo-mining conditions.

The thesis concludes with parametric studies performed on the mechanical properties of the continuum and those of the explicitly introduced bedding planes around the tunnels, and optimization studies performed on the cable bolts used in the modeling studies. The parametric studies on the continuum mechanical properties showed that, for both tunnels, the rock mass deformation is most sensitive to changes in cohesion and internal friction angle, followed by changes in elastic modulus of the equivalent continuum. The tensile strength was not found to influence the deformations in any way since it is a failure indicator or criterion. Parameterization of bedding plane deformability and frictional properties indicated that the tunnel deformations are most sensitive to changes in bedding plane basic friction angle, followed by the joint normal stiffness (JKN) and to some extent, the joint shear stiffness (JKS). This lays out guidelines for future rock testing routines at the mine site. The support optimization studies aimed at linking cable diameters (and in turn, the steel strengths) and grout strengths to the cable FS and grout failures. The studies illustrated the importance of ensuring stiffness compatibility between the steel and grout to ensure that neither tensile failures of steel, nor shear failures of grout dominate.

Supplementary data including raw deformation data, output data from parametric studies and abstracts from accepted/submitted manuscripts resulting from this research are available in Appendices A-C.

7.2. Recommendations for future work

Future work on this research could focus on using other constitutive models for representing the continuum and the discontinuum, such as the strain-softening model for the continuum and continuously yielding joint model for the bedding planes to observe post-failure behavior. Additionally, the study could benefit from using creep constitutive models to gain insight on long-term time dependence of the rock mass. Extensive field instrumentation and real-time monitoring of tunnel stability, in addition to thorough in-situ stress measurements, fracture mapping and in-situ mechanical property measurements would provide more reliable input properties for the modeling. Finally, modeling performed on the entire mine, including tunnel networks and shafts would provide significant insight into the global behavior of the rock mass.

REFERENCES

Aydan, Ö., Ulusay, R., & Tokashiki, N. (2015). Rock Mass Quality Rating (RMQR) System and its Application to the Estimation of Geomechanical Characteristics of Rock Masses. *Engineering Geology for Society and Territory-Volume 6*, 769-772. Springer International Publishing.

Barla, G., & Barla, M. (2000). Continuum and discontinuum modelling in tunnel engineering. *The Mining Geological Petroleum Engineering Bulletin*, *12*, 45–57.

Barton, N., Lien, R., & Lunde, J. (1974). Engineering classification of rock masses for the design of tunnel support. *Rock mechanics*, *6*(4), 189-236.

Beer, G. (2010). Application of the Boundary Element Method to the Simulation in Tunneling. C*adernos de Engenharia de Estruturas*, 1–12.

Bieniawski, Z. T. (1974). Engineering classification of jointed rock masses. discussions of paper by ZT Bieniawski, trans. s. afr. instn. civ. engrs. v15, n12, Dec. 1973, and authors reply: 4F, 4T, 39R. Trans. S. Afr. Instn. Civ. Engrs. V16, N7, July, 1974, P239–254. *International Journal of Rock Mechanics and Mining Sciences & Geomechanics Abstracts*, *11*(12), p. 244). Pergamon.

Bieniawski, Z. T. (1989). *Engineering rock mass classifications: a complete manual for engineers and geologists in mining, civil, and petroleum engineering*. John Wiley & Sons.

Bizjak, K. F., & Petkovšek, B. (2004). Displacement analysis of tunnel support in soft rock around a shallow highway tunnel at Golovec. *Engineering Geology*, *75*(1), 89-106.

Brady, B., & Bray, J. (1978). The boundary element method for determining stresses and displacements around long openings in a triaxial stress field. *International Journal of Rock Mechanics and Mining Sciences & Geomechanics Abstracts*, *15*(1), 21–28.

Cai, F., Yang, Q.Q., Su, Z.M., (2013). DDA simulations of large landslides triggered by the Wenchuan. In: *11th International Conference on Analysis of Discontinuous Deformation (ICADD11)*, Fukuoka, Japan, pp. 201–206.

Cai, M. (2011). Rock mass characterization and rock property variability considerations for tunnel and cavern design. *Rock mechanics and rock engineering*, *44*(4), 379-399.

Cai, M., Kaiser, P. K., Uno, H., Tasaka, Y., & Minami, M. (2004). Estimation of rock mass deformation modulus and strength of jointed hard rock masses using the GSI system. *International Journal of Rock Mechanics and Mining Sciences*, *41*(1), 3-19.

Cardarelli, E., Marrone, C., & Orlando, L. (2003). Evaluation of tunnel stability using integrated geophysical methods. *Journal of Applied Geophysics*, *52*(2), 93-102.

Cecil, O. S. (1970). Shotcrete support in rock tunnels in Scandinavia. *Civil Engineering*.

Celada, B., Tardáguila, I., Varona, P., Rodríguez, A., & Bieniawski, Z. T. (2014). Innovating Tunnel Design by an Improved Experience-based RMR System. In *World Tunnel Congress. Proceedings… Foz do Iguaçu, Brazil* (p. 9).

Chen, B. R., Feng, X. T., Ming, H. J., Zhou, H., Zeng, X. H., Feng, G. L., & Xiao, Y. X. (2012b). Evolution law and mechanism of rock burst in deep tunnel: time delayed rock burst. *Chin J Rock Mech Eng*, *31*(3), 561-569. (In Chinese)

Chen, C. N., Huang, W.-Y., & Tseng, C.-T. (2011). Stress redistribution and ground arch development during tunneling. *Tunnelling and Underground Space Technology*, *26*(1), 228–235. doi:10.1016/j.tust.2010.06.012

Chen, H., Qi, H., Long, R., & Zhang, M. (2012a). Research on 10-year tendency of China coal mine accidents and the characteristics of human factors. *Safety science*, *50*(4), 745-750.

Cheng, C., & Sun, X. M. (2010, August). Brittle Failure Due to Excavation Induced Stress Change-a Case Study of Jinping II Hydropower Station. In *International Symposium on In-Situ Rock Stress*. International Society for Rock Mechanics.

Cheng, Y. M. (1998). Advancements and improvement in discontinuous deformation analysis. *Computers and Geotechnics*, *22*(2), 153–163. doi:10.1016/S0266-352X(98)00002-0

Chengping, Z., Limin, L., Haoran, S., & Dingli, Z. (2010). Numerical Analysis of Metro Tunneling-Induced Stratum Deformation and Settlement by Using FLAC3D. In *2010 International Conference on Intelligent Computation Technology and Automation* (pp. 817–820). IEEE. doi:10.1109/ICICTA.2010.218

China Coal Society Open Pit Mine Committee (2010) China Open Pit Coalmining Development Report (1914–2007). China Coal Industry Publishing House, Beijing

Chun, B. S., Ryu, W. R., Sagong, M., & Do, J. N. (2009). Indirect estimation of the rock deformation modulus based on polynomial and multiple regression analyses of the RMR system. *International Journal of Rock Mechanics and Mining Sciences*, *46*(3), 649-658.

Cichowicz, A., Milev, A. M., & Durrheim, R. J. (2000). Rock mass behaviour under seismic loading in a deep mine environment: implications for stope support. *Journal-South African Institute of Mining and Metallurgy*, *100*(2), 121-128.

Clough, R. W. (1958, November). Structural analysis by means of a matrix algebra program. In *Proceedings of the First Conference on Electronic Computation, American Society of Civil Engineers, Kansas City, MO* (pp. 109-132).

Clough, R. W. (1960, September). The finite element method in plane stress analysis. *In Proceedings of the Second ASCE Conference on Electronic Computations, Pittsburgh, PA*.

Clough, R. W. (1990). Original formulation of the finite element method. *Finite Elements in Analysis and Design*, *7*(2), 89-101.

Coggan, J., Gao, F., Stead, D., & Elmo, D. (2012). Numerical modelling of the effects of weak immediate roof lithology on coal mine roadway stability. *International Journal of Coal Geology*, *90*, 100-109.

Compiling Committee of China (2010) China Coal Industry Yearbook 2009. China Coal Industry Press, Beijing

Cording, E. J., & Deere, D. U. (1972). Rock tunnel supports and field measurements. North American Rapid Excavation and Tunneling Conference, Chicago 1972. In *Proceedings* (Vol. 1, pp. 567-600).

Cummings, R. A., Kendorski, F. S., & Bieniawski, Z. T. (1982). Caving rock mass classification and support estimation. *US Bureau of Mines Contract Report J, 100103*.

Cundall, P. A. (1971). A computer model for simulating progressive, large-scale movements in blocky rock systems. In *The International Symposium on Rock Mechanics* (Vol. 2, pp. 47–65).

Cundall, P. A. (1988). Formulation of a three-dimensional distinct element model—Part I. A scheme to detect and represent contacts in a system composed of many polyhedral blocks. *International Journal of Rock Mechanics and Mining Sciences & Geomechanics Abstracts*, *25*(3), 107-116.

Cundall, P. A., & Hart, R. D. (1985). *Development of generalized 2-D and 3-D distinct element programs for modeling jointed rock*. Itasca Consulting Group Inc Minneapolis, MN.

Cundall, P. A., & Hart, R. D. (1992). Numerical modelling of discontinua. *Engineering computations*, *9*(2), 101-113.

Cundall, P. A., & Strack, O. D. (1979). A discrete numerical model for granular assemblies. *Geotechnique*, *29*(1), 47-65.

Damjanac, B., & Cundall, P. (2016). Application of distinct element methods to simulation of hydraulic fracturing in naturally fractured reservoirs. *Computers and Geotechnics*, *71*, 283-294.

Dasgupta, B., Dham, R., & Lorig, L. J. (1995, January). Three dimensional discontinuum analysis of the underground powerhouse for Sardar Sarovar Project, India. In *8th ISRM Congress*. International Society for Rock Mechanics.

Deb, D., & Das, K. C. (2009). Extended finite element method (XFEM) for analysis of cohesive rock joint. *Journal of Scientific & Industrial Research*, *68*, 575-583.

Deere, D. U., Hendron, A. J., Patton, F. D., & Cording, E. J. (1966, January). Design of surface and near-surface construction in rock. In *The 8th US Symposium on Rock Mechanics (USRMS)*. American Rock Mechanics Association.

Deere, D. U., Peck, R. B., Parker, H. W., Monsees, J. E., & Schmidt, B. (1970). Design of tunnel support systems. *Highway Research Record*, (339).

Delisio, A., Zhao, J., & Einstein, H. H. (2013). Analysis and prediction of TBM performance in blocky rock conditions at the Lötschberg Base Tunnel. *Tunnelling and Underground Space Technology*, *33*, 131-142.

Eberhardt, E., Stead, D., Coggan, J., & Willenberg, H. (2003). Hybrid finite-/discrete-element modelling of progressive failure in massive rock slopes. In M. Handley & D. Stacey (Eds.), *10th Congress of the International Society for Rock Mechanics* (pp. 275–280). Johannesburg: The South African Institute of Mining and Metallurgy. Retrieved from http://www.eoas.ubc.ca/personal/erik/e-papers/03EE_ISRMCongress-Elfen.pdf

Elmo, D. (2006). Evaluation of a hybrid FEM/DEM approach for determination of rock mass strength using a combination of discontinuity mapping and fracture mechanics modelling, with particular emphasis on modelling of jointed pillars (Ph.D.). University of Exeter, Exeter UK.

Elmo, D., & Stead, D. (2010). An integrated numerical modelling–discrete fracture network approach applied to the characterisation of rock mass strength of naturally fractured pillars. *Rock Mechanics and Rock Engineering*, *43*(1), 3-19.

Elmo, D., Stead, D., Eberhardt, E., & Vyazmensky, A. (2013). Applications of finite/discrete element modeling to rock engineering problems. *International Journal of Geomechanics*, *13*(5), 565-580.

Fairhurst, C. (2003). Stress estimation in rock: a brief history and review. *International Journal of Rock Mechanics and Mining Sciences*, *40*(7), 957-973.

Fairhurst, C., & Pei, J. (1990). A comparison between the distinct element method and the finite element method for analysis of the stability of an excavation in jointed rock. *Tunnelling and Underground Space Technology*, *5*(1-2), 111–117. doi:10.1016/0886-7798(90)90066-S

Firpo, G., Salvini, R., Francioni, M., & Ranjith, P. G. (2011). Use of digital terrestrial photogrammetry in rocky slope stability analysis by distinct elements numerical methods. *International Journal of Rock Mechanics and Mining Sciences*, *48*(7), 1045-1054.

Fraldi, M., & Guarracino, F. (2011). Evaluation of impending collapse in circular tunnels by analytical and numerical approaches. *Tunnelling and Underground Space Technology*, *26*(4), 507-516.

Gao, F. Q., & Kang, H. P. (2008). Effect of pre-tensioned rock bolts on stress redistribution around a roadway—insight from numerical modeling. *Journal of China University of Mining and Technology*, *18*(4), 509-515.

Gengye, C., Bin, L., Mingfu, W., Zhe, H., & Wei, L. (2005). Analysis of stress monitoring of a large-span highway tunnel in Hanjialing mountain. *Chinese Journal of Rock Mechanics and Engineering*, *24*(5), 509-5. (In Chinese)

Ghee, E. H., Zhu, B. T., & Wines, D. R. (2006). Numerical analysis of twin road tunnels using two-and three-dimensional modelling techniques. In *Fourth International FLAC symposium on numerical modelling in geomechanics*.

Goodman, R. E., & Shi, G. H. (1988). The application of block theory to the design of rock bolt supports for tunnels. *Computers and Geotechnics*, *5*(1), 74.

Goodman, R. E., Taylor, R. L., & Brekke, T. L. (1968). A model for the mechanics of jointed rock. *Journal of Soil Mechanics & Foundations Div*.

Güler, G., Quaye, G. B., Jager, A. J., Reddy, N., Schweitzer, J. K., Malan, D. F., & Milev, A. (2000, November). Rock mass behaviour in ultra-deep South African gold mines and its impact on the behaviour of stope support. In *ISRM International Symposium*. International Society for Rock Mechanics.

Hamdi, P., Stead, D., & Elmo, D. (2014). Damage characterization during laboratory strength testing: A 3D-finite-discrete element approach. *Computers and Geotechnics*, *60*, 33–46. doi:10.1016/j.compgeo.2014.03.011

Hamidi, J. K., Shahriar, K., Rezai, B., & Rostami, J. (2010). Performance prediction of hard rock TBM using Rock Mass Rating (RMR) system. *Tunneling and Underground Space Technology*, *25*(4), 333-345.

Hao, Y. H., & Azzam, R. (2005). The plastic zones and displacements around underground openings in rock masses containing a fault. *Tunnelling and Underground Space Technology*, *20*, 41–61. doi:10.1016/j.tust.2004.05.003

Hasanpour, R. (2014). Advance numerical simulation of tunneling by using a double shield TBM. *Computers and Geotechnics*, *57*, 37–52. doi:10.1016/j.compgeo.2014.01.002

Hasanpour, R., Rostami, J., & Ünver, B. (2014). 3D finite difference model for simulation of double shield TBM tunneling in squeezing grounds. *Tunnelling and Underground Space Technology*, *40*, 109–126. doi:10.1016/j.tust.2013.09.012

He, M. C. (2006). Rock mechanics and hazard control in deep mining engineering in China. In *Proceedings of the 4th Asian Rock Mechanics Symposium. Singapore: World Scientific Publishing Co., Ltd* (pp. 29-46).

He, M. C., Xie, H. P., Peng, S. P., & Jiang, Y. D. (2005). Study on rock mechanics in deep mining engineering. *Chinese Journal of Rock Mechanics and Engineering*, *24*(16), 2803-2813. (In Chinese)

He X, & Song L (2012) Status and future tasks of coal mining safety in China. *Safety Science*, *50*(4):894–898. doi:10.1016/j.ssci.2011.08.012

Heidbach, O., Tingay, M., Barth, A., Reinecker, J., Kurfeß, D., & Müller, B. (2008). The world stress map database release 2008, doi: 10.1594/GFZ. *WSM. Rel2008*.

Hoek, E. (1994). Strength of rock and rock masses. *ISRM News Journal*, *2*(2), 4-16.

Hoek, E., & Brown, E. T. (1997). Practical estimates of rock mass strength. *International Journal of Rock Mechanics and Mining Sciences*, *34*(8), 1165-1186.

Hsiao, F. Y., Chern, J. C., & Chic, S. Y. (2012, January). Post-Peak strength estimation for tunneling in marble. In *ISRM Regional Symposium-7th Asian Rock Mechanics Symposium*. International Society for Rock Mechanics.

Irie, K., Koyama, T., Hamasaki, E., et al. (2009).DDA Simulations for Huge Landslides in Aratozawa Area, Miyagi, Japan Caused by Iwate-Miyagi Nairiku Earthquake. In: *9th International Conference on Analysis of Discontinuous Deformation (ICADD9)*, Singapore, pp. 153–160.

Itasca (2008) 3DEC user's guide. Itasca Consulting Group Inc., Minnesota

Jian-ping, Z., Ren-ke, W., Ai-min, W., Yang, L., & Wang, Z. (2012). Optimization Support Controlling Large Deformation of Tunnel in Deep Mine based on Discontinuous Deformation Analysis. *Procedia Environmental Sciences*, *12*(Icese 2011), 1045–1054. doi:10.1016/j.proenv.2012.01.386

Jing, L. (2003). A review of techniques, advances and outstanding issues in numerical modelling for rock mechanics and rock engineering. *International Journal of Rock Mechanics and Mining Sciences*, *40*(3), 283-353.

Jing, Z. J., Xie, F. R., Cui, X. F., & Zhang, J. F. (2013). Modern tectonic stress field deeply in Xuzhou Coal Mine. *Journal of Coal Science and Engineering (China)*, *19*(1), 14-18.

Jun, W., Caichu, X., Hehua, Z., Yongsheng, L., Zhiliang, L., & Xiaoju, C. (2004). Site monitoring and analysis of non-symmetrical multi-arch highway tunnel. *Chinese Journal of Rock Mechanics and Engineering*, *23*(2), 267-271. (In Chinese)

Kang, H. (2014). Support technologies for deep and complex roadways in underground coal mines: a review. *International Journal of Coal Science & Technology*, *1*(3), 261-277.

Kang, H., Zhang, X., Si, L., Wu, Y., & Gao, F. (2010). In-situ stress measurements and stress distribution characteristics in underground coal mines in China. *Engineering Geology*, *116*(3), 333-345.

Ke, C.-C., Kuo, C.-L., Hsu, S.-M., Liu, S.-C., & Chen, C.-S. (2012). Two-Dimensional Fracture Mechanics Analysis Using a Single-Domain Boundary Element Method. *Mathematical Problems in Engineering*, *2012*, 1–26. doi:10.1155/2012/581493

Kendorski, F. S., Cummings, R. A., Bieniawski, Z. T., & Skinner, E. H. (1983, June). A rock mass classification scheme for the planning of caving mine drift supports. In *Proceedings of rapid excavations tunneling conference. Amer Inst Mechan Engg, New York* (pp. 191-223).

Klopčič, J., & Logar, J. (2014). Effect of relative orientation of anisotropy planes to tunnel axis on the magnitude of tunnelling displacements. *International Journal of Rock Mechanics and Mining Sciences*, *71*, 235–248. doi:10.1016/j.ijrmms.2014.02.024

Kontogianni, V., Papantonopoulos, C., & Stiros, S. (2008). Delayed failure at the Messochora tunnel, Greece. *Tunnelling and Underground Space Technology*, *23*(3), 232-240.

Kulatilake, P. H., Park, J., & Um, J. G. (2004). Estimation of rock mass strength and deformability in 3-D for a 30 m cube at a depth of 485 m at Äspö hard rock laboratory. *Geotechnical and Geological Engineering*, *22*(3), 313-330.

Kulatilake, P. H. S. W, & Shu, B. (2015). Prediction of Rock Mass Deformations in Three Dimensions for a Part of an Open Pit Mine and Comparison with Field Deformation Monitoring Data. *Geotechnical and Geological Engineering*, *33*(6), 1551-1568.

Kulatilake, P. H. S. W., Ucpirti, H., Wang, S., Radberg, G., & Stephansson, O. (1992). Use of the distinct element method to perform stress analysis in rock with non-persistent joints and to study the effect of joint geometry parameters on the strength and deformability of rock masses. *Rock Mechanics and Rock Engineering*, *25*(4), 253-274.

Kulatilake, P. H. S. W., Wang, S., & Stephansson, O. (1993). Effect of finite size joints on the deformability of jointed rock in three dimensions. *International journal of rock mechanics and mining sciences & geomechanics abstracts*, *30*(5), 479-501.

Kulatilake, P. H. S. W., Wu, Q., Yu, Z., & Jiang, F. (2013). Investigation of stability of a tunnel in a deep coal mine in China. *International Journal of Mining Science and Technology*, *23*(4), 579–589.

Ladanyi, B. (1982). Borehole creep and relaxation tests in ice-rich permafrost. In *Proc. 4th Can. Permafrost Conf., Calgary*, pp. 406-415.

Laubscher, D. H. (1977). Geomechanics classification of jointed rock masses-mining applications. *Trans. Instn. Min. Metall*, *86*, A1-8.

Lauffer, H. (1958). Gebirgsklassifizierung für den Stollenbau. *Geologie und Bauwesen*, *24*(1), 46-51.

Lisjak, A., & Grasselli, G. (2014). A review of discrete modeling techniques for fracturing processes in discontinuous rock masses. *Journal of Rock Mechanics and Geotechnical Engineering*, *6*(4), 301-314.

Lisjak, A., Grasselli, G., & Vietor, T. (2014). Continuum-discontinuum analysis of failure mechanisms around unsupported circular excavations in anisotropic clay shales. *International Journal of Rock Mechanics and Mining Sciences*, *65*, 96–115. doi:10.1016/j.ijrmms.2013.10.006

Liu, Q., Bai, S., Xiao, C., & Gao, W. (2007). Study on surrounding rock stability of Longtan tunnel based on in-situ monitoring measurements. *Yanshilixue Yu Gongcheng*

Xuebao/Chinese Journal of Rock Mechanics and Engineering, *26*(10), 1982-1990. (In Chinese)

Liu, Y. J., & Li, Y. X. (2014). Revisit of the equivalence of the displacement discontinuity method and boundary element method for solving crack problems. *Engineering Analysis with Boundary Elements*, *47*, 64–67. doi:10.1016/j.enganabound.2014.06.006

Lizhong, W., Yayuan, H., Bailin, W., & Yunmin, C. (2003). Stability analysis and monitoring for tunnel in loose soils during construction . *Chinese Journal of Rock Mechanics and Engineering*, *4*, 020. (In Chinese)

Lu, S. (2005). The geological structure character of Xinwen mine area and its seeking coal orientation. *Hebei Coal*, *4*, 003.

Ma, J., Cui, G. X., Yong, Q., & Zhou, G. Q. (2008). Experimental research on unloading properties of clay under high stress. *Journal of China University of Mining and Technology*, *18*(1), 122-124.

Ma, Y.M. (1999).Development of discontinuous deformation analysis the first ten years (1986-1996), In *Proceedings Third International Conference on Analysis of Discontinuous Deformation*, Vail, Colorado, USA, pp. 17-32.

Macklin, S. R., Varley, P., Varona, P., & Merino, C. (2012). The investigation and design for a unique architectural space – The Chillida Cavern, Mount Tindaya, Fuerteventura. *Tunnelling and Underground Space Technology*, *31*, 9–19. doi:10.1016/j.tust.2012.04.001

MacLaughlin, M. M., & Doolin, D. M. (2006). Review of validation of the discontinuous deformation analysis (DDA) method. *International journal for numerical and analytical methods in geomechanics*, *30*(4), 271-305.

Maerten, F., Maerten, L., & Pollard, D. D. (2014). iBem3D, a three-dimensional iterative boundary element method using angular dislocations for modeling geologic structures. *Computers & Geosciences*, *72*, 1–17. doi:10.1016/j.cageo.2014.06.007

Mahabadi, O. K., Lisjak, A., Munjiza, A., & Grasselli, G. (2012). Y-Geo : New Combined Finite-Discrete Element Numerical Code for Geomechanical Applications. *International Journal of Geomechanics*, *12*(6), 676–688. doi:10.1061/(ASCE)GM.1943-5622.0000216.

Marschall, P., Distinguin, M., Shao, H., Bossart, P., Enachescu, C., & Trick, T. (2006, January). Creation and evolution of damage zones around a microtunnel in a claystone formation of the Swiss Jura Mountains. In *SPE International Symposium and Exhibition on Formation Damage Control*. Society of Petroleum Engineers.

Marti, J., & Cundall, P. (1982). Mixed discretization procedure for accurate modelling of plastic collapse. *International Journal for Numerical and Analytical Methods in Geomechanics*, *6*(1), 129-139.

Martino, J. B., & Chandler, N. A. (2004). Excavation-induced damage studies at the underground research laboratory. *International Journal of Rock Mechanics and Mining Sciences*, *41*(8), 1413-1426.

Merritt, A. H. (1972, June). Geologic prediction for underground excavations. In *N Am Rapid Excav & Tunnelling Conf Proc* (Vol. 1).

Munjiza, A., Owen, D. R. J., & Bicanic, N. (1995). A Combined Finite-Discrete Element Method in Transient Dynamics of Fracturing Solids. *Engineering Computations*, *12*(2), 145–174. doi:dx.doi.org/10.1108/02644409510799532

Nagtegaal, J. C., Parks, D. M., & Rice, J. R. (1974). On numerically accurate finite element solutions in the fully plastic range. *Computer methods in applied mechanics and engineering*, *4*(2), 153-177.

Ohnishi, Y., Sasaki, T., Koyama, T., Hagiwara, I., Miki, S., & Shimauchi, T. (2014). Recent insights into analytical precision and modelling of DDA and NMM for practical problems. *Geomechanics and Geoengineering*, *9*(2), 97-112.

Palmstrom, A. (1982). The volumetric joint count—a useful and simple measure of the degree of rock mass jointing. In *IAEG Congress, New Delhi* (Vol. 221).

Pan, X. D., & Reed, M. B. (1991, January). A coupled distinct element—finite element method for large deformation analysis of rock masses. In *International Journal of Rock Mechanics and Mining Sciences & Geomechanics Abstracts* (Vol. 28, No. 1, pp. 93-99). Pergamon.

Porathur, J. L., Srikrishnan, S., Verma, C. P., Jhanwar, J. C., & Pal Roy, P. (2014). Slope stability assessment approach for multiple seams Highwall Mining extractions. *International Journal of Rock Mechanics and Mining Sciences, 70,* 444–449. doi:10.1016/j.ijrmms.2014.04.023

Prazeres, P. G. C., Thoeni, K., & Beer, G. (2012). Nonlinear analysis of NATM tunnel construction with the boundary element method. *Computers and Geotechnics, 40,* 160–173. doi:10.1016/j.compgeo.2011.10.005

Price, D. G. (2008). De Freitas, M. H., ed. Engineering Geology: Principles and Practice. Springer. ISBN 3540292497

Rachez, X., & Gentier, S. (2010). 3D-hydromechanical behavior of a stimulated fractured rock mass. In *World Geothermal Congress 2010* (pp. 8-p).

Read, R. S. (2004). 20 years of excavation response studies at AECL's Underground Research Laboratory. *International Journal of Rock Mechanics and Mining Sciences*, *41*(8), 1251-1275.

Rockfield Software Ltd (2011) ELFEN User manual. Swansea, UK.

Sakurai, S. (1997). Lessons learned from field measurements in tunnelling. *Tunneling and underground space technology*, *12*(4), 453-460.

Scheldt, T. (2003). *Comparison of continuous and discontinuous modelling for computational rock mechanics* (Doctoral dissertation, Norwegian University of Science and Technology).

Schweitzer, J. K., & Johnson, R. A. (1997). Geotechnical classification of deep and ultra-deep Witwatersrand mining areas, South Africa. *Mineralium Deposita*, *32*(4), 335-348.

Shen, J., & Karakus, M. (2014). Three-dimensional numerical analysis for rock slope stability using shear strength reduction method. *Canadian Geotechnical Journal*, *51*(2), 164–172. doi:10.1139/cgj-2013-0191

Shi, G. H., & Goodman, R. E. (1985). Two dimensional discontinuous deformation analysis. *International Journal for Numerical and Analytical Methods in Geomechanics*, *9*(6), 541-556.

Shi, G. H. (1992). Discontinuous deformation analysis: a new numerical model for the statics and dynamics of deformable block structures. *Engineering computations*, *9*(2), 157-168.

Shi, G. (2007). Applications of Discontinuous Deformation Analysis (DDA) to Rock Engineering. In *International Seminar on Computational Mechanics (ISCM 2007)* (pp. 136–147).

Shi, G. H. (2014). Application of discontinuous deformation analysis on stability analysis of slopes and underground power houses. *Geomechanics and Geoengineering*, *9*(2), 80–96. doi:10.1080/17486025.2013.871065

Singh, M., & Rao, K. S. (2005). Empirical methods to estimate the strength of jointed rock masses. *Engineering Geology*, *77*(1), 127-137.

Singh, R., Mandal, P. K., Singh, A. K., & Singh, T. N. (2001). Cable-bolting-based semi-mechanised depillaring of a thick coal seam. *International Journal of Rock Mechanics and Mining Sciences*, *38*(2), 245-257.

Singh, T. N., Pradhan, S. P., & Vishal, V. (2013). Stability of slopes in a fire-prone mine in Jharia Coalfield, India. *Arabian Journal of Geosciences*, *6*(2), 419–427. doi:10.1007/s12517-011-0341-4

Stefanou, I., Psycharis, I., & Georgopoulos, I. O. (2011). Dynamic response of reinforced masonry columns in classical monuments. *Construction and Building Materials*, *25*(12), 4325-4337.

Stephansson, O., & Shen, B. (1991). Modelling of faulted rock mass response to glaciation, thermal loading and seismicity. *Quarterly Journal of Engineering Geology and Hydrogeology*, *24*(4), 355-362.

Sun, L., Zhao, G. F., & Zhao, J. (2013). Particle manifold method (PMM): A new continuum-discontinuum numerical model for geomechanics. *International Journal for Numerical and Analytical Methods in Geomechanics*, *37*(12), 1711–1736. doi:10.1002/nag

Sun, S. J., Wang, L., Zhang, D. F., & Wang, H. P. (2011). Time-history response analysis of surrounding rock mass in process of excavating deep tunnel. *Journal of China Coal Society*, *36*(5), 738-746.

Sun, X. M., Feng, C., Jun, Y., & Cao, W. F. (2009). Numerical simulation of the effect of coupling support of bolt-mesh-anchor in deep tunnel. *Mining Science and Technology (China)*, *19*(3), 352-357.

Szostak-Chrzanowski, A., Chrzanowski, A., & Massiéra, M. (2005). Use of deformation monitoring results in solving geomechanical problems—case studies. *Engineering Geology*, *79*(1), 3-12.

Terzaghi, K., Proctor, R. V., & White, T. L. (1946). Rock tunneling with steel supports. *Commmercial Shearing and Stamping Company, Youngstown, Ohio*.

Vakili, A., & Hebblewhite, B. K. (2010). A new cavability assessment criterion for longwall top coal caving. *International Journal of Rock Mechanics and Mining Sciences*, *47*(8), 1317-1329.

Vardakos, S. S., Gutierrez, M. S., & Barton, N. R. (2007). Back-analysis of Shimizu Tunnel No. 3 by distinct element modeling. *Tunnelling and Underground Space Technology*, *22*(4), 401–413. doi:10.1016/j.tust.2006.10.001

Vogel, M., & Rast, H. P. (2000). AlpTransit—safety in construction as a challenge: health and safety aspects in very deep tunnel construction. *Tunnelling and Underground Space Technology*, *15*(4), 481-484.

Vyazmensky, A., Elmo, D., & Stead, D. (2010). Role of rock mass fabric and faulting in the development of block caving induced surface subsidence. *Rock mechanics and rock engineering*, *43*(5), 533-556.

Wang, L. G., & Miao, X. X. (2006). Numerical simulation of coal floor fault activation influenced by mining. *Journal of China University of Mining and Technology*, *16*(4), 385-388.

Wang, M., Kulatilake, P. H. S. W., Um, J., & Narvaiz, J. (2002). Estimation of REV size and three-dimensional hydraulic conductivity tensor for a fractured rock mass through a single well packer test and discrete fracture fluid flow modeling. *International Journal of Rock Mechanics and Mining Sciences*, *39*(7), 887-904.

Wang, M., Song, H., Zheng, D., & Chen, S. (2006). On mechanism of zonal disintegration within rock mass around deep tunnel and definition of'deep rock engineering'. *Yanshilixue Yu Gongcheng Xuebao/Chinese Journal of Rock Mechanics and Engineering*, *25*(9), 1771-1776. (In Chinese)

Wang, Q. S., Li, X. B., Zhao, G. Y., Peng, S., & Yao, J. R. (2008). Experiment on mechanical properties of steel fiber reinforced concrete and application in deep underground engineering. *Journal of China University of Mining and Technology*, *18*(1), 64-81.

Wang, W. H., Li, X. B., Zuo, Y. J., Zhou, Z. L., & Zhang, Y. P. (2006). 3DEC modeling on effect of joints and interlayer on wave propagation. *Transactions of Nonferrous Metals Society of China*, *16*(3), 728-734.

Wang, X., Kulatilake, P. H. S. W., & Song, W. D. (2012). Stability investigations around a mine tunnel through three-dimensional discontinuum and continuum stress analyses. *Tunnelling and Underground Space Technology*, *32*, 98–112.

Wang, X. Y., Bai, J. B., Chen, Y., & Hu, Z. C. (2010). Stress relaxation effect and control technology in surrounding rock in deep entry. *Journal of China Coal Society*, *35*(7), 1072-1077. (In Chinese)

Wickham, G. E., Tiedemann, H. R., & Skinner, E. H. (1972, June). Support determinations based on geologic predictions. In *N Am Rapid Excav & Tunnelling Conf Proc* (Vol. 1).

Wu, A., Yang, Q., Ma, G., Lu, B., & Li, X. (2011). Study on the Formation Mechanism of Tangjiashan Landslide Triggered by Wenchuan Earthquake Using DDA Simulation. *International Journal of Computational Methods*, *08*(02), 229–245. doi:10.1142/S0219876211002563

Wu, J.-H.(2010). Seismic landslide simulations in discontinuous deformation analysis.*Computers and Geotechnics*, *37*(5), 594–601. doi:10.1016/j.compgeo.2010.03.007

Wu, J.-H., & Chen, C.-H.(2011). Application of DDA to simulate characteristics of the Tsaolinglandslide.*Computers and Geotechnics*, *38*(5), 741–750.

Wu, J. H., Ohnishi, Y., Shi, G. H., & Nishiyama, S. (2005). Theory of three-dimensional discontinuous deformation analysis and its application to a slope toppling at Amatoribashi, Japan. *International Journal of Geomechanics*, *5*(3), 179-195.

Wu, Q., & Kulatilake, P. H. S. W. (2012a). REV and its properties on fracture system and mechanical properties, and an orthotropic constitutive model for a jointed rock mass in a dam site in China. *Computers and Geotechnics*, *43*, 124-142.

Wu, Q., & Kulatilake, P. H. S. W. (2012b). Application of equivalent continuum and discontinuum stress analyses in three-dimensions to investigate stability of a rock tunnel in a dam site in China. *Computers and Geotechnics*, *46*, 48-68.

Wu, R., Xu, J. H., Li, C., Wang, Z. L., & Qin, S. (2015). Stress distribution of mine roof with the boundary element method. *Engineering Analysis with Boundary Elements*, *50*, 39–46. doi:10.1016/j.enganabound.2014.07.009

Wu, W., Feng, X., Zhang, C., & Qiu, S. (2011). Classification of failure modes and controlling measures for surrounding rock of deep tunnel in hard rock. *Chin J Rock Mech Eng*, *30*(9), 1782-1801. (In Chinese)

Xiao-guang, J., & Xiao-hong, L. (2007). Numerical Modeling of Three-dimension Stress Field in Deep Tunnel of High Geo-stress Area. *Journal of Chongqing University (Natural Science Edition)*, *6*, 023. (In Chinese)

Xie, F. R., Jing, Z. J., Du, Y., Cui, X. F., & Huang, X. M. (2009). Modern tectonic stress field in Xiezhuang Coal Mine. *Journal of China Coal Society*, *2*, 012. (In Chinese)

Xu, N., Kulatilake, P. H. S. W., Tian, H., Wu, X., Nan, Y., & Wei, T. (2013). Surface subsidence prediction for the WUTONG mine using a 3-D finite difference method. *Computers and Geotechnics*, *48*, 134–145. doi:10.1016/j.compgeo.2012.09.014

Yaodong, J., Yixin, Z., Wengang, L., & Qi, L. (2004). Research on Floor Heave of Roadway in Deep Mining. *Chinese Journal of Rock Mechanics and Engineering*, *14*, 020. (In Chinese)

Yang, C., Luo, Z., Hu, G., & Liu, X. (2007). Application of a microseismic monitoring system in deep mining. *Journal of University of Science and Technology Beijing, Mineral, Metallurgy, Material*, *14*(1), 6-8.

Yuan, S., Zhang, Z., Deng, K., & Li, C. (2010, October). Thermal hazard in Chinese coal mines and measures of its control. In *Mine Safety and Efficient Exploitation Facing Challenges of the 21st Century: International Mining Forum 2010* (p. 15). CRC Press.

Yuyong, J., & Jian, Z. (2004). On using DEM for simulating response of jointed rock to underground explosion. *Chinese Journal of Rock Mechanics and Engineering*, *23*(2), 5.

Zhang, Q., Chen, X., Lin, B., Liu, D., & Zhang, N. (2009a). Study of 3D geomechanical model test of zonal disintegration of surrounding rock of deep tunnel. *Chinese Journal of Rock Mechanics and Engineering*, *9*, 005. (In Chinese)

Zhang, N., Wang, C., Gao, M., & Zhao, Y. (2009b). Roadway support difficulty classification and controlling techniques for Huainan deep coal mining. *Chinese Journal of Rock Mechanics and Engineering*, *12*, 010. (In Chinese)

Zhang, Y., Chen, G., Zheng, L., Wu J. (2013a). Detailed investigation of near-fault earthquake loading induced displacement of sliding system by the Discontinuous Deformation Analysis (DDA). In: *11th International Conference on Analysis of Discontinuous Deformation (ICADD11)*, Fukuoka, Japan, pp. 153–156.

Zhang, W., Zhang, D., & Xu, M. (2013b). Fast Drivage Technology for Large Sections of Deep Coal-Rock Roadway in Complicated Geological Conditions. *The Electronic Journal of Geotechnical Engineering*, *18*/J.

Zheng, W., Zhuang, X., Tannant, D. D., Cai, Y., & Nunoo, S. (2014). Unified Continuum/Discontinuum Modelling Framework for Slope Stability Assessment. *Engineering Geology*, *179*, 90–101. doi:10.1016/j.enggeo.2014.06.014

Zhao, Z.Y., Bao, H.R., and Tian, Q., 2011. On the complementation of augmented Lagrangian method in the 2D discontinuous deformation analysis. In: *J. Zhao, Y. Ohnishi, G.F. Zhao and T. Sasaki eds. Advances in Discontinuous Numerical Methods and Applications in Geomechanics and Geoengineering. ICADD10*,HA, CRC Press, 181–187.

Zhou, J. W., Xu, W. Y., Li, M. W., Zhou, X. Q., & Shi, C. (2009). Application of rock strain softening model to numerical analysis of deep tunnel. *Chin J Rock Mech Eng*, *28*(6), 1116-1127. (In Chinese)

Zhou, X., & Qian, Q. (2007). Zonal fracturing mechanism in deep tunnel. *Yanshilixue Yu Gongcheng Xuebao/Chinese Journal of Rock Mechanics and Engineering*, *26*(5), 877-885. (In Chinese)

Zoback, M. L. (1992). First-and second-order patterns of stress in the lithosphere: The world stress map project. *Journal of Geophysical Research: Solid Earth*, *97*(B8), 11703-11728.

APPENDIX A: RAW DEFORMATION DATA

Table A.1: Deformation measurements (in mm) for the horseshoe tunnel

Day	Wall increment	Wall deformation	Roof increment	Roof deformation	Floor increment	Floor deformation
0	0	0	0	0	0	0
3	1	1	0	0	1	1
57	6	7	8	8	7	8
66	1	8	1	9	1	9
77	1	9	1	10	0	9
105	1	10	2	12	3	12
121	1	11	1	13	1	13
134	1	12	2	15	3	16
142	0	12	1	16	1	17
159	1	13	0	16	0	17
164	2	15	1	17	3	20
167	0	15	0	17	0	20
172	0	15	0	17	0	20
180	2	17	0	17	0	20
196	0	17	2	19	5	25
207	2	19	2	21	3	28
213	0	19	2	23	3	31

216	0	19	4	27	0	31
233	0	19	4	31	6	37
240	2	21	0	31	3	40
257	2	23	2	33	4	44
266	0	23	1	34	3	47
300	1	24	0	34	0	47
331	0	24	0	34	2	49
342	0	24	0	34	3	52
350	0	24	0	34	0	52

Table A.2: Deformation measurements (in mm) for the inverted arch tunnel

Day	Wall increment	Wall deformation	Roof increment	Roof deformation	Floor increment	Floor deformation
0	0	0	0	0	0	0
3	2	2	1	1	0	0
57	5	7	2	3	1	1
66	1	8	1	4	1	2
77	1	9	2	6	2	4
105	2	11	4	10	3	7
121	1	12	2	12	0	7
134	0	12	0	12	10	17
142	0	12	0	12	0	17
159	0	12	0	12	0	17
164	4	16	0	12	0	17
167	0	16	1	13	0	17
172	0	16	1	14	1	18
180	1	17	0	14	0	18
196	1	18	1	15	0	18
207	0	18	2	17	1	19
213	0	18	10	27	10	29
216	0	18	0	27	0	29
233	1	19	1	28	1	30
240	3	22	2	30	1	31

257	1	23	2	32	1	32
266	1	24	1	33	1	33
300	3	27	6	39	5	38
331	3	30	3	42	11	49
342	2	32	2	44	1	50
350	0	32	0	44	0	50

APPENDIX B: SUPPLEMENTARY MATERIAL FOR PARAMETRIC ANALYSES

Table B.1: Results from parametric changes in continuum cohesion for the horseshoe (HS) tunnel

Deviation from mean	Deformations (mm)			Factor of Safety		Grout bond failure (%)	
	Roof (mm)	Wall (mm)	Floor (mm)	First Support	Second Support	First Support	Second Support
-30	49.8	53	60.8	1.03	1.19	16.66	14.12
-15	39.7	37.2	48.9	1.06	1.17	11.2	10.31
0	36.5	32.1	44.6	1.09	1.2	11.11	10.92
15	33.8	27.5	42.8	1.13	1.24	11.14	11.39
30	30.8	23.2	40.2	1.23	1.32	10.17	10.25

Table B.2: Results from parametric changes in continuum cohesion for the inverted-arch (IA) tunnel

Deviation from mean	Deformations (mm)			Factor of Safety		Grout bond failure (%)	
	Roof (mm)	Wall (mm)	Floor (mm)	First Support	Second Support	First Support	Second Support
-30	48.8	54.2	59.9	1.03	1.12	17.1	13.33
-15	42.8	43.7	50.9	1.06	1.15	13.5	12.1
0	37.9	36	44.5	1.11	1.19	12.94	11.71
15	33.7	30.1	40	1.15	1.21	10.97	11.53
30	31	26.1	36.5	1.26	1.28	10.19	10.89

Table B.3: Results from parametric changes in continuum friction angle for the HS tunnel

Deviation from mean	Deformations (mm)			Factor of Safety		Grout bond failure (%)	
	Roof (mm)	Wall (mm)	Floor (mm)	First Support	Second Support	First Support	Second Support
-30	54.1	62.5	61.7	1.03	1.09	17.42	14.41
-15	42.4	42.1	50	1.05	1.16	14.35	11.49
0	36.5	32.1	44.6	1.09	1.2	11.11	10.92
15	32	25.1	43.3	1.19	1.28	10.59	10.51
30	29.6	21.6	39.8	1.37	1.43	10.12	10.9

Table B.4: Results from parametric changes in continuum friction angle for the IA tunnel

Deviation from mean	Deformations (mm)			Factor of Safety		Grout bond failure (%)	
	Roof (mm)	Wall (mm)	Floor (mm)	First Support	Second Support	First Support	Second Support
-30	52.9	65	63.4	1.03	1.12	17.45	15.98
-15	44.9	47.7	52.7	1.07	1.15	14.49	12.12
0	37.9	36	44.5	1.11	1.19	12.94	11.71
15	32.4	27.5	39.6	1.22	1.23	10.44	11.43
30	28.7	22.5	34.5	1.41	1.35	10.35	10.19

Table B.5: Results from parametric changes in continuum elastic modulus for HS tunnel

Deviation from mean	Deformations (mm)			Factor of Safety		Grout bond failure (%)	
	Roof (mm)	Wall (mm)	Floor (mm)	First Support	Second Support	First Support	Second Support
-30	45	39.2	56.3	1.06	1.16	11.11	9.62
-15	39.8	35	48	1.08	1.19	11.13	11.02
0	36.5	32.1	44.6	1.09	1.2	11.11	10.92
15	34.6	30.5	42.2	1.09	1.21	11.14	11.35
30	32.1	27.8	38	1.12	1.21	11.05	11.3

Table B.6: Results from parametric changes in continuum elastic modulus for IA tunnel

Deviation from mean	Deformations (mm)			Factor of Safety		Grout bond failure (%)	
	Roof (mm)	Wall (mm)	Floor (mm)	First Support	Second Support	First Support	Second Support
-30	47	45.8	57.2	1.07	1.17	13.21	11.29
-15	42.2	40.7	50.6	1.1	1.18	13.09	11.67
0	37.9	36	44.5	1.11	1.19	12.94	11.71
15	35.8	34.5	42.9	1.1	1.19	12.93	13.38
30	33.7	32	40	1.11	1.2	12.89	13.55

Table B.7: Results from parametric changes in continuum tensile strength for HS tunnel

Deviation from mean	Deformations (mm)			Factor of Safety		Grout bond failure (%)	
	Roof (mm)	Wall (mm)	Floor (mm)	First Support	Second Support	First Support	Second Support
-30	37	32.8	45.1	1.09	1.2	11.15	11.23
-15	36.9	32.3	45.1	1.09	1.2	11.15	11.21
0	36.5	32.1	44.6	1.09	1.2	11.11	10.92
15	36.5	32.1	44.6	1.09	1.2	11.11	10.92
30	36.5	32.1	44.6	1.09	1.2	11.11	10.92

Table B.8: Results from parametric changes in continuum tensile strength for IA tunnel

Deviation from mean	Deformations (mm)			Factor of Safety		Grout bond failure (%)	
	Roof (mm)	Wall (mm)	Floor (mm)	First Support	Second Support	First Support	Second Support
-30	38	36.9	45.6	1.11	1.19	12.94	11.94
-15	37.9	36.6	45.5	1.11	1.19	12.94	11.71
0	37.9	36	44.5	1.11	1.19	12.94	11.71
15	37.9	36	44.5	1.11	1.19	12.94	11.71
30	37.9	36	44.3	1.11	1.19	12.94	11.71

Table B.9: Results from parametric changes in bedding plane joint normal stiffness (JKN) for the HS tunnel

Deviation from mean	Deformations (mm)			Factor of Safety		Grout bond failure (%)	
	Roof (mm)	Wall (mm)	Floor (mm)	First Support	Second Support	First Support	Second Support
-30	41.9	34.9	50.8	1.03	1.15	12.83	10.9
-15	38.5	32.6	45.5	1.06	1.17	11.13	10.59
0	36.5	32.1	44.6	1.09	1.2	11.11	10.92
15	34.7	30.5	44	1.12	1.21	10.66	10.33
30	33.7	29.9	43	1.14	1.22	10.14	10.39

Table B.10: Results from parametric changes in bedding plane JKN for the IA tunnel

Deviation from mean	Deformations (mm)			Factor of Safety		Grout bond failure (%)	
	Roof (mm)	Wall (mm)	Floor (mm)	First Support	Second Support	First Support	Second Support
-30	42.9	39.5	51.8	1.04	1.14	13.3	12.65
-15	40.5	38.5	48.4	1.1	1.17	13.1	12.83
0	37.9	36	44.5	1.11	1.19	12.94	11.71
15	37.3	36	44.5	1.13	1.2	12.93	12.83
30	36.2	35.6	42.9	1.14	1.21	12.08	12.61

Table B.11: Results from parametric changes in bedding plane joint shear stiffness (JKS) for the HS tunnel

Deviation from mean	Deformations (mm)			Factor of Safety		Grout bond failure (%)	
	Roof (mm)	Wall (mm)	Floor (mm)	First Support	Second Support	First Support	Second Support
-30	38.3	34.3	47.2	1.08	1.2	11.44	11.37
-15	37.5	33.5	46.5	1.08	1.2	11.2	11.23
0	36.5	32.1	44.6	1.09	1.2	11.11	10.92
15	35.5	30.3	44.5	1.1	1.19	11.07	10.33
30	35.3	29.3	44.5	1.1	1.19	11.07	10.27

Table B.12: Results from parametric changes in bedding plane JKS for the IA tunnel

Deviation from mean	Deformations (mm)			Factor of Safety		Grout bond failure (%)	
	Roof (mm)	Wall (mm)	Floor (mm)	First Support	Second Support	First Support	Second Support
-30	39.4	38.9	46.9	1.09	1.19	13.14	11.96
-15	38.4	37.5	46	1.1	1.19	13.03	11.93
0	37.9	36	44.5	1.11	1.19	12.94	11.71
15	37.3	35.3	44	1.1	1.19	12.39	11.94
30	36.4	34.3	43.5	1.14	1.19	11.35	11.47

Table B.13: Results from parametric changes in bedding plane basic friction angle for the HS tunnel

Deviation from mean	Deformations (mm)			Factor of Safety		Grout bond failure (%)	
	Roof (mm)	Wall (mm)	Floor (mm)	First Support	Second Support	First Support	Second Support
-30	43.2	41.5	53.4	1.04	1.15	16.23	13.51
-15	39.6	35.5	48.4	1.06	1.18	12.3	11.67
0	36.5	32.1	44.6	1.09	1.2	11.11	10.92
15	34.8	29.5	42	1.12	1.22	11.05	10.57
30	33.3	28.7	40.2	1.14	1.23	11	9.84

Table B.14: Results from parametric changes in bedding plane basic friction angle for the IA tunnel

Deviation from mean	Deformations (mm)			Factor of Safety		Grout bond failure (%)	
	Roof (mm)	Wall (mm)	Floor (mm)	First Support	Second Support	First Support	Second Support
-30	46.2	51	56.9	1.04	1.15	17.33	15.78
-15	41.2	42.5	50.3	1.08	1.17	13.78	13.04
0	37.9	36	44.5	1.11	1.19	12.94	11.71
15	35.2	31.9	41.1	1.14	1.2	11.44	10.96
30	33.7	29.8	37.9	1.18	1.2	10.15	10.56

Table B.15: Results of variation of cable diameters for IA tunnel

Diameter (mm) – First/second support	Roof (mm)	Wall (mm)	Floor (mm)	Average FS		Grout bond failure (%)	
				1st Support	2nd Support	1st Support	2nd Support
16/19	37.9	36	44.5	1.11	1.19	12.94	11.71
19/22	37.1	34.9	44.2	1.13	1.22	15.22	14.88
22/26	36.2	33.4	44.1	1.18	1.3	22	20.48
26/29	35.6	32.4	43.9	1.27	1.38	28.8	23.24

Table B.16: Results of variation of grout uniaxial compressive strengths for IA tunnel

Grout UCS (MPa)	Roof (mm)	Wall (mm)	Floor (mm)	Average FS		Grout bond failure (%)	
				1st Support	2nd Support	1st Support	2nd Support
25	38.5	36.8	45.3	1.17	1.32	34.5	30.03
35	38.2	36.5	44.9	1.12	1.22	22.14	20.38
45	38	36.4	44.9	1.11	1.2	14.85	14.72
55	37.9	36	44.5	1.11	1.19	12.94	11.71

APPENDIX C: MANUSCRIPTS FROM THIS WORK

C.1: Rock Mechanics and Rock Engineering

One manuscript containing some of the results in this thesis has been published in the peer-reviewed journal *Rock Mechanics and Rock Engineering*. The abstract of the paper (doi: 10.1007/s00603-015-0885-9) is given below:

Title: Discontinuum–Equivalent Continuum Analysis of the Stability of Tunnels in a Deep Coal Mine Using the Distinct Element Method

Abstract: An imperative task for successful underground mining is to ensure the stability of underground structures. This is more so for deep excavations which may be under significantly high stresses. In this manuscript, we present stability studies on two tunnels, a horseshoe-shaped and an inverted arch-shaped tunnel, in a deep coal mine in China, performed using the 3DEC distinct element code. The rock mass mechanical property values for the tunnel shapes have been estimated through a back-analysis procedure using available field deformation data. The back-analysis has been carried out through a pseudo-time dependent support installation routine which incorporates the effect of time through a stress-relaxation mechanism. The back-analysis indicates that the rock mass cohesion, tensile strength, uniaxial compressive strength, and elastic modulus values are about 35–45 % of the corresponding intact rock property values. Additionally, the importance of incorporating stress relaxation before support installation has been illustrated through the increased support factor of safety and reduced grout failures. The calibrated models have been analyzed for different supported and unsupported cases to

estimate the significance and adequacy of the current supports being used in the mine and to suggest a possible optimization. The effects of supports have been demonstrated using deformations and yield zones around the tunnels, and average factors of safety and grout failures of the supports. The use of longer supports and floor bolting has provided greater stability for the rock masses around the tunnels. Finally, a comparison between the two differently shaped tunnels establishes that the inverted arch tunnel may be more efficient in reducing roof sag and floor heave for the existing geo-mining conditions.

C.2: American Rock Mechanics Association Symposium

A second paper with some material from the research detailed in the thesis has been accepted for presentation at the *American Rock Mechanics Association Symposium 2016* at Houston. The abstract is given below:

Title: Distinct Element Method Based Stability Analysis of Tunnels in a Deep Coal Mine in China

Abstract: Stability studies on two tunnels, a horseshoe-shaped and an inverted arch-shaped tunnel, in a deep coal mine in China, have been performed using the 3DEC distinct element code and presented in this study. A pseudo time-dependent support installation procedure has been developed to incorporate the stress relaxation and deformation due to time gap between excavation and support installation. The utility of incorporating stress relaxation before support installation has been explored through observation of support factors of safety and grout failures. The numerical models have been analyzed for different support configurations and unsupported situations. The reinforcement provided by the supports has been demonstrated using changes in tunnel

deformations and sizes of yield zones around the tunnels, in addition to observations of support factors of safety and grout failures. Results indicate that using longer supports and floor bolting would provide higher stability for the rock masses around the tunnels. A comparison between the closure strains in the two tunnels indicates that the inverted arch tunnel may be more stable under the existing geo-mining conditions at the site. Finally, parametric studies point to the importance of cohesion and friction angle estimation for intact rock, and basic friction angle estimation for the rock mass, to ensure robust numerical results.